ไฮโดรจิเนชันของคาร์บอนไดออกไซด์โดยตัวเร่งปฏิกิริยาโคบอลต์บนตัวรองรับเมโซพอรัสไทเทเนีย

นายเอกรัตน์ บัวพัน
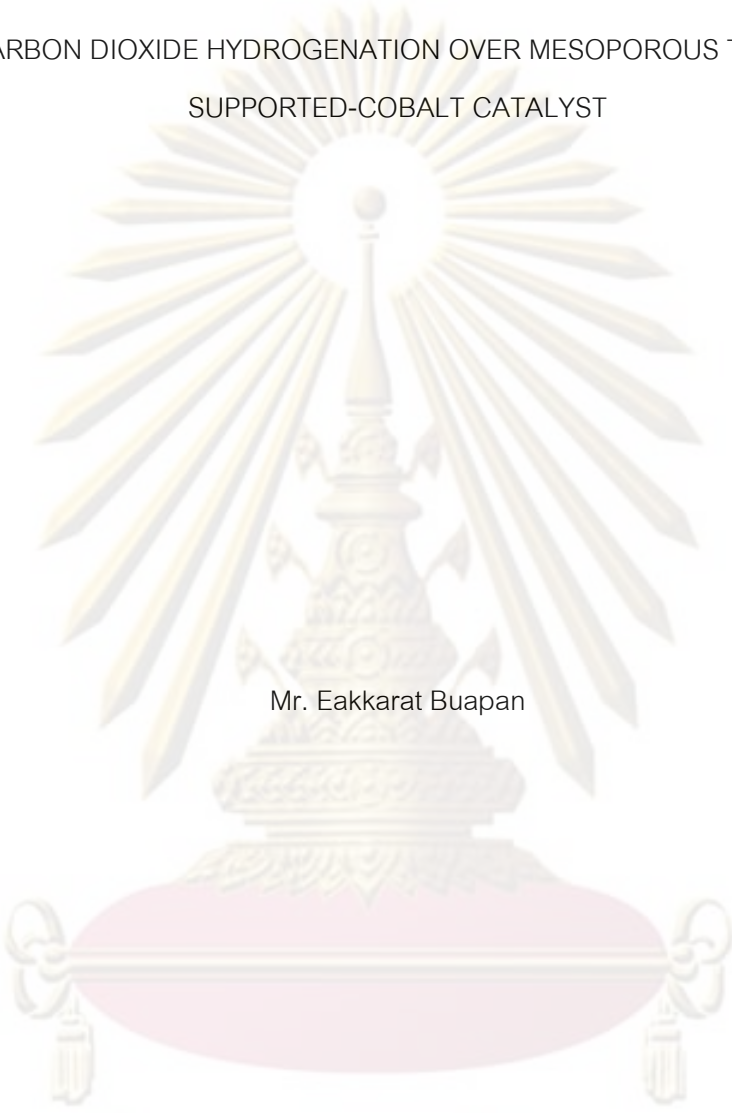
CARBON DIOXIDE HYDROGENATION OVER MESOPOROUS TITANIA

SUPPORTED-COBALT CATALYST

Mr. Eakkarat Buapan

A Thesis Submitted in Partial Fulfillment of the Requirements

for the Degree of Master of Engineering Program in Chemical Engineering

Department of Chemical Engineering

Faculty of Engineering

Chulalongkorn University

Academic Year 2009

Thesis Title   CARBON DIOXIDE HYDROGENATION OVER MESOPOROUS
                  TITANIA SUPPORTED-COBALT CATALYST

By   Mr. Eakkarat Buapan

Field of Study   Chemical Engineering

Thesis Advisor   Associate Professor Bunjerd jongsomjit, Ph.D.

Accepted by the Faculty of Engineering, Chulalongkorn University in Partial
Fulfillment of the Requirements for the Master's Degree

.... Dean of the Faculty of Engineering

(Associate Professor Boonsom Lerdhirunwong, Dr.Ing)

THESIS COMMITTEE

.... Chairman

(Associate Professor Muenduen Phisalaphong, Ph.D.)

.... Thesis Advisor

(Associate Professor Bunjerd Jongsomjit, Ph.D.)

.... Examiner

(Assistant Professor Joongjai Panpranot, Ph.D.)

.... External Examiner

(Assistant Professor Okorn Mekasuwandumrong. D.Eng.)

เอกรัตน์ บัวพัน: ไฮโดรจิเนชันของคาร์บอนไดออกไซด์โดยตัวเร่งปฏิกิริยาโคบอลต์บน
ตัวรองรับเมโซพอรัสไทเทเนีย (CARBON DIOXIDE HYDROGENATION OVER
MESOPOROUS TITANIA SUPPORTED-COBALT CATALYST)
อ. ที่ปรึกษาวิทยานิพนธ์หลัก: รศ.ดร. บรรเจิด จงสมจิตร, 98 หน้า.

ปฏิกิริยาไฮโดรจิเนชันของคาร์บอนไดออกไซด์ของตัวเร่งปฏิกิริยาโคบอลต์บนตัว
รองรับเมโซพอรัสไทเทเนีย (เฟสผสมและเฟสรูไทบริสุทธิ์) ซึ่งได้จากการสังเคราะห์โดย
กระบวนการออกซิไดซ์และเปปไทเซชันระหว่างไทเทเนียมคาร์ไบด์ด้วยกรดไนตริกเข้มข้น (5
โมลาห์, 70 องศาเซลเซียส เป็นเวลา 8 และ 48 ชั่วโมง) อีกทั้งผลของการปรับปรุงตัวรองรับ
ด้วยรูทีเนียมได้ถูกทำการศึกษา จากการทดลองพบว่า ตัวเร่งปฏิกิริยาโคบอลต์บนตัวรองรับ
เฟสผสมและรูไทบริสุทธิ์ ซึ่งมีพื้นที่ผิวจำเพาะและปริมาตรรูพรุนสูงกว่าบนตัวรองรับที่ใช้
ในทางการค้า ส่งผลให้มีส่วนว่องไว การกระจายตัวของโลหะโคบอลต์และ พื้นที่โลหะว่องไว
ที่สูงกว่า แต่ค่าการเปลี่ยนแปลง และอัตราการเกิดปฏิกิริยามีค่าต่ำกว่า สาเหตุเนื่องมาจาก
ปริมาณคาร์บอนหลงเหลือในตัวรองรับจากกระบวนการสังเคราะห์ ซึ่งมีปริมาณสูงกว่าตัว
รองรับเชิงการค้าถึง 4.5 เท่า อีกทั้งการเกิดสารประกอบโคบอลต์ไททาเนท ซึ่งส่งผลให้
ความสามารถในการถูกรีดิวซ์ของตัวเร่งปฏิกิริยาลดลงโดยไม่ทำให้อุณหภูมิในการรีดิวซ์
เปลี่ยนไป เมื่อทำการปรับปรุงตัวรองรับด้วยโลหะรูทีเนียม พบว่าการกระจายตัวของโลหะโค
บอลต์ดีขึ้นและช่วยเพิ่มความสามารถในการรีดิวซ์ของตัวเร่งปฏิกิริยาที่อุณหภูมิต่ำ อีกทั้ง
สภาวะการแคลไซด์ที่อุณหภูมิสูงกว่าสภาวะที่ไม่ได้ปรับปรุง (300 และ 500 องศาเซลเซียส)
ส่งผลให้ปริมาณคาร์บอนถูกลดลงมาอยู่ในระดับเดียวกับตัวรองรับเชิงการค้า แต่พื้นที่ผิว
จำเพาะและปริมาตรรูพรุนก็ลดลงมาอยู่ในระดับเดียวกันด้วย ค่าการเปลี่ยนแปลงและ อัตราการ
เกิดปฏิกิริยาเคมีจึงมีค่าสูงขึ้น แต่ยังคงไม่เห็นความแตกต่างอย่างชัดเจนเมื่อเทียบกับตัวเร่ง
ปฏิกิริยาบนตัวรองรับเชิงการค้า

ภาควิชา	วิศวกรรมเคมี	ลายมือชื่อนิสิต	เอกรัตน์ ยังฯ
สาขาวิชา	วิศวกรรมเคมี	ลายมือชื่อ อ.ที่ปรึกษาวิทยานิพนธ์หลัก	
ปีการศึกษา	2552		

#5070650821: MAJOR CHEMICAL ENGINEERING

KEYWORDS : MESOPOROUS TITANIA/TITANIUM CARBIDE/NITRIC ACID/ACID-CATALYZED/PEPTIZATION/COBALT CATALSYT; CO_2 HYDROGENATION

EAKKARAT BUAPAN: CARBON DIOXIDE HYDROGENATION OVER MESOPOROUS TITANIA SUPPORTED-COBALT CATALYST THESIS ADVISOR: ASSOC. PROF. BUNJERD JONGSOMJIT, Ph.D., 98 pp.

CO_2 hydrogenation of Co-catalysts on mesoporous titania (mixed and pure rutile phases), which was synthesized by oxidation and peptization process between TiC-precursor and aqueous nitric acid (5 M, 70 °C, 8 and 48 h), and effect of ruthenium (Ru) metal promoted on catalyst support were investigated. It was found that Co/Mixed phase and Co/R had higher specific surface area, pore volume, active site, %Co dispersion and active metal surface area than those of Co/P25 (commercial one), which showed lower conversion and reaction rate value. Due to high carbon residue (about 4.5 times higher than commercial one) on the supports from synthesis process and the formation of cobalt titanate, it resulted in a decrease in the degree of reduction without any significant change in the reduction behaviors. When the catalyst supports were promoted with ruthenium metal, it enhances dispersion and reduction efficiency of cobalt species. Moreover, with Ru-promoted catalyst, the calcined temperature is higher than that of the unpromoted one. Carbon residue was removed to the same level of commercial support, but specific surface area was decreased to this level, too. Conversion and rate of CO_2 hydrogenation took up to high value, but not significant compared to the Co-catalyst using the commercial support.

Department : Chemical Engineering   Student's Signature ....

Field of Study : Chemical Engineering   Advisor's Signature ....

Academic Year : 2009

ACKNOWLEDGEMENTS

CONTENTS

LIST OF TABLES

LIST OF FIGURES

LIST OF SCHEMES

CHAPTER I

INTRODUCTION

1.1 Rationale

Global warming caused by a noticeable increase of carbon dioxide emission into the atmosphere is an important and urgent problem. Catalytic hydrogenation of CO_2 has been recently attracting considerable attention as one of the chemical fixation and recycling technologies for emitted CO_2. Most of the research has emphasized that the supports such as C, Al_2O_3, SiO_2, ZrO_2, TiO_2 etc. can significantly influence activity/selectivity properties of the active phase for surface reaction (Sou, 1997, Storsaeter, 2005). Titanium (IV) oxide (TiO_2 of titania) has received considerable attention in heterogeneous catalysis due to its high chemical stability, high photoactivity, nontoxicity, low cost, and is used in many applications such as environmental remediation, chemical synthesis and energy production and storage (Kryukova, 2007, Ozcan, 2007; Yu, 2007). However, the properties of titania itself may not be completely satisfied for all purpose based on CO_2 hydrogenation activity, since some intrinsic undesirable properties, such as the relative low surface area and pore size lead to an unsatisfied CO_2 conversion (Bando, 1997, Suo, 1997). Since Antonelli and Ying (1995) reported a modified sol–gel synthesis of hexagonally packed mesoporous TiO_2, the TiO_2 has attracted much attention because of its high surface area and large, uniform pores. This is a great importance in catalysis and solar cell applications. Many efforts have been made in order to generate the active mesoporous supported catalysts which are more active and more stable.

With the aim of providing further insights of the reactivity of carbon dioxide on a Co-based catalyst, the effect of mesoporous titania support, which was synthesized by acid catalyzed-TiC and Ru-promotion on the Co-based mesoporous titania catalyst for CO_2 hydrogenation was investigated, the sample properties were characterized using thermal gravimetric/differential thermal analysis (TG/DTA). N_2 physisorption (BET), x-ray diffraction (XRD), scanning electron microscopy (SEM), energy dispersive x-ray spectroscopy (EDX), transmission electron microscopy (TEM), thermal conductivity detector (TCD), x-ray photoelectron spectroscopy (XPS), CO-Pulse chemisorptions, temperature-programmed reduction (TPR) and Inductive couple plasma/optical emission spectrometer (ICP/OES) plasma gas-chromatography (GC). The reaction study of CO_2 hydrogenation was carried out in order to measure activity and product selectivity under methanation condition.

1.2 Objective

The objective of this research was to investigate the effect of mesoporous titania support, which was synthesized by acid catalyzed-TiC and Ru-promotion on the Co-based mesoporous titania catalyst for CO_2 hydrogenation regarding CO_2 conversion and selectivity.

1.3 Research scope

- Preparation of mesoporous titania support via acid catalyzed-TiC method
- Characterization of the mesoporous titania support samples by TG/DTA, XRD, BET SEM/TEM and TCD
- Preparation of unpromoted and promoted mesoporous titania with 0.5 %wt Ru by incipient wetness impregnation method.
- Preparation of supported Co-catalyst on the unpromoted and promoted mesoporous titania (20%wt) by incipient wetness impregnation method.

- Characterization of the catalyst samples using XRD, BET, TPR, CO-pulse chemisorptions, SEM/EDX, TEM, ICP, TCD and XPS.
- Investigation of the catalytic activity of Co/TiO_2 catalyst in the CO_2 hydrogenation reaction at 220 °C, 1 atm with H_2/CO ratio of 10 under methanation condition.

1.4 Research Methodology

```
                    ┌─────────────────────────────────────┐
                    │  Preparation mesoporous titania support │
                    └─────────────────────────────────────┘
```

Mesoporous titania support	Ru-promoted mesoporous titania support

Support Characterization

- TG/DTA   - XRD
- BET   - TCD
- SEM   - TEM

Impregnate Co onto the support

- XRD   - BET
- SEM/EDX   - TEM
- TPR   - XPS
- CO chemisorptions
- ICP/OES

Catalyst precursor

CO_2 hydrogenation reaction

GC analysis

Discussion and conclusion
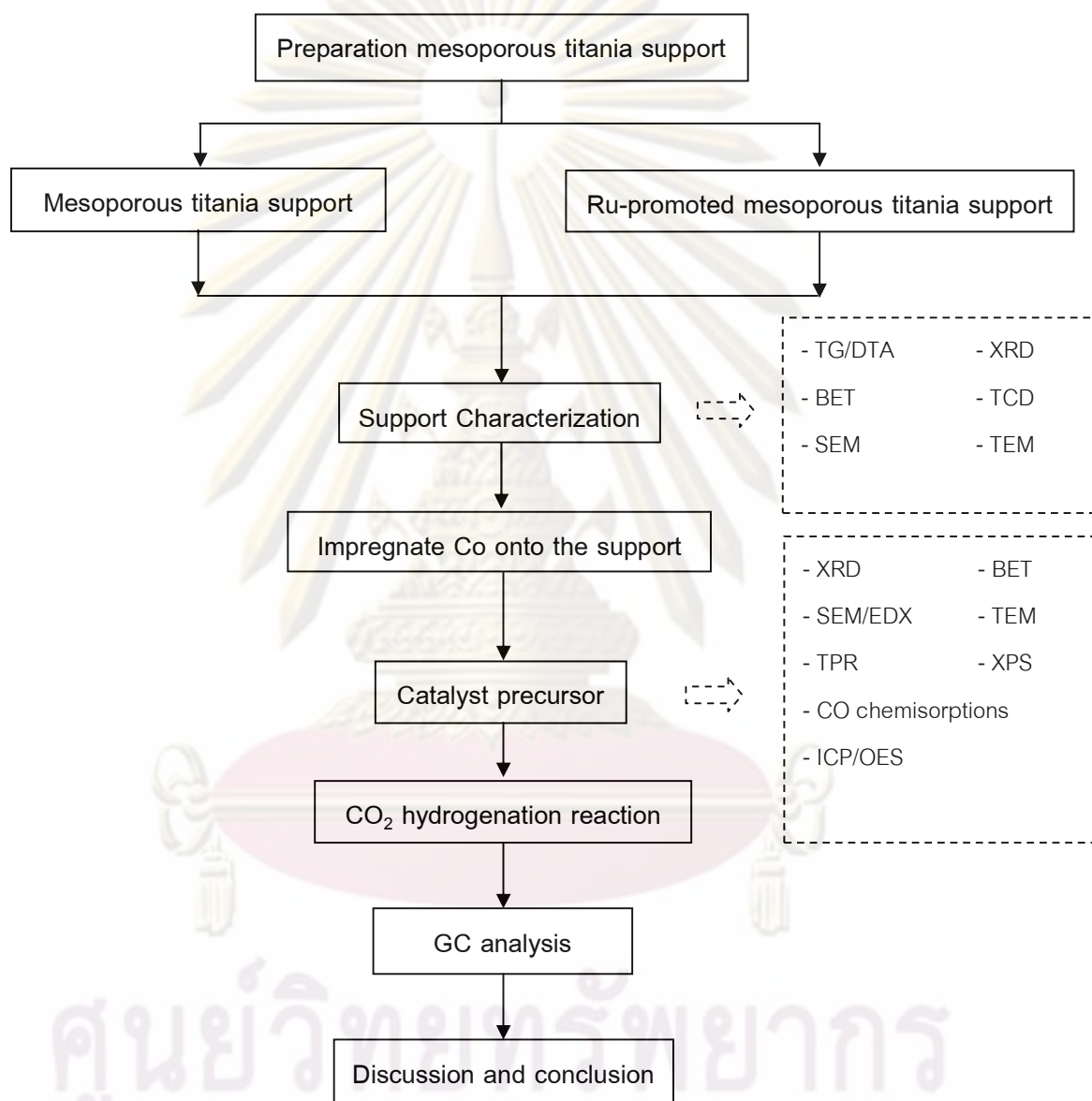
Scheme 1.1 diagram of research methodology

CHAPTER II

THEORY

2.1 CO_2 Hydrogenation

CO_2 is currently used as an additive in the synthesis of methanol from CO and H_2 (Aresta, 1998), and it is believed that reduced forms of CO_2 are kinetically important intermediates in this process. Homogeneous catalysts are also known that mediate the rapid hydrogenation of CO_2 to formate (Leitner, 1998). Because this reaction is not thermodynamically favored, amines and supercritical CO_2 have been used to drive this reaction. Under the appropriate conditions, very high turnover numbers and rates can be achieved. For example, they examined complexes of the general type $[R_2P-(X)-PR_2]Rh$-(hfacac) (X = bridging group; hfacac = 1,3-bis-(trifluoromethyl)-acetonylacetonate) (Fornika, 1995). All of the compounds are active catalysts for formic acid production from H_2 and CO_2, but the most effective has X = $(CH_2)_4$ and R = cyclohexyl and exhibits a turnover frequency of 1335 h^{-1} at 25 °C and 40 atm of 1:1 H_2: CO_2. The selectivity to formic acid is nearly 100%; the suggested pathway is indicated in **Scheme** 2.1. Recently, efficient heterogeneous catalysts have been developed for CO_2 hydrogenation to methanol, and pilot-scale plants based on this technology have been demonstrated (Ushikoshi, 1998). However, the thermodynamics for methanol production from H_2 and CO_2 are not as favorable as that for production of methanol from H_2 and CO. For example, at 200 °C the equilibrium yield of methanol from CO_2 is slightly less than 40% while the yield from CO is greater than 80% (Arakawa, 1998). The reduction of CO_2 can be rendered more favorable by the use of hybrid catalysts that dehydrate methanol to form dimethyl ether (Dubois, 1992).

P = P(cyclohexyl)$_2$
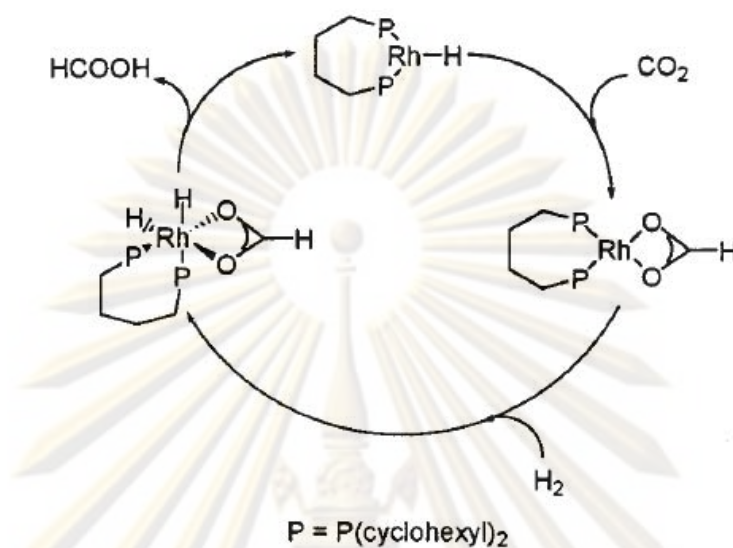
Scheme 2.1 Proposed of Rhodium-Catalyzed CO_2 hydrogenation mechanism to formic acid
(Fornika, 1995).

Other copper-based catalysts have also been used for methanol synthesis. Fisher and Bell (Fisher, 1997) studied $Cu/ZrO_2/SiO_2$ catalysts by in-situ infrared spectroscopy and suggested the pathway shown in **Scheme 2.2** for the route to methanol. Ethanol has also been produced by the hydrogenation of CO_2 (Kusama, 1996). This fuel is attractive because it has a somewhat higher energy density than methanol and it is not as toxic. However, the selectivity for ethanol production is generally low (<40%). The hydrogenation of CO_2 to methane and higher hydrocarbons is also known. For C_2 and higher hydrocarbons, hybrid catalysts such as $Cu-ZnO-Cr_2O_3$ and H-Y zeolite are generally used. Pioneering work has been carried out by Noyori *et al.* (1996) on the catalytic synthesis of formic acid derivatives by CO_2 hydrogenation, together with other substrates, in supercritical CO_2. In part because of the high solubility of H_2 in $scCO_2$, an economical synthesis of dimethylformamide is achieved. The process is superior to conventional methods because of its high efficiency (TON = 4.2×10^5, where TON = moles of product per

mole of catalyst) and high selectivity; the catalyst precursor is $(Me_3P)_4RuCl_2$, and the operating temperature is 100 °C.
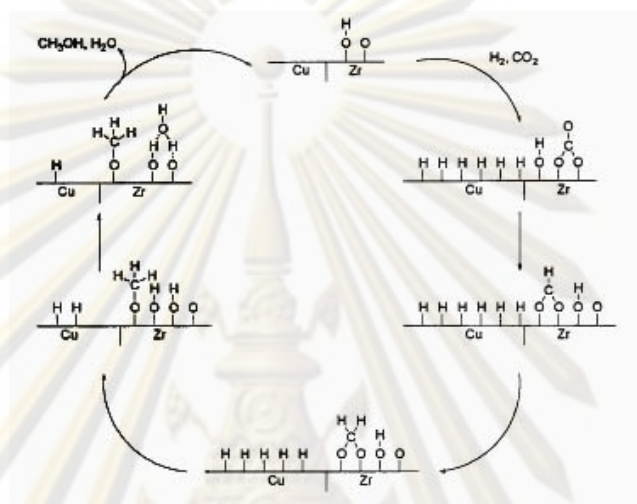
Scheme 2.2 Proposed heterogeneous catalyst CO_2 hydrogenation mechanism to methanol (Fisher, 1997)

Lahtinen *et al.* (1994) were investigated C, CO and CO_2 hydrogenation on cobalt foil model catalysts. It found that the reactions produce mainly methane but with selectivity of 98, 80, and 99 wt% at 525 K for C, CO, and CO_2, respectively. These authors also proposed the reaction mechanisms for C, CO and CO_2 hydrogenation shown in **Table 2.1**. Trovarelli *et al.* (1990) suggested that the hydrogenation of CO_2 to hydrocarbons proceeded through the formation of CO as intermediate. According to other authors (Gines, 1997), CO_2 hydrogenation on metal catalysts occurred through a consecutive mechanism in which CO_2 was first converted to CO by the reverse water gas shift (RWGS) reaction, and then CO was hydrogenated to hydrocarbon.

Table 2.1 The reaction mechanisms proposed for C, CO and CO_2 hydrogenation.

(Lahtinen, 1994)

C Hydrogenation	CO Hydrogenation	CO_2 hydrogenation		
	$CO + {}^* \Leftrightarrow CO^*$	$CO2 + {}^* \Leftrightarrow CO2^*$		
$H_2 + 2^* \Leftrightarrow 2H^*$	$H_2 + 2^* \Leftrightarrow 2H^*$	$H_2 + 2^* \Leftrightarrow 2H^*$		
		$CO_2^* + Co \Leftrightarrow CO^* + CoO$		
	$CO^* + Co \Leftrightarrow C^* + CoO$	$CO^* + Co \Leftrightarrow C^* + CoO$	$CO^* + H^* \Leftrightarrow COH^* + {}^*$	
$C^* + H^* \Leftrightarrow CH^* + {}^*$	$C^* + H^* \Leftrightarrow CH^* + {}^*$	$C^* + H^* \Leftrightarrow CH^* + {}^*$	$COH^* + H^* \Leftrightarrow H_2CO^* + {}^*$	
$CH^* + H^* \Leftrightarrow CH_2^* + {}^*$		$CH^* + H^* \Leftrightarrow CH_2^* + {}^*$	$HCO^* + Co \Leftrightarrow CH_2^* + CoO$	
$CH_2^* + H^* \Leftrightarrow CH_3^*$	$CH_2^* + H^* \Leftrightarrow CH_3^*$	$CH_2^* + H^* \Leftrightarrow CH_3^*$		
$CH_3^* + H^* \Leftrightarrow CH_4 + 2^*$	$CH_3^* + H^* \Leftrightarrow CH_4 + 2^*$	$CH_3^* + H^* \Leftrightarrow CH_4 + 2^*$		
	$CoO + H^* \longrightarrow OH^* + Co$	$CoO + H^* \longrightarrow OH^* + Co$		
	$OH^* + H^* \Leftrightarrow H_2O + 2^*$	$OH^* + H^* \Leftrightarrow H_2O + 2^*$		
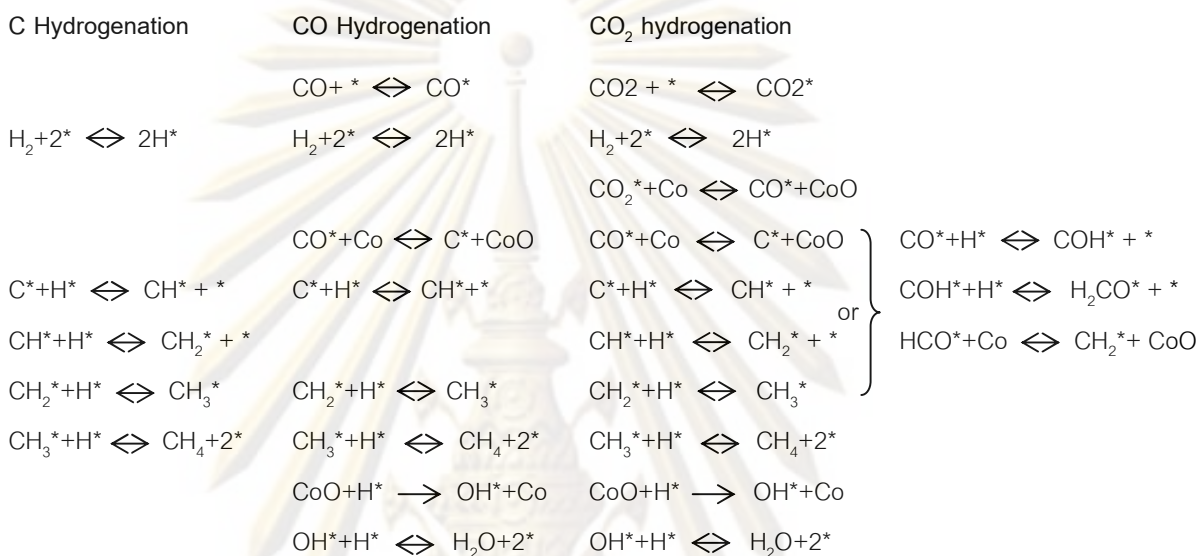
2.2 Titanium (IV) Oxide, TiO_2, (Fujishima, 1999)

Titanium (IV) oxide, TiO_2, occurs naturally in three crystalline forms;

1. Anatase, which tends to be more stable at lower temperatures. This type generally shows a higher photoactivity than other types of titanium dioxide.

2. Brookite, which is usually found only in minerals and has a structure belonging to orthorhombic crystal system.

3. Rutile, which tends to more stable at high temperatures. The application of almost rutile type is used in industrial products such as paints, cosmetics foodstuffs and sometimes found in igneous rocks.

Both of anatase and rutile type have a structure belonging to tetragonal crystal system but they are not isomorphous (**Figure** 2.1). The two tetragonal crystal types are more common because they are easy to make. Anatase occurs usually in near-regular octahedral, and rutile forms slender prismatic crystal, which are frequently twinned. Rutile is the thermally stable form and is one of the two most important ores of titanium.

The three allotropic forms of titanium dioxide have been prepared artificially but only rutile, the thermally stable form, has been obtained in the form of transparent large single crystal. The transformation form anatase to rutile is accompanied by the evolution of ca. 12.6 kJ/mol (3.01 kcal/mol), but the rate of transformation is greatly affected by temperature and by the presence of other substance which may either catalyze of inhibit the reaction. The lowest temperature at which conversion of anatase to rutile takes place at a measurable rate is ca. 700 °C, but this is not a transition temperature. The change is not reversible; °G for the change from anatase to rutile is always negative.
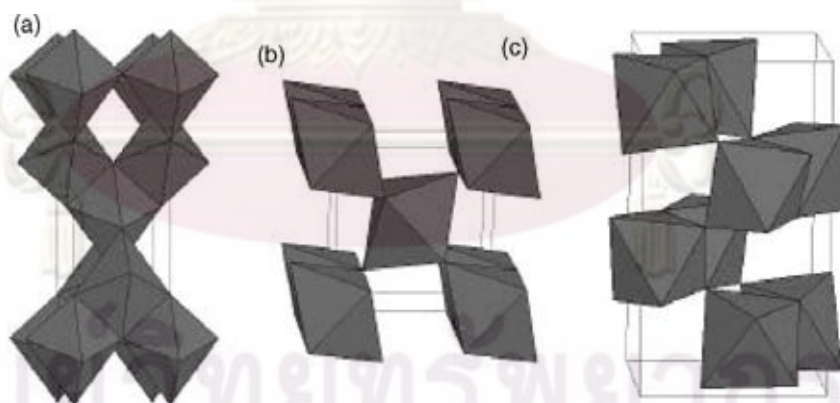
Figure 2.1 Crystal structures of anatase (a), rutile (b), and brookite (c) TiO_2. (Carp, 2004)

Table 2.2 Crystallographic properties of anatase, brookite, and rutile.

Properties	Anatase	Brookite	Rutile
Crystal structure	Tetragonal	Orthorhombic	Tetragonal
Optical	Uniaxial, negative	Biaxial, positive	Uniaxial, negative
Density, g/cm^3	3.9	4.0	4.23
Harness, Mohs scale	$5\frac{1}{2} - 6$	$5\frac{1}{2} - 6$	$7 - 7\frac{1}{2}$
Unit cell	$D_4a^{19}.4TiO_2$	$D_2h^{15}.8TiO_2$	$D_4h^{12}.3TiO_2$
Dimension, nm			
a	0.3758	0.9166	0.4584
b		0.5436	
c	0.9514	0.5135	2.953

Brookite has been produced by heating amorphous titanium (IV) oxide, prepared from alkyl titanates of sodium titanate with sodium or potassium hydroxide in an autoclave at 200 to 600 °C for several days. The important commercial forms of titanium (IV) oxide are anatase and rutile, and these can readily be distinguished by X-ray diffraction spectrometry.

Since both anatase and rutile are tetragonal, they are both anisotropic, and their physical properties, e.g. refractive index, vary according to the direction relative to the crystal axes. In most applications of these substances, the distinction between crystallographic directions is lost because of the random orientation of large numbers of small particles, and it is mean value of the property that is significant.

Measurement of physical properties, in which the crystallographic directions are taken into account, may be made of both natural and synthetic rutile, natural anatase

crystals, and natural brookite crystals. Measurements of the refractive index of titanium dioxide must be made by using a crystal that is suitably orientated with respect to the crystallographic axis as a prism in a spectrometer. Crystals of suitable size of all three modifications occur naturally and have been studied. However, rutile is the only form that can be obtained in large artificial crystals from melts. The refractive index of rutile is 2.75. The dielectric constant of rutile varies with direction in the crystal and with any variation from the stoichiometric formula, TiO_2; an average value for rutile in powder from is 114. The dielectric constant of anatase powder is 48.

Titanium dioxide is thermally stable (mp 1855 °C) and very resistant to chemical attack. When it is heated strongly under vacuum, there is a slight loss of oxygen corresponding to a change in composition to $TiO_{1.97}$. The product is dark blue but reverts to the original white color when it is heated in air.

2.3 Cobalt (Young, 1960, Othmer, 1991)

2.3.1 General

Cobalt, a transition series metallic element having atomic number 27, is similar to silver in appearance. Cobalt and cobalt compounds have expended from use colorants in glasses and ground coat fits for pottery to drying agents in paints and lacquers, animal and human nutrients, electroplating materials, and high temperature alloys, hard facing alloys, and high speed tools, and magnetic alloys, alloys used for prosthetics, and used in radiology. Cobalt is also as a catalyst for hydrocarbon refining from crude oil for the synthesis of heating fuel.

2.3.2 Physical Properties

The electronic structure of cobalt is $[Ar]3d^7 4s^2$. At room temperature the crystalline structure of the α (or ε) form, is close-packed hexagonal (cph) and lattice parameters are a = 0.2501 nm and c = 0.4066 nm. Above approximately 417 °C, a face-centered cubic (fcc) allotrope, the γ (or β) form, having a lattice parameter a = 0.3554 nm, becomes the stable crystalline form. The scale formed on unalloyed cobalt during exposure to air or oxygen at high temperature is double-layered. In the range of 300 to 900 °C, the scale consists of a thin layer of mixed cobalt oxide, Co_3O_4, on the outside and cobalt (II) oxide, CoO, layer next to metal. Cobalt (III) oxide, Co_2O_3, may be formed at temperatures below 300 °C. above 900 °C, Co_3O_4 decomposes and both layers, although of different appearance, are composed of CoO only. Scales formed below 600 °C and above 750 °C appear to be stable to cracking on cooling, whereas those produced at 600-750 °C cracks and flake off the surface.

Cobalt forms numerous compounds and complexes of industrial importance. Cobalt, atomic weight 58.933, is one of the first transition series of Group 9 (VIIIB). There are thirteen know isotope, but only three are significant: ^{59}Co is the only stable and naturally occurring isotope; ^{60}Co has a half-life of 5.3 years and is a common source of γ-source for MÖssbauer spectroscopy. Cobalt exists in the +2 or +3 valance states for the major of its compounds and complexes. A multitude of complexes of the cobalt (III) ion exists, but few stable simple salt are know. Octahedral stereochemistry is the most common for cobalt (II) ion as well as for cobalt (III). Cobalt (II) forms numerous simple compounds and complexes, most of which are octahedral or tetrahedral in nature; cobalt (II) forms more tetrahedral complex than other transition-metal ions. Because of the small stability difference between octahedral and tetrahedral complexes of cobalt (II), both can be found equilibrium for a number of complexes. Typically, octahedral cobalt (II) salts and complexes are pink to brownish red; most of the tetrahedral Co (II) species are blue.

Table 2.3 Physical properties of cobalt (Othmer, 1991)

Property	Value
atomic number	27
atomic weight	58.93
transformation temperature, °C	417
heat of transformation, J/g[a]	251
melting point, °C	1493
latent heat of fusion, ΔH_{fus} J/g[a]	395
boiling point, , °C	3100
latent heat of vaporization at bp, ΔH_{vap} kJ/g[a]	6276
specific heat, J/(g· °C)[a]	
15-100°C	0.442
molten metal	0.560
coefficient of thermalexpansion, °C^{-1}	
cph at room temperature	12.5
fcc at 417 °C	14.2
thermal conductivity at 25 °C, W/(m·K)	69.16
thermal neutron absorption, Bohr atom	34.8
resistivity, at 20 °C[b], 10^{-8} Ω·m	6.24
Curie temperature, °C	1121

Table 2.3 Physical properties of cobalt (cont.)

Property	Value		
saturation induction, $4\pi I_s$, T[c]	1.870		
permeability, μ			
initial	68		
max	245		
residual induction, T[c]	0.490		
coercive force, A/m	708		
Young's modulus, Gpac	211		
Poisson's ratio	0.32		
Hardness[f], diamond pyramid, of %Co	99.9	99.98[e]	
At 20 °C	225	253	
At 300 °C	141	145	
At 600 °C	62	43	
At 900 °C	22	17	
strength of 99.99 %cobalt, MPa[g]	as cast	annealed	sintered
tensile	237	588	679
tensile yield	138	193	302
compressive	841	808	
compressive yield	291	387	

[a] To convert J to cal, divided by 4.184.

[b] conductivity = 27.6 % of International Annealed Copper Standard.

[c] To convert T to gauss, multiply by 10^4.

[d] To convert GPa to psi , multiply by 145,000.

[e] Zone refined.

[f] Vickers, [g] To convert MPa to psi , multiply by 145.

2.3.3 Cobalt Oxides

Cobalt has three well-know oxides: Cobalt (II) oxide, CoO, is an olive green, cubic crystalline material. Cobalt (II) oxide is the final product formed when the carbonate or the other oxides are calcined to a sufficiently high temperature, preferably in a neutral or slightly reducing atmosphere. Pure cobalt (II) oxide is a difficult substance to prepare, since it readily takes up oxygen even at room temperature to re-form a higher oxide. Above about 850 °C, cobalt (II) oxide form is the stable oxide. The product of commerce is usually dark gray and contains 77-78 wt% cobalt. Cobalt (II) oxide is soluble in water, ammonia solution, and organic solvents, but dissolves in strong mineral acids. It is used in glass decorating and coloring and is a precursor for the production of cobalt chemical.

Cobalt (II) oxide, Co_2O_3, is form when cobalt compounds are heated at a low temperature in the presence of an excess of air. Some authorities told that cobalt (III) oxide exists only in the hydrate form. The lower hydrate may be made as a black power by oxidizing neutral cobalt solutions with substances like sodium hypochlorite. Co_2O_3 or $Co_2O_3.H_2O$ is completely converted to Co_3O_4 at temperatures above 265 °C. Co_3O_4 will absorb oxygen in a sufficient quantity to correspond to the higher oxide Co_2O_3.

Cobalt oxide, Co_3O_4, is formed when cobalt compounds, such as the carbonate or the hydrated sesquioxide, are heated in air at temperatures above approximately 265 °C and not exceeding 800 °C.

2.4 Co-based catalyst

Supported cobalt (Co) catalysts are the preferred catalysts for the synthesis of heavy hydrocarbons from carbon dioxide and hydrogen because of their high activity, high selectivity for linear hydrocarbons, and low activity for the water gas shift reaction. It is

known that reduced cobalt metal, rather than its oxides or carbides, is the most active phase for CO_2 hydrogenation in such catalysts. Investigations have been done to determine the nature of cobalt species on various supports such as alumina, silica, titania, magnesia, carbon, and zeolites. The influence of various types of cobalt precursors used was also investigated. It was found that the used of organic precursors such as Co (III) acetyl acetate resulting in an increase of CO conversion compared to that of cobalt nitrate (Kraum, 1999).
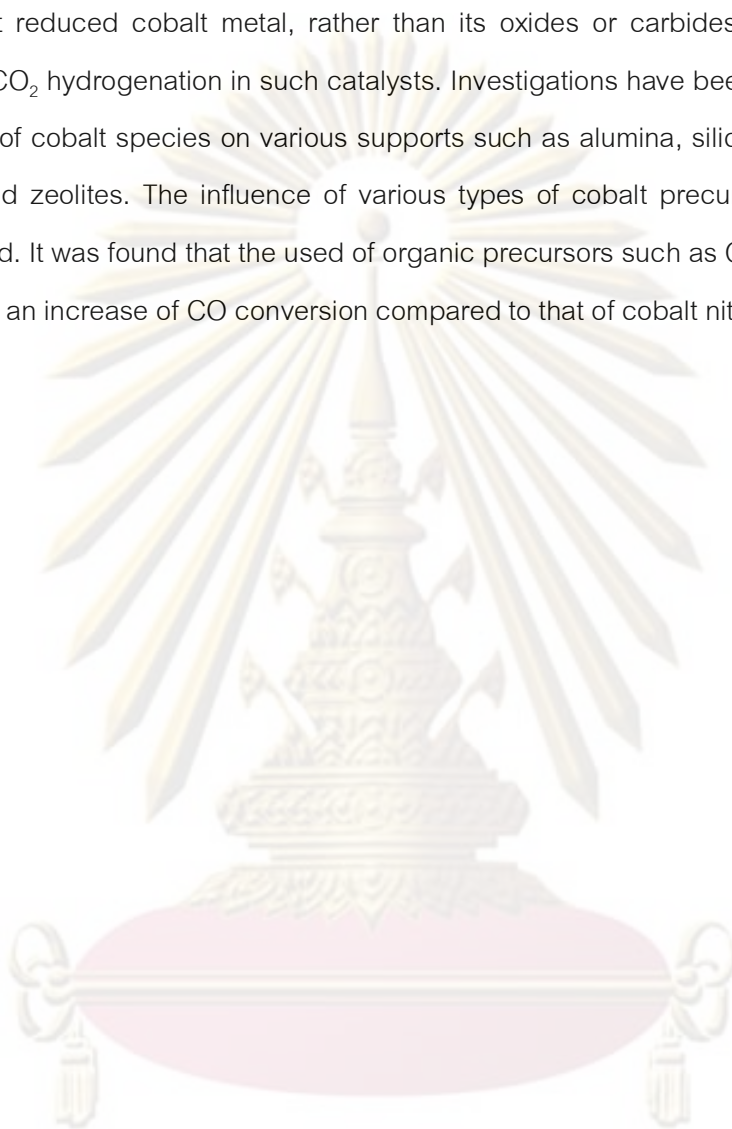
CHAPTER III

LITERATURE REVIEW

CO$_2$ hydrogenation (methanation) is a well-known catalytic reaction used to produce light-hydrocarbon fuel (methane). Generally, supported cobalt catalyst is employed for this process due to its good activity, selectivity and low reverse water-gas shift reaction (RWGS). Moreover, several factors have shown to affect the performance of Co-catalysts for CO$_2$ hydrogenation such as preparation method and addition of a supported promoting agent.

3.1 CO$_2$ hydrogenation with Heterogeneous catalysts

In a previous study, characterization of TiO$_2$-, ZrO$_2$- and Al$_2$O$_3$-supported iron catalysts as used for CO$_2$ hydrogenation (Suo, 1997) was investigated. It was found that TiO$_2$- and ZrO$_2$-supported iron oxides show good activity and C$_{2+}$ selectivity. In addition, Bando *et al*. (1997) found that Cu/TiO$_2$ showed the highest turnover frequency among Cu/Al$_2$O$_3$, Cu/SiO$_2$. Moreover, the CO and CO$_2$ hydrogenation on Co/SiO$_2$ under Fisher-Tropsch synthesis conditions was also studied (Zhang, 2002). It was found that CO$_2$ and CO hydrogenation appears to follow different reaction pathways and main product is methane with relative low activity of CO$_2$ hydrogenation and otained similar catalytic activities but the selectivity were very different, FTS product distributions were observed with an $\propto$ of about 0.80; in contrast, the CO$_2$ hydrogenation products contained about 70% or more of methane and proposed reaction pathway for CO and CO$_2$ hydrogenation.

Hydrogenation of CO_2 (Sakurai, 1996, Sakurai, 1995) and CO (Sakurai, 1995, Vannice, 1983, Mori, 1987) over TiO_2-supported noble metal catalysts have been intensively studied.

Cobalt-based catalysts are preferred for the synthesis of high molecular weight paraffins (Dry, 2002, Iglesia, 1997, Chu, 2007), as they own high activity, high selectivity to linear hydrocarbons, low activities for the water-gas shift reaction, and lower price compared to those of noble metal. The catalytically active phase of the reaction is metallic cobalt; the behavior of cobalt catalysts strongly depends on the dispersion and reducibility of cobalt species. Design of efficient cobalt catalyst with high concentration of cobalt metal sites, high catalysts activity and high selectivity to desired products still remains a challenge (Hong, 2009). Jongsomjit *et al*. (2005) were investigated cobalt dispersion on titania consisting various rutile:anatase ratios. It was found that the number of reduced cobalt metal surface with presence of optimum rutile phase in titania up to 19% resulted in highly dispersed cobalt oxide species. It was proposed a volcano conceptual model on dependence of dispersion with rutile phase on the number of reduced cobalt metal surface atoms for Co/TiO_2.

3.2 Titania (TiO_2) supported Co-catalysts

The strong metal support interaction (SMSI) between the titania support and Co metal is used to determined the cobalt dispersion and reduction behavior of Co/TiO_2 catalyst. The synthesis of highly dispersed cobalt on TiO_2 support requires the strong interaction between cobalt and support. However, too strong interaction can produce the Co-support compound as a suboxide at an interface that is high resistant to reduction. Active sites in Cobalt catalyst were found in many directions such as unsupported metallic cobalt and cobalt monocrystals were active, for large cobalt metal particles the reaction rate is proportional to the number of cobalt surface sites (Soled, 2003). In addition, the active

cobalt metallic phases, a working FT catalyst, could contain several other cobalt species: cobalt carbide, cobalt oxides, cobalt support mixed compounds, etc. These species are probably not directly involved in FT synthesis. Cobalt carbide formation seems to be related to a deactivation process. Oxidized cobalt species (Co_3O_4, CoO, etc.) do not catalyze FT synthesis either. Oxidation of cobalt metallic species during the reaction leads to catalyst deactivation and reduces FT reaction rates. At the same time, cobalt oxidized species could probably affect the rate of several side and secondary reactions, such as water-gas shift, olefin isomerization, reinsertion, and hydrogenolysis (Khodakov, 2007).

In many recent years, titania-supported Co catalysts have been widely studied by many authors, especially for the application of FT in a continuous stirred tank reactor (CSTR) (Jacobs, 2002). The anatase:rutile phase of titania can affect to the catalytic activity of Co/TiO_2 catalyst. The formerly study reported that both activity and selectivity of CO hydrogenation reaction were altered by changing the rutile:anatase ratios in the titania support (Jongsomjit, 2005). The activity of a $Co/\gamma\text{-}Al_2O_3$ catalyst could affect by addition of CO during H_2 reduction results in increasing both Co reducibility and dispersion (Jongsomjit, 2002). The Co support compound formation (Co-SCF) was found to lower activity of the Co catalyst. In addition, Co-SCF was found during standard reduction resulting in a lower reducibility of the Co catalyst and it is non-reducible at temperature < $800^{\circ}C$ during TRP difference from $CoTiO_3$.

Type of supported also affect to the phase composition and interaction of cabalt with support. The study of type of supported cobalt catalyst (CoO_x/SiO_2, CoO_x/TiO_2 and CoO_x/Al_2O_3) has been studied. From the result, it showed that the interaction of cobalt oxide with supports was much stronger in the kinds of Al_2O_3 and TiO_2, while no conclusive evidence of any interaction was found for SiO_2 (Wang, 2006). The support interactions on the reduction of cobalt oxide species were observed in the order Al_2O_3 > TiO_2> SiO_2. Besides, the amounts of cobalt metal loading also affect the reducibility by decreasing interactions with the support. Co/TiO_2 also use as catalyst for dry reforming of methane for

generating synthesis gas and is related to the generation of fuel for fuel cells (Nagaoka, 2002).

3.3 Mesoporous titania synthesis

Mesoporous TiO_2 has been paying much attention, because of its high specific surface area and high porosity. It is extensively used in the photocatalysis fields, catalytic support and solar cells. Since Antonelli and Ying (1995) reported a modified sol-gel synthesis of hexagonally packed mesoporous TiO_2 by using alkyl phosphate surfactants and titanium isopropoxide bisacetylacetonate, many researches have been performed broadly on synthesis of mesoporous TiO_2 by several methods. Up to date, most of the synthesis process use amine (Wang, 2003, Wu, 2003), ionic (Wang, 2006, Li, 2007), block polymer (Liu, 2008) or nonionic surfactants (Kluson, 2001) as the structure-directing agent (template) which could be removed by either calcinations or solvent extraction process. However, the mesoporous framework could be collapsed by thermal treatment at high temperature that leads to surface area and pore volume reduction. A simple and environmentally benign template-free sol-gel process mesoporous TiO_2 was first demonstrated by Liu et al. (Liu, 2004). Nitric acid was used as a catalyst and the calcined TiO_2 produced without a structure-directing template has a high surface of 106 m^2g^{-1}. Raveendran et al. (2008) have demonstrated a template-free method to prepare spherical anatase mesoporous TiO_2 in the nanometer/submicron size ranged by simple room-temperature, hydrolytic condensation of titanium butoxide (TiOB) dispersed in ethyl acetate. The TiO_2 exhibits high surface area (388 m^2g^{-1}), while the formation of the mesoporous organization may be attributed to the self-assembly of TiOB molecules through site-specific intermolecular interactions, the role of ethyl acetate may be in dispersing the bulk TiOB associations into thermodynamically stable spherical assemblies, retaining their meso-scale

order. Huang *et al*. (2005) prepared the high surface area mesoporous TiO_2 by a sol-gel process at ambient temperature using tetrabutyl titanate as precursor, inorganic acid i.e. HCl, HNO_3, H_2SO_4 and HPO_3 as catalysts, in the absence of any template. Shieh *et al*. (2007) presented a novel reaction between TiC and aqueous HNO_3 producing anatase TiO_2 with a narrow diameter distribution of mesopores. The reaction was performed in one step condition (70 °C) with a short reaction time (1 h) without any surfactants or polymers as templates. Avoidance of any structure-directing template during synthesis of mesoporous TiO_2 is highly important from both environmental and industrial points of view.

3.4 CO_2 hydrogenation with promoted-support catalyst

Perez-Alonso *et al*. (2008) was investigated the carbon dioxide hydrogenation over Fe-Ce catalyst. Unpormoted and Ce-pormoted Fe catalysts have been tested. Under the selected reaction conditions (573 K, 1.01 MPa, H_2/CO = 3, GHSV = 15.5 $Lh^{-1}g^{-1}$cat), both materials show similar catalytic performance, reaching similar conversion levels and yielding hydrocarbons (C_1–C_{10}) with high selectivity. The chain growth probability (α) obtained is very similar in both cases (0.44). Although Ce incorporation into the base iron catalyst does not modify the CO_2 hydrogenation performance, the promoter addition shortens the time required to reach stationary-state operation in a great extent (from 70 to 30 h). Yaccato *et al*. (2005) were investigated the competition of CO and CO_2 methanation over ZnO_2 supported noble metal catalysts in high throughput scanning mass spectrometer. It found that the highest methanation activity is seen for Ru and Rh whereas Pt is found to be the most active and selective catalyst for the reverse WGS reaction (highest CO_2 loss without concomitant methanation side reaction). Whereas Cu, Au, Co, and Ag are only slightly active and Pd only moderately active, Ir, Na-doped Co, Re, K-doped Pt and the chloride precursor $PtCl_4$ are more active and WGS selective. Pt and Na-doped Pt as well as

Ni methanize, but with their trajectories emanating from the reverse WGS equilibrium point in the lower left quadrant, indicating 'shift-assisted' methanation with the faster WGS reaction dominating, at 350 °C and 1% metal loading. Pt ammine nitrite, hydroxide and tetramethylammonium hexahydroxoplatinate are the most active among the Pt precursorsscreened and show good methanation activity. However, Rh and Ru are the most active methanizers. High methanation activity is accompanied by high water formation rates, much beyond the WGS mass balance diagonal that requires water to scale linearly with CO_2 consumption. In summary, the activity ranking of the active metals is given by the following order:

Cu; Au; Co; Ag < Pd < Ir; NaCo; Re; KPt; PtCl < NaPt< Pt; Ni < Rh < KNaRu < Ru

Lee *et al*. (2004) were investigated the promotion of hydrocarbon selectivity in CO_2 hydrogenation by Ru component over Fe-K/Al_2O_3 catalyst. It found that Ru promoter enhance CO_2 conversion from 36% to 41% and promote C_{5+} selectivity. It was reported that Ru promotion in Al_2O_3-supported iron catalysts enhanced the catalytic activity and higher hydrocarbon selectivity.

CHAPTER IV

EXPERIMENTAL

4.1 Chemicals

The chemicals used in this experiment are specified as follows:

1.   TiC precursor available from Aldrich.

2.   Cobalt (II) nitrate hexahydrate 98% available from Aldrich.

3.   Ruthenium (III) nitrosyl nitrate, solution in dilute nitric acid, 1.5%

         $[Ru(NO(NO_3)_3]$ available from Aldrich

4.   Nitric Acid

5.   Ethanol

4.2 Catalyst Preparation

4.2.1   Preparation of mesoporous titania

TiC in black powder form (Aldrich, nominally less than 4 um in particle size) 1.4 g. was added to 16 ml of aqueous HNO_3 solution (5 M) at 70 °C with a vigorous stir condition. After 4, 8, 24, 48 and 72 h reaction time, a fine gray was collected by centrifuging then it was washed with ethanol and de-ionized water for several times and was dried at 70 °C over night in an oven to remove the water. The dried sample was subsequently calcined in a tube furnace with air (95 ml/min) by heating to 200 °C at a rate of 10 °C/min and held at that temperature for 30 min. Then, the as-prepared samples were cool down to room temperature in N_2 flow (75 ml/min). Next, the acid concentration was increased to 9 M (70

°C) and reaction temperature was raised up to 80 °C and 100 °C (5 M HNO_3) which both case were operated only at 24, 48 and 72 h to investigate the TiO_2 phase transformation rate with strong acid concentration and high temperature condition.

4.2.2 Cobalt loading

The catalysts were prepared by incipient wetness impregnation with aqueous solution of cobalt (II) nitrate hexahydrate. The certain amount of cobalt (20 wt% loading) will be dissolved de-ionized water and then impregnated into the support. The cobalt solution is dropped slowly to the support and then the catalyst is dried in the oven at 110 °C for 12 h. The catalyst is calcined in air at 300 °C for 2 h using a ramp rate of 1 °C/min.

4.2.3 Promoted mesoporous titania preparation

A promoted-titania support was co-impregnation prepared by the incipient wetness impregnation. A Ruthenium (III) nitrosyl nitrate [$Ru(NO(NO_3)_3$] (0.5 wt% loading) was dissolved in de-ionized water which its volume equaled to pore volume of catalyst and then impregnated on to prepared titania. The Ru solution was dropped slowly to the titania support. The modified-titania would be dried at 383 K for 12 h and calcained in air flow at 773K for 4 h.

4.2.4 Catalyst Nomenclature

Part I: Preparation of mesoporous titania

Nomenclature of sample is given as follows $TiO_2\_A\_B\_C$

where A is HNO_3 concentration in M

B is reaction temperature in °C

C is reaction time in h

i.e. TiO_2_5M_70C_8h means TiO_2 obtained using 5 M HNO_3, at 70 °C for 8 h.

Part II: Catalyst for CO_2 hydrogenation

Nomenclature of sample is given as follows CoRu/A

Where Co is 20%wt of cobalt impregnated

Ru is 0.5%wt ruthenium promoted

A is the support used i.e. P25, Mixed and R refer to degussa P25, mixed phase titania and pure rutile phase , respectively.

I.e. CoRu/P25 means 0.5%wt ruthenium promoted degussa P25 support which impregnated with 20%wt Co.

4.3 Catalyst Characterization

4.3.1 X-ray diffraction (XRD)

XRD was performed to determine the bulk phase of catalysts by SIEMENS D 5000 X-ray diffractometer using CuK_α radiation with Ni filter in the 2θ range of 20-80 degrees resolution 0.04°. The crystallite size was calculated from Scherrer's equation.

4.3.2 Carbon analyzer

At least 0.3 mg of sample was analyze by elemental analyzer or CHNS/O analyzer with perkin elmer, PE2400 series II. The sample was decomposed to gas phase by

high thermal treated and carbon content was detected by thermal conductivity detector (TCD).

4.3.3 N_2 Physisorption

The catalyst 0.1 gram was study BET surface area, pore volume and pore diameter were measured by N_2 adsorption–desorption isotherm at liquid nitrogen temperature (-196 °C) using a Micromeritics ASAP 2020. The surface area and pore distribution were calculated according to Brunauer-Emmett-Teller (BET) and Barret-Joyner-Halenda (BJH) methods, consecutively.

4.3.4 CO-Pulse Chemisorptions

The active sites and the relative percentages dispersion of cobalt catalyst were determined by CO-pulse chemisorptions technique using Micromeritics ChemiSorb 2750 (pulse chemisorption system) and ASAP 2101C V.3.00 software. It was carried out using 10 mg of a sample and reduced in H_2 flow rate at 50 ml/min with heated from room temperature to 350 °C at rate 10 °C/min and held at this temperature for 3 h after the cooled down to room temperature in a He flow. Desorbed CO was measured using thermal conductivity detector. Pulsing was continued until no further carbon monoxide adsorption was observed.

4.3.5 Temperature-Programmed Reduction (TPR)

TPR was used to determine the reduction behaviors of the samples using a Micrometritics Chemisorb 2750.

1. The catalyst sample 0.1 g was used in the sample cell.

2. Prior to operation, the catalysts were heated up to 200 °C in flowing nitrogen and held at this temperature for 1 h.

3. After the catalyst sample was cooled down to room temperature, the carrier gas was 5% H_2 in Ar (30 CC/min) were ramping from 35 to 800 °C at 10 °C/min.

4. A cold trap was placed before the detector to remove water produced during the reaction.

5. A thermal conductivity detector (TCD) was used to determine the amount of hydrogen consumption during TPR.

4.3.6 X-ray photoelectron spectroscopy (XPS)

The XPS analysis was performed originally using an AMICUS spectrometer equipped with a Mg Ka X-ray radiation. For a typical analysis, the source was operated at voltage of 15 kV and current of 12 mA. The pressure in the analysis chamber was less than 10^{-5} Pa. The AMICUS system is computer controlled using the AMICUS "VISION 2"software.

4.3.7 Transmission Electron Microscopy (TEM)

The morphology and size of the catalyst was observed using JEOL JEM 2010, operating at 200 kV.

4.3.8 Thermal Gravimetric Analysis (TGA)

Thermal gravimetric analysis (TGA) and differential thermal analysis (DTA) were performed using an SDT Analyzer Model Q600 from TA Instruments, USA. The TGA/DTA analyses of the spent catalysts were carried out from room temperature to 1000 °C at a heating rate of 10 °C/min in oxygen.

4.4 Reaction study in CO_2 hydrogenation

4.4.1 Materials

The reactant gas used for the reaction study was the carbon dioxide in hydrogen feed stream as supplied by Thai Industrial Gas Limited (TIG). The gas mixture contained 8.80±2vol% CO_2 in H_2 (22 CC/min). The total flow rate was 30 CC/min with the H_2/CO_2 ratio of 10/1. Ultra high purity hydrogen (50 CC/min) and high purity argon (8 CC/min) manufactured by Thai Industrial Gas Limited (TIG) were used for reduction and balanced flow rate.

4.4.2 Apparatus

Flow diagram of CO_2 hydrogenation system is shown in **Figure 4.1**. The system consists of a reactor, an automatic temperature controller, an electrical furnace and a gas controlling system.

4.4.2.1 Reactor

The reactor was made from a stainless steel tube (O.D. 3/8"). Two sampling points were provided above and below the catalyst bed. Catalyst was placed between two quartz wool layers.

4.4.2.2 Automation Temperature Controller

This unit consisted of a magnetic switch connected to a variable voltage transformer and a solid-state relay temperature controller model no. SS2425DZ connected to a thermocouple. Reactor temperature was measured at the bottom of the catalyst bed in

the reactor. The temperature control set point is adjustable within the range of 0-800 °C at the maximum voltage output of 220 volt.

4.4.2.3 Electrical Furnace

The furnace supplied heat to the reactor for CO_2 hydrogenation. The reactor could be operated from temperature up to 800 °C at the maximum voltage of 220 volt.

4.4.2.4 Gas Controlling System

Reactant for the system was each equipped with a pressure regulator and an on-off valve and the gas flow rates were adjusted by using metering valves.

4.4.2.5 Gas Chromatography

The composition of hydrocarbons in the product stream was analyzed by a Shimadzu GC14B (VZ10) gas chromatograph equipped with a flame ionization detector. A Shimadzu GC8A (molecular sieve 5A) gas chromatography equipped with a thermal conductivity detector was used to analyze CO and H_2 in the feed and product streams. The operating conditions for each instrument are shown in the **Table 4.1**.

4.4.3 Procedures

1. Using 0.1 g of catalyst packed in the middle of the stainless steel microrector, which is located in the electrical furnace.
2. A flow rate of Ar = 8 CC/min, 8.80% CO_2 in H_2 = 22 CC/min and H_2 = 50 CC/min in a fixed-bed flow reactor. A relatively high H_2/CO ratio was used to minimize deactivation due to carbon deposition during reaction.

3. The catalyst sample was reduced *in situ* in flowing H_2 at 350 $^{\circ}$C for 3 h prior to CO_2 hydrogenation.

4. CO_2 hydrogenation was carried out at 220 $^{\circ}$C and 1 atm total pressure in flowing 8.80% CO_2 in H_2.

5. The effluent was analyzed using gas chromatography technique. [Thermal conductivity detector (TDC) was used for separation of carbon monoxide (CO) and methane (CH_4) and flame ionization detector (FID) were used for separation of light hydrocarbon such as methane (CH_4), ethane (C_2H_6), propane (C_3H_8), etc. In all cases, steady-state was reached within 6 h.
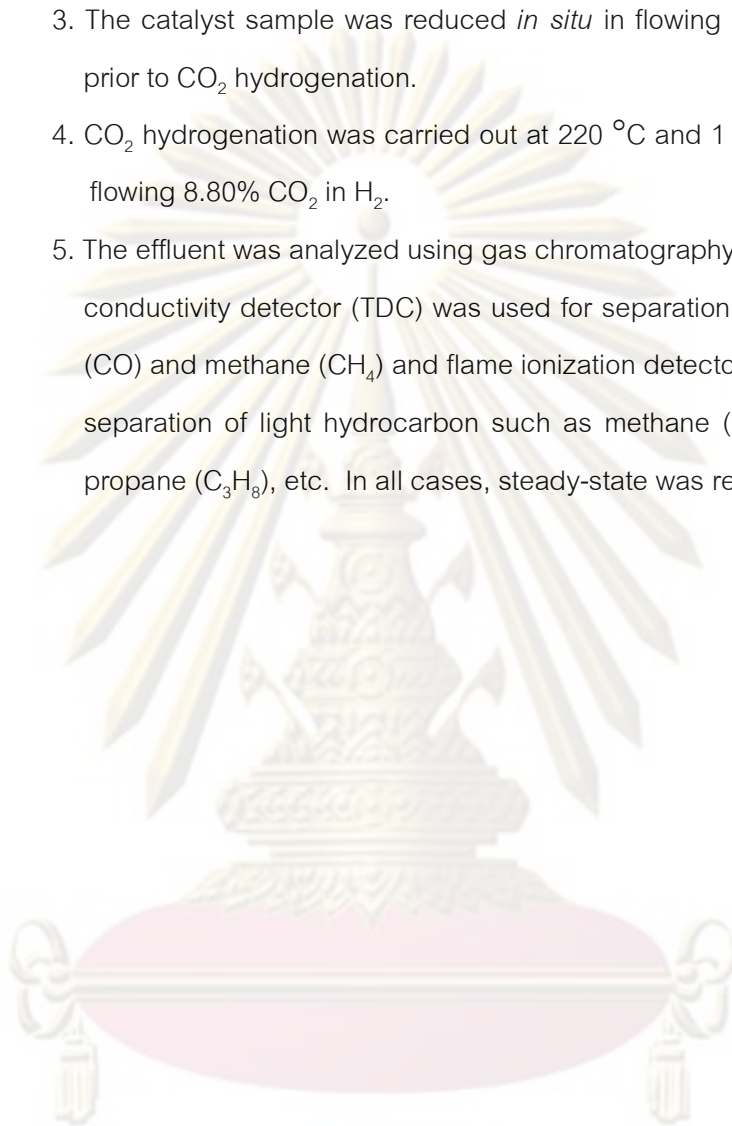
Table 4.1 Operating condition for gas chromatograph

Gas Chromagraph	SHIMADZU GC-8A	SHIMADZU GC-14B
Detector	TCD	FID
Column	Porapak Q	VZ10
- Column material	SUS	-
- Length	2 m	-
- Outer diameter	4 mm	-
- Inner diameter	3 mm	-
- Mesh range	60/80	60/80
- Maximum temperature	350 °C	80 °C
Carrier gas	He (99.999%)	H_2 (99.999%)
Carrier gas flow	40 cc/min	-
Column gas	He (99.999%)	Air, H_2
Column gas flow	40 cc/min	-
Column temperature		
- initial (°C)	60	70
- final (°C)	60	70
Injector temperature (°C)	100	100
Detector temperature (°C)	100	150
Current (mA)	80	-
Analysed gas	Ar, CO_2, H_2	Hydrocarbon C_1-C_4
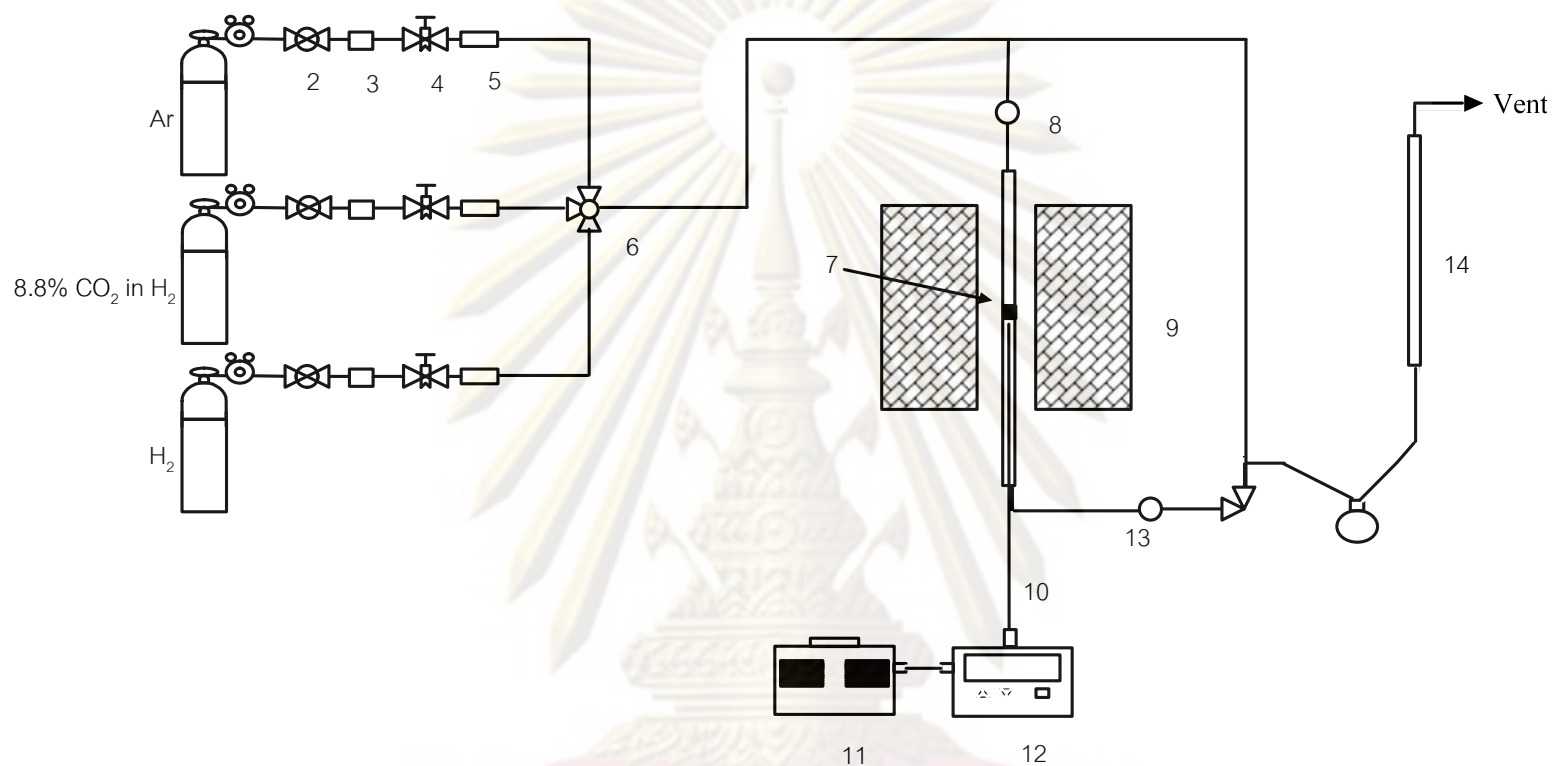
1. Pressure Regulator   2. On-Off Value   3. Gas Filter   4. Metering Valve

5. Back Pressure   6. 3-way Valve   7.Catalyst Bed   8. Sampling point

9. Furnace   10. Thermocouple   11. Variable Voltage Transformer   12. Temperature Controller

13. Heating Line   14. Bubble Flow Meter

Figure 4.1 Flow diagram of CO_2 hydrogenation system

CHAPTER V

RESULTS AND DISCUSSION

This chapter is divided into two sections: 5.1) the study of mesoporous titania form acid catalyzed-TiC and 5.2) Comparison of catalytic activity between Co-catalyst on prepared-TiO_2, with and without ruthenium promoted, with commercial grade TiO_2 (Degussa-P25). For CO_2 hydrogenation, 20wt% Co loading was used and carried out at 220°C and 1 atm, $CO_2/H_2/Ar$ = 20/2/8.

For catalyst characterization, the catalysts were characterized by several techniques i.e. TG/DTA, XRD, BET, TCD, SEM, TEM, TPR, ICP, CO-pulse chemisorptions, Raman spectroscopy and XPS.

5.1 The study of mesoporous titania synthesis from acid catalyzed-TiC

5.1.1 Characterization of TG/DTA

When the prepared-TiO_2 at for 0, 4, 8, 24, 48 and 72 h with 5 M HNO_3 at 70 °C were completely calcined, the samples were first characterized with TGA/DTA technique. The TGA/DTA curves of TiC precursor are shown in **Figure 5.1** indicating that the TiC weight increased approximately about 30% (theoretical value), which was in a good agreement with the exact value about 28%, corresponding with TiC oxidation diagram in **Scheme 5.1**.

$$TiC + 2O_2 \rightarrow TiO_2 + CO_2$$
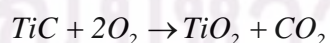
Scheme 5.1 The oxidizing reaction of TiC presurcor
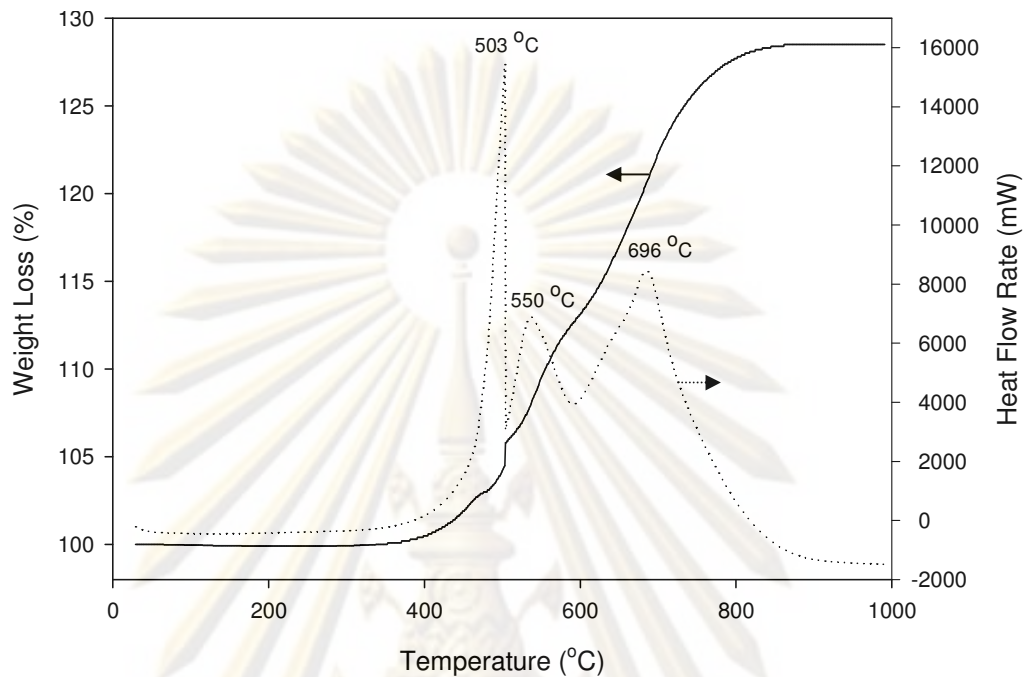
Figure 5.1 TG/DTA curve of the TiC precursor (without reaction)

The exothermic oxidation initially took place from 400 °C and completely oxidized at 850 °C. It is divided into three regions, 400-520 °C, 520-600 °C and 600-850 °C. These three regions correspond roughly to the DTA results from Shen *et al*. (2006) and Shimada and Mochdsuki (2004). They investigated the oxidation behavior of TiC in dry oxygen, wet oxygen and water vapor and prepared carbon doped anatse TiO_2 obtained from TiC. Shimada *et al*. (1996, 2004) also proposed the oxidation mechanism of TiC that was oxidized to oxycarbide (TiC_xO_{1-x}) followed by titanium suboxides, such as TiO, Ti_3O_5 or Ti_4O_9, which produced the heat and CO_2 evolved in a first stage. Then, the oxidation at stages 2 and 3 were related to the transformation of anatase and rutile phase, respectively. The schematic diagram of TiC oxidizing reaction is shown in **Scheme 5.2** as follow:

$$TiC \xrightarrow{\text{300-450 }^\circ\text{C}} TiC_xO_{1-x} \xrightarrow{\text{450-550 }^\circ\text{C}} TiO_2 \xrightarrow{\text{> 550 }^\circ\text{C}} TiO_2$$

Titanium suboxide   Anatase   Rutile
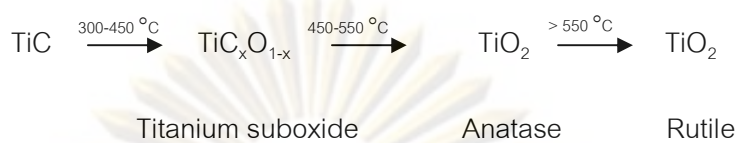
Scheme 5.2 The transformation diagram from TiC to TiO_2. (Shen, 2006, Shimada, 2004)

.

On contrary, the TGA/DTA curves of samples after 8 h as shown in **Figures 5.2 and 5.3**, the TiC precursor was already oxidized to TiO_2. The TGA/DTA show the weight lost around 15-20%, mainly from removal of the physisorbed water and the decomposition of acid species around 230 °C. It was observed that their weights were constant after around 400 °C due to the energy used to transform from amorphous-TiO_2 to anatase TiO_2 and from the anatase to the rutile one at 375 °C and 550 °C, respectively (Rajesh, 2008).
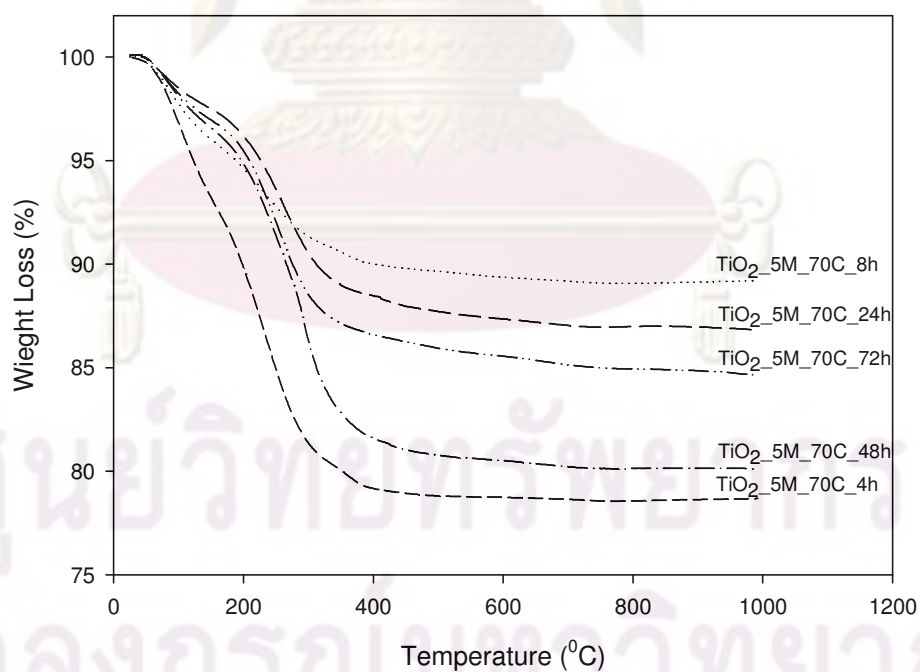
Figure 5.2 TGA curves of the oxidized-TiC for various reaction times.
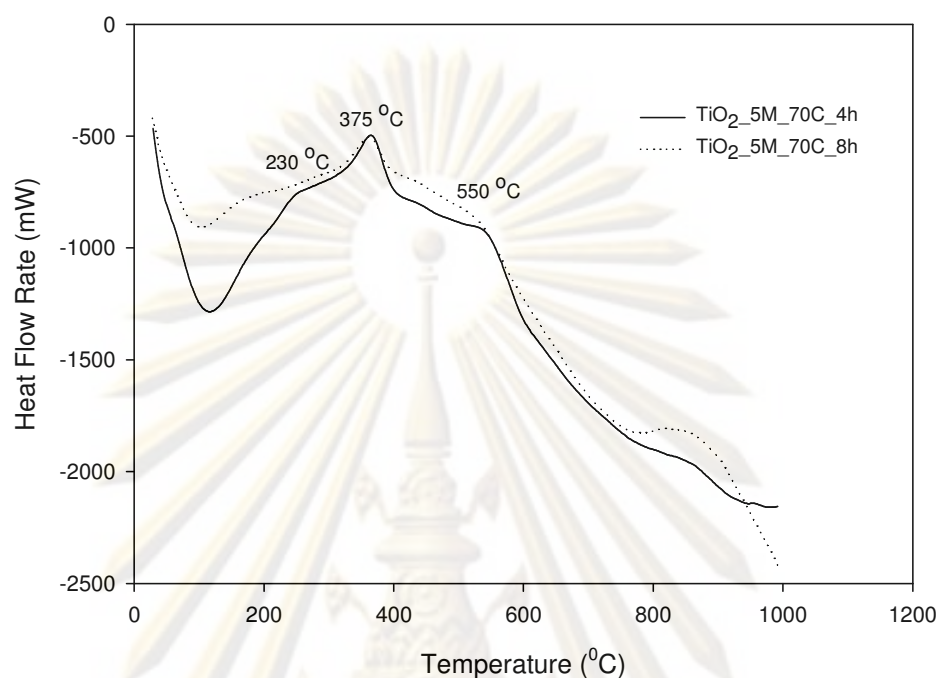
Figure 5.3 DTA curve of the oxidized-TiC for 4 h and 8 h

5.1.2 Characterization by XRD

Based on the XRD patterns in **Figure 5.4**, the mixed phase TiO_2 was simultaneously produced during the oxidation reaction. It showed that the TiC precursor was completely oxidized to mixed phase TiO_2 (45% anatase) after 8 h. After that, anatase phase was transformed the rutile one around 48 h. The calculated crystallite size based on Debye-Scherrer equation for all prepared TiO_2 is approximately 3.7 nm. The anatase phase content and crystallite size were shown in **Table 5.1**. Shieh *et al*. (2007) proposed that the formation of TiO_2 through the reaction of TiC with aqueous nitric acid (5 M) at 70 °C is unique. No TiO_2 was generated with the reactions of TiC using other oxidizing agents, i.e. HCl, H_2SO_4, H_3PO_4, $KMnO_4$, $K_2Cr_2O_7$, $Na_2S_2O_7$, Na_2CrO_4 (5 M aqueous solutions) and H_2O_2 (30%). The formation of the TiO_2 mesoporous structure is likely caused by mesopore-

etching of TiC particles and transformation of TiC pore walls into TiO_2 by HNO_3. Instead, TiC is probably transformed by HNO_3 into Ti_mX_n species which further hydrolyzes and condenses to form the amorphous TiO_2. The schematic of TiO_2 formation diagram is shown in **Scheme 5.3**.
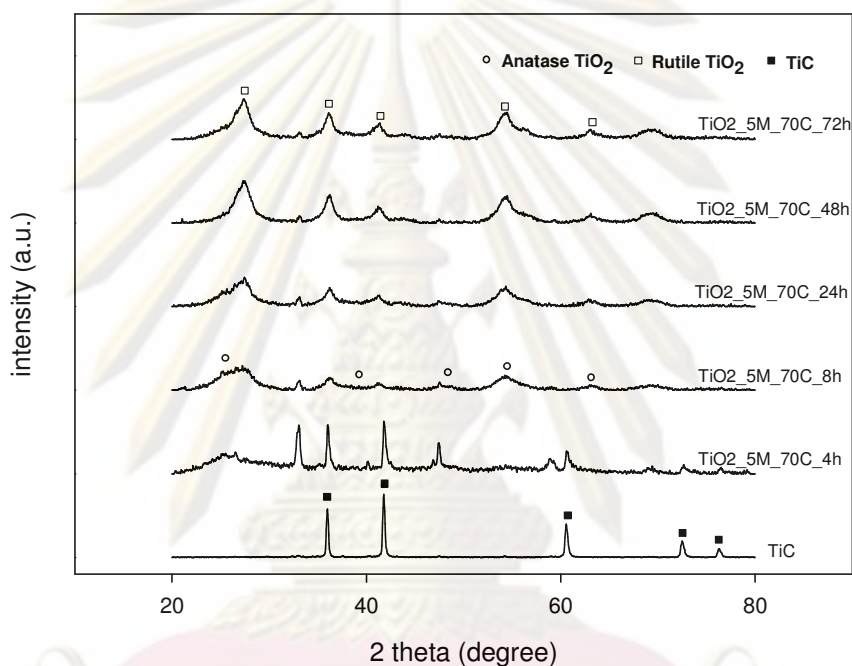
Figure 5.4 XRD patterns of oxidized-TiC for various reaction times
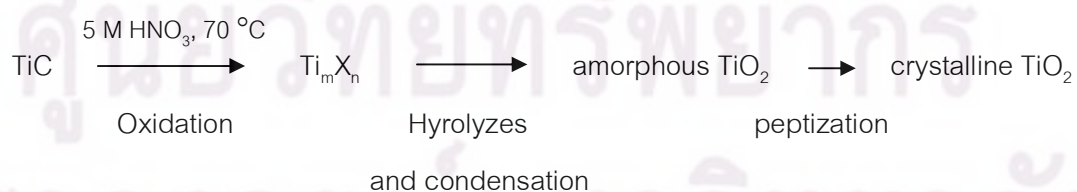
Scheme 5.3 The TiO_2 formation diagram from TiC oxidation follows by peptization process

Table 5.1 Characteristics of Degassa P25, TiC and TiO_2 obtained from TiC at different conditions

Sample	%Anatase	d_{xrd}^a (nm)	BET surface area (m^2/g)	Pore size (nm)	Pore volume (cm^3/g)	Carbon Content (%)
Degussa P-25	100	21.5	59	8.74	0.146	1.07
TiC	n.o.	200.0	4	17.22	0.006	16.42
TiO$_2$_5M_70C_4h	n.o.	n.o.	181	3.82	0.120	9.14
TiO$_2$_5M_70C_8h	45	3.5	306	3.78	0.239	3.80
TiO$_2$_5M_70C_24h	34	3.9	248	3.55	0.194	3.42
TiO$_2$_5M_70C_48h	0	3.9	163	5.33	0.129	3.12
TiO$_2$_5M_70C_72h	0	3.6	205	4.46	0.151	2.94

^{a} calculated by Debye-Scherrer equation.

5.1.3 BET surface area

The pore size, pore volume and BET surface area of TiC precursor, Degussa TiO_2 (P25) and all calcined samples are summarized in **Table 5.1**. At 8 h, the obtained mixed phase TiO_2 showed the highest pore volume and BET surface area at 0.239 cm^{3}g^{-1} and 306 m^{2}g^{-1}, respectively while the pure rutile TiO_2, which was obtained after 48 h, showed lower pore volume and BET surface area at 0.129 cm^{3}g^{-1} and 163 m^{2}g^{-1}, respectively. The N$_2$ adsorption/desorption isotherms are shown in **Figure 5.5**. The isotherm alteration from type-III isotherm (nonporous or macroporous material) of TiO_2-P25 to mesoporous type-IV isotherm with a hysteresis loop revealed a typical shape of network pores, at 8 h and a little hysteresis loop at 24 h. After that, it gradually changed back to nonporous type-II isotherm at 48 and 72 h with 100% of rutile phase. The pore size

distribution of all prepared samples is shown in **Figure 5.6** and it was found that all samples have pore size around 3-4 nm within the mesoporous scale.
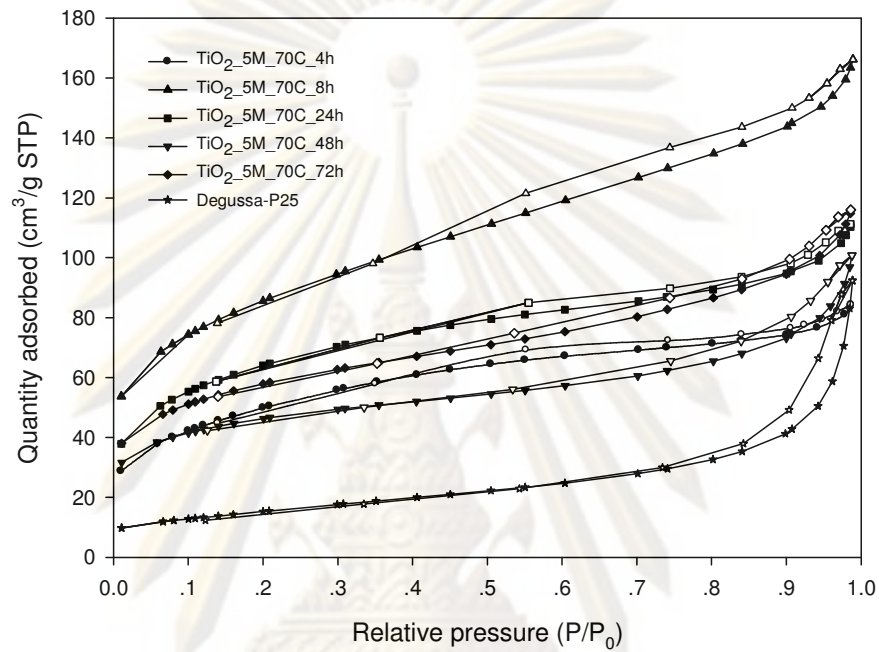
Figure 5.5 N_2 adsorption/desorption isotherms of oxidized-TiC with 5 M HNO_3 at 70 °C for various reaction times
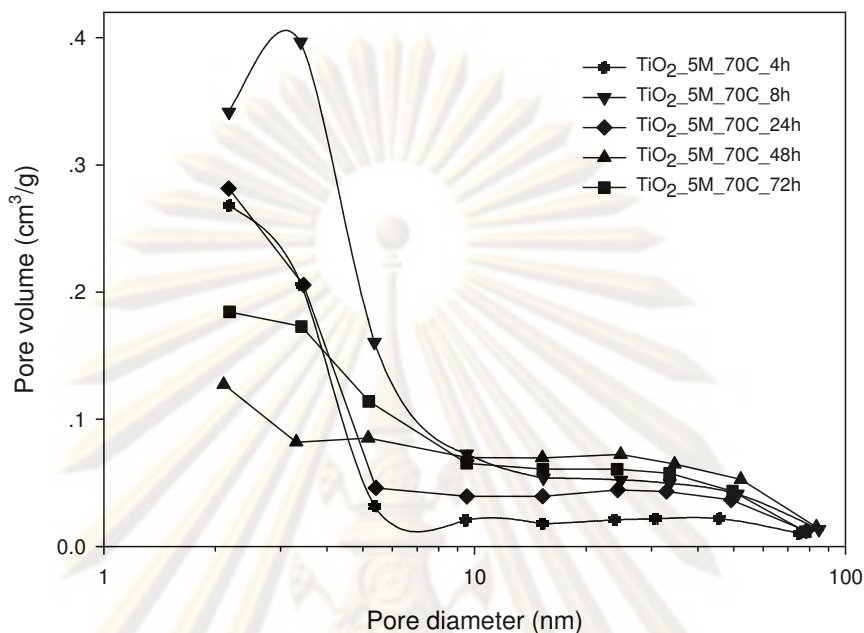
Figure 5.6 Pore size distributions of oxidized-TiC with 5 M HNO_3 at 70 °C for various

reaction times

5.1.4 Carbon content

In the early period with 8 h, the carbon content dramatically decreased perhaps due to the extreme oxidation of the carbon with aqueous nitric solution (gas from the oxidation reaction can be detected in the initial stage). Slow oxidation of the carbon after 8 h affected the amount of carbon gradually decreased with the values around 3.80% at 8 h to 2.94% at 72 h as shown in **Figure 5.7**.
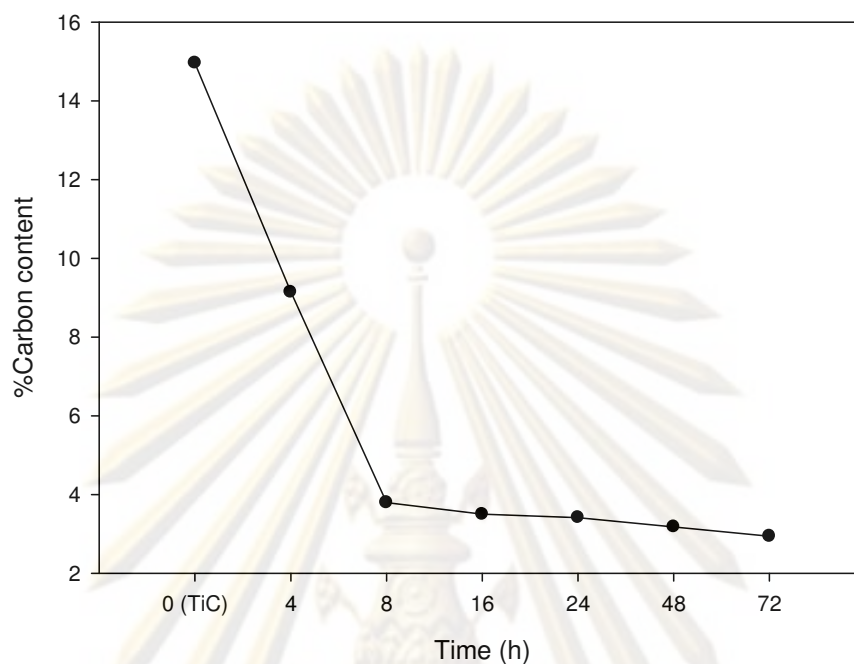
Figure 5.7 %Carbon content of oxidized TiC with 5 M HNO_3 at 70 °C at various reaction

    times.

5.1.5 SEM and TEM

    The effect of reaction time on the morphology for all prepared TiO_2 was studied by SEM and TEM techniques. **Figure 5.8** shows the SEM micrographs of TiC precursor (a) and prepared TiO_2 at 8 h (b). **Figure 5.8**-(a) image displays a particle size of TiC that is less than 10 um with smooth surface and sharp edges, clearly seen from the larger particle. In **Figure 5.8**-(b), the primary particles within nanocrystallite size, were agglomerated to form secondary particles with quite spherical shape with ca. 28 um, rough surface and without sharp edges. The morphology of prepared TiO_2 particles was also examined by TEM which was depicted in **Figure 5.9** (a–c). As shown in the TEM images, tiny crystals as well as clusters composed of a number of very fine crystals were seen after

the 8 h (5.9-a), which consisted of anatase (~4 nm with quite spherical shape) and the rutile phase with quite rod-like shape. At 48 (**Figure 5.9**-b), the rod-like shape of prepared TiO_2 was observed, and then at 72 h the more tiny fine crystalline of prepared rutile TiO_2 was evident (5.9-c), corresponding to the XRD results as mentioned before

5.1.6 Effect of acid concentration and reaction temperature

When either the acid concentration or reaction temperature was increased, phase transformation from anatase phase to rutile one was accelerated. This can be observed from ratio of anatase phase decreased to 0% and 40% with 9 M HNO_3 and 80 °C for 24 h. While both of the crystallite size and pore size were approximately similar with increased reaction parameters. With strong acidity and high reaction temperature, the mesoporous structure was also accelerated to collapse during oxidation process, resulting in decreased pore volume and BET surface area. From the summarized data in **Table 5.2**, pore volume and BET surface area of prepared TiO_2 with 9 M HNO_3 at 70 °C for 24 h were reduced from 248 m^2g^{-1} to 131 m^2g^{-1} and 0.194 cm^3g^{-1} to 0.086 cm^3g^{-1}, respectively. Considering at high reaction temperature, the prepared TiO_2 lost its pore volume at 100 °C with 5 M HNO_3 for 24 h. The BET surface area decreased with increasing reaction temperature.
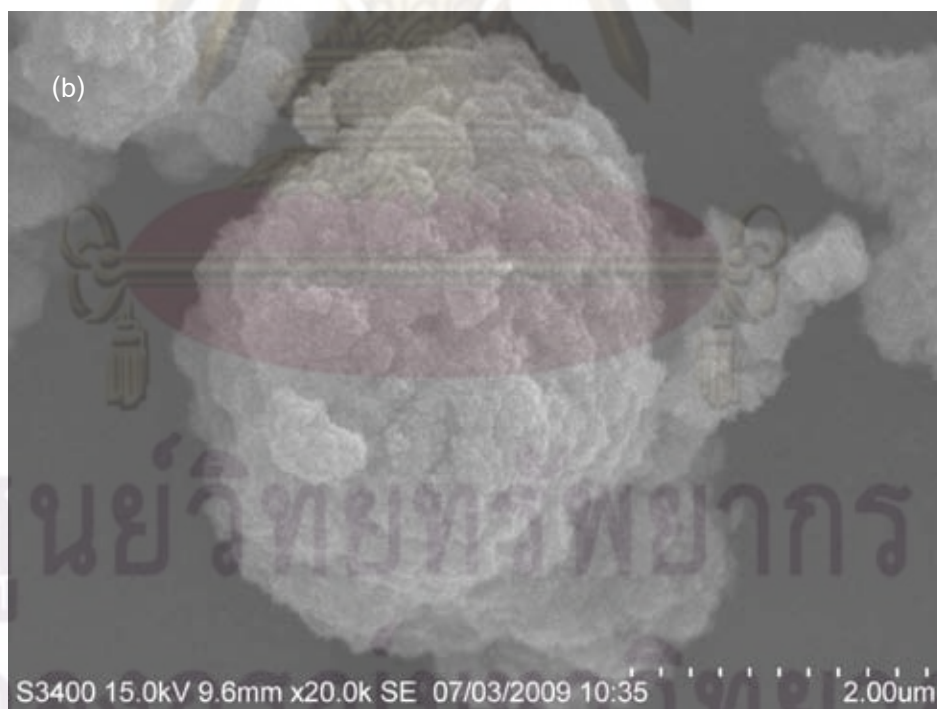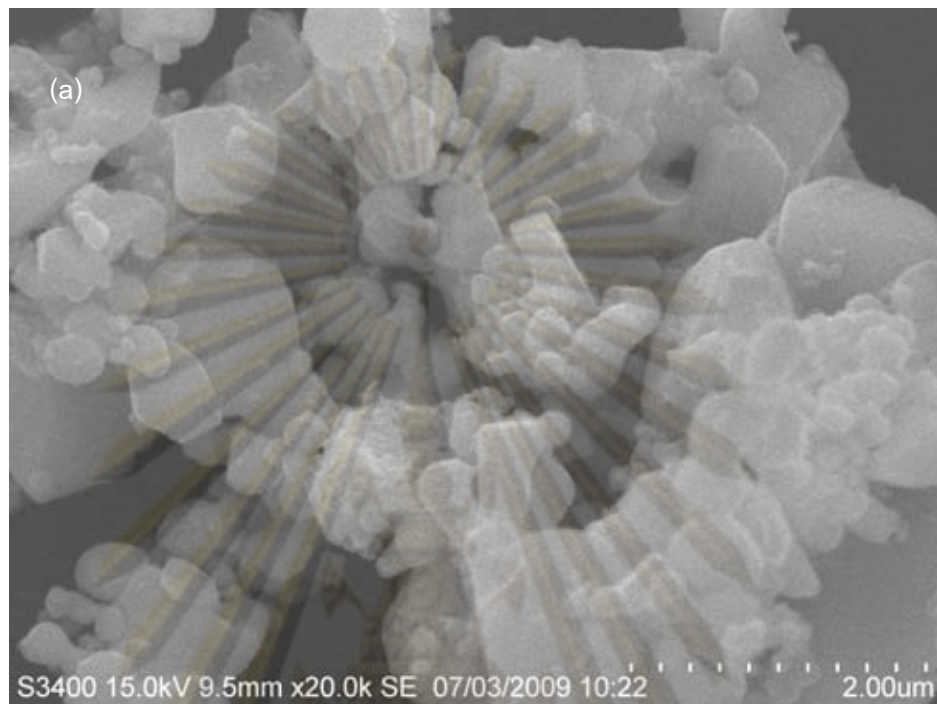
Figure 5.8 SEM images of TiC precursor (a) and the TiO$_2$_5M_70C_8h (b)
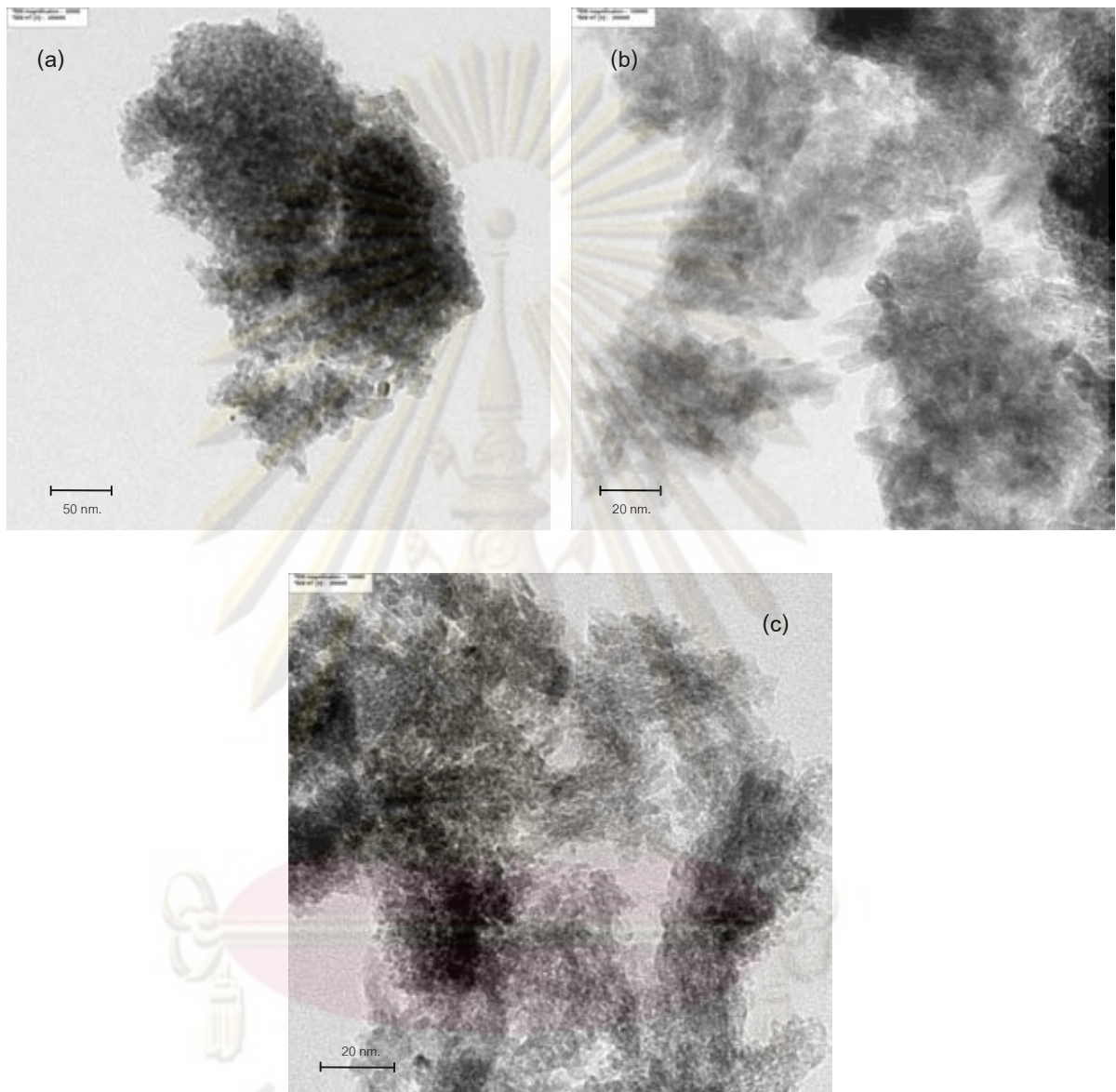
Figure 5.9 TEM images of the TiO$_2$_5M_ 70C_8h (a), TiO2_5M_ 70C_48h (b)

and TiO$_2$_5M_70C_72h (c)

Table 5.2 Phase composition, crystalline size (d_{xrd}), total pore volume, BET surface area and

of oxidized TiC when increase acid concentration and reaction temperature

Sample	%Anatase	d_{xrd} ^{a} (nm)	BET surface area (m^2/g)	Pore size (nm)	Pore volume (cm^3/g)
TiO$_2$_9M_70C_24h	0	3.1	131	4.25	0.086
TiO$_2$_9M_70C_48h	0	3.5	160	5.31	0.129
TiO$_2$_5M_80C_24h	40	4.0	185	3.82	0.138
TiO$_2$_9M_100C_24h	35	4.4	152	4.02	0.122

^{a} calculated by Debye-Scherrer equation.

5.1.7 Peptization process

After the amorphous TiO$_2$ has been generated, it still holds in acid condition waiting for TiC to be completely oxidized. Peptization process could be adopted to explain the effect of reaction time, concentration of peptizing agent (5 M HNO$_3$), and reaction temperature. Peptization is a process to redisperse a coagulated colloid by electrostatic force. When an acid is added to TiO$_2$ precipitates, the TiO$_2$ particles dissolve and recrystallize into anatase or rutile phase as a function of peptization temperature (Jung, 2004). It involves three possible processes that could occur simultaneously: (i) agglomerates break down into particles of colloidal dimensions by providing chemical, thermal or mechanical energies, (ii) particle charging by proton adsorption, which in turn stabilizes the suspension through electrostatic repulsion and (iii) particle reagglomeration may occur as a consequence of incomplete peptization. Bacsa et al. (2005) reported an improvement of the anatase-to-rutile phase transformation by peptizing the hydrolyzed precipitates with nitric acid; however, the l00% rutile phase was not obtained. Bischoff and

Anderson (Bischoff, 1995) found that acid peptization of TiO_2 particles favored the formation of rutile, in comparison with the situation that occurred at higher temperatures. It is generally accepted that the adsorption of protons on the surface of hydrous TiO_2 particles creates a net positive charge, and thus yields an electrostatically stabilized sol during acid peptization. However, this adsorption model of peptization cannot explain why the rutile phase forms after peptization at a low temperature. Moreover, Yang *et al.* (2000, 2005) prepared rutile rod-like particle by hydrothermal method using HNO_3 peptization. They found that when HNO_3 was added to the amorphous titania, deoxolation could possibly occur via **Scheme 5.4**.
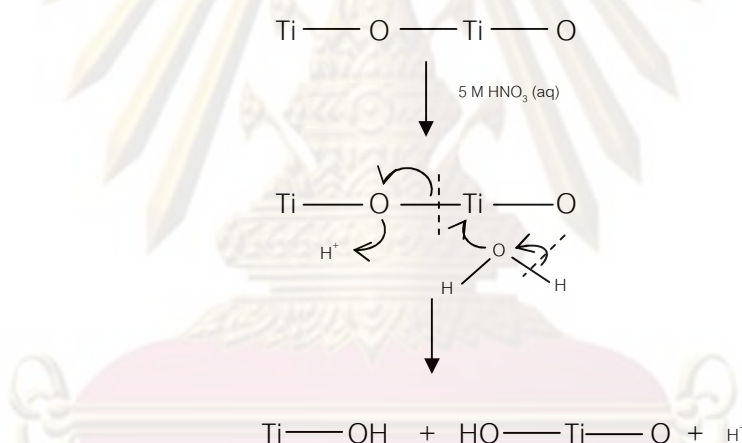
Scheme 5.4 Redrawn of the deoxolation process of peptizing titanium dioxize based on Yang et al. (2000, 2005)

Its electrophilic proton (H^+) will attack the oxygen atom between two titanium atoms, making it more electrophilic. Thus, the titanium atom becomes more able to attract the electron density from the O atom in H_2O and break the oxolation bonds $\equiv$Ti-O-Ti$\equiv$ to form HO-Ti$\equiv$. The reduction in number of oxolation bonds among titanium atoms lowered

the agglomerate degree and finally peptized the amorphous precipitate. The particles obtained by drying the sol exhibit the XRD patterns both of the anatase and the rutile phase. This indicates that edge-shared bonding among the $[TiO_6]$ octahedral as a typical feature of anatase is dominant in the $[TiO_6]$ octahedral arrangement and that a few corner-shared bondings of $[TiO_6]$ octahedral typical of the rutile phase have also been formed as well with increasing reaction time or acidity (H^+ concentration), corresponding to the work of Zhang and Gao (2001). They investigated the effect of peptization process on phase transformation of TiO_2 nanoparticles, more oxolation bonds among titanium atoms were broken and produced more OH groups around a single titanium atom, which facilitated the movement of the titanium atom, which had been confined to its adjacent neighbors before peptization. Condensations among titania hydrates could take place among several titanium species, leading to structural rearrangements towards the formation of corner-shared octahedral chains characteristic of the rutile phase. As a matter of fact, XRD patterns of the peptized samples with 8 h reaction time (5 M HNO_3 at 70 °C) indicated that the as-formed powder is the anatase and rutile phase. Matijevic *et al*. (1981) found that raising the temperature of an acidified solution containing metal ions could lead to a forced hydrolysis .The first step in this process is a rapid nucleation. Therefore, crystallization could result in the formation of a metastable polymorph. Moreover, Bischoff and Anderson (1995) demonstrated the high acid peptization results in an increase the solubility of titania. The most likely material to dissolve is the amorphous titania. The acid increases the solubility of titania, but the slow crystallization at low temperature yields the more stable rutile form.

5.2 Comparison of catalytic activity between Co-catalyst on prepared-TiO$_2$, with and without ruthenium promoted, with commercial grade TiO$_2$ (Degussa-P25).

The reaction study was carried out in CO$_2$ hydrogenation to determine the overall activity of the catalyst samples. First, the catalysts were reduced in H$_2$ at 350 °C for 3 h in a fixed-bed flow reactor. Then, the reaction test was carried out with flow rate of H$_2$/CO$_2$/Ar = 20/2/8 cm^3/min.

5.2.1 Characterization by XRD

The bulk crystalline phases of samples were determined using XRD technique. XRD patterns of the Co-catalysts are shown in **Figure 5.10**. They strong diffraction peaks at 25.4°, 38.0°, 48.0°, 54.0°, 55.1°, 62.8°, and 70.0° indicating the TiO$_2$ in the anatase phase as well as at 27.5°, 38.0°, 42.0°, 54.5°, and 55.8° were matched with the rutile phase. The strong peaks at 31.8°, 37.5°, 45.3°, and 65.3° corresponded with Co$_3$O$_4$. The XRD peaks of CoTiO3 along with Co$_3$O$_4$ on the Co/TiO$_2$ catalyst at 23°, 32°, 35°, 49°, 52°, 62° and 64° were not observed (Kraum, 1999). For ruthenium- promoted support, the ruthenium identify patterns were not observed because of very low amount of ruthenium concentration (0.5 %wt). The XRD patterns of used catalysts are exhibited in **Figure 5.11**, it was found that, for ruthenium-support promoted catalyst, support crystallite structures were still remained after the reaction.

Table 5.3 summarizes the crystalline size of supports (2θ~25° with anatase and 2θ~27° with rutile phase) and Co$_3$O$_4$ (2θ~36.8°) calculated by using the Debye-Scherrer equation. The crystallite sizes of Co$_3$O$_4$ on both of with Ru-promoted support and without Ru-promoted supports for Co-catalysts decreased with decreasing support pore diameter and the crystalline size (Borg, 2008). However, the Co$_3$O$_4$ crystalline sizes of Ru-promoted samples should be smaller than those of the un-promoted catalysts because Ru would enhance cobalt dispersion. In this study, the Co$_3$O$_4$ crystalline sizes might be

secondary particle and the second calcinations of catalysts resulted in growth crystallite size.
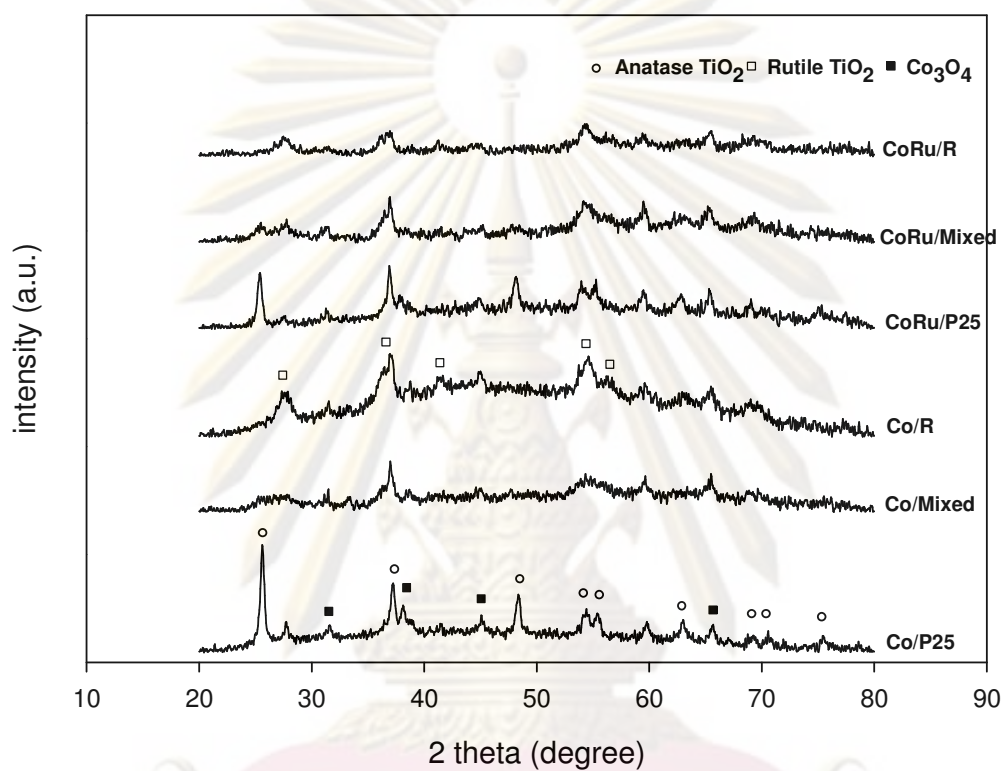
Figure 5.10 The XRD patterns of Co-catalysts before CO_2 hydrogenation.
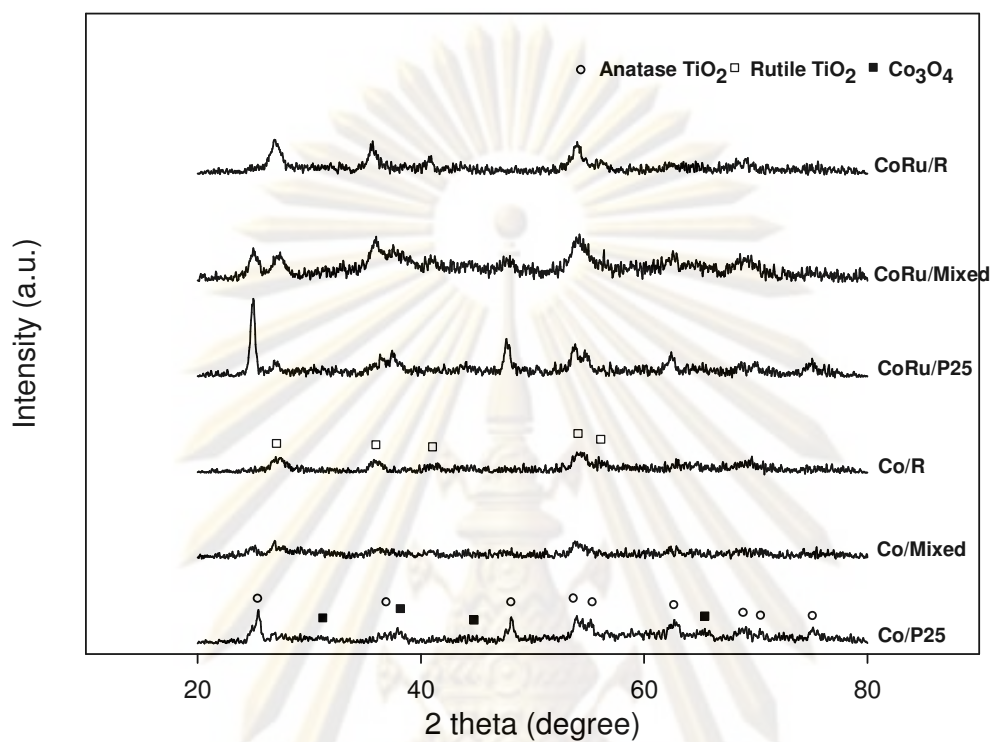
Figure 5.11 The XRD patterns of Co-catalysts after CO_2 hydrogenation.

Table 5.3 The crystallite size of TiO_2 and Co_3O_4 on Co-catalysts with various supports. (With Ru-promoted and without Ru-promoted)

Catalysts	Crystallite size (nm)	
	TiO_2	Co_3O_4
Co/P25	21.5	36.6
Co/Mixed	3.5	5.4
Co/R	3.9	5.2
CoRu/P25	n.d.	18.1
CoRu/Mixed	n.d.	11.0
CoRu/R	n.d.	10.8

5.2.2 BET surface area

BET surface areas of Co-catalysts are shown in **Table 5.4**. The surface areas and pore volume decreased in all catalysts, indicating that some pore blockage by cobalt oxide clusters occurred. **Figure 5.12** illustrates adsorption-desorption isotherms of cobalt on different supports. Only Co/Mixed catalyst still remained hysteresis loop which referred to mesoporous framework. For promoted catalysts, the thermal treatment after impregnation (calcinations) affected to dramatically decreasing of surface area because of the collapse of mesoporous frameworks. **Figure 5.13** shows the pore size distribution of Co-catalysts. From this figure, it was observed that the pore sizes of Co/P25 and CoRu/P25 were larger than those of others. Impregnation, drying, calcination, and addition of Ru did not change pore size distribution of promoted and un-promoted catalysts, but reduced the nitrogen uptake.

Table 5.4 BET surface area, pore volume and pore sizes of the Co-catalysts.

Samples	Surface area (m^2/g)	Pore volume(cm^3/g)	Average pore size(nm)
Degussa-P25	59	0.15	8.7
Mixed	306	0.24	3.8
Rutile (R)	163	0.13	5.3
Co/P25	50	0.16	12.8
Co/Mixed	147	0.13	3.5
Co/R	117	0.11	3.7
CoRu/P25	46	0.19	16.8
CoRu/Mixed	71	0.09	5.4
CoRu/R	60	0.09	6.1
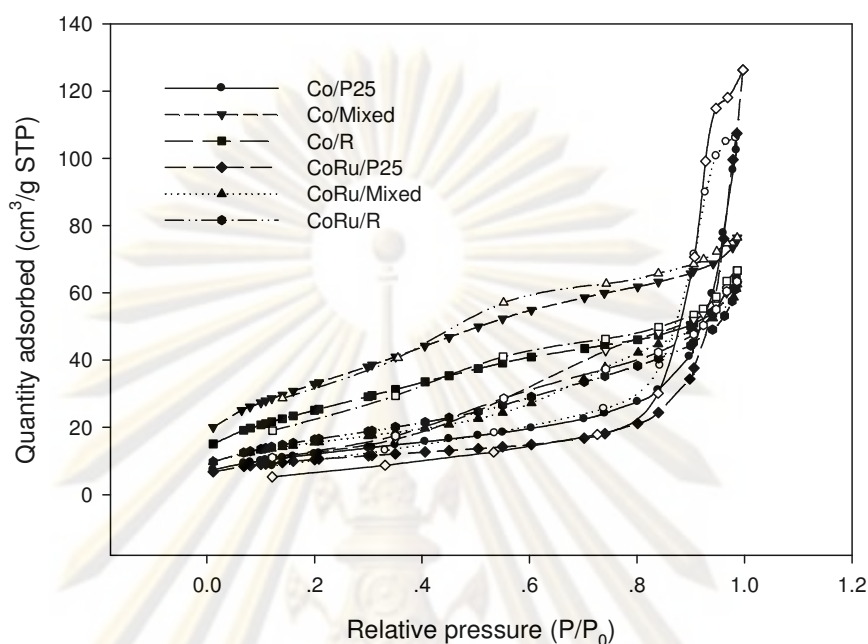
Figure 5.12 N_2 adsorption/desorption isotherms of the Co-catalysts on various supports with Ru-promoted and without Ru promoted.

5.2.3 Temperature programmed reduction analysis (TPR)

The TPR profiles of all Co-catalysts are given in **Figure 5.14**. The reduction temperature around 200-300 °C referred to reduction of residual cobalt nitrate remaining after calcination (Kogelbauer, 1996). For Co/P25 catalysts, Co_3O_4 was reduced to CoO around 331 °C and CoO to metallic Co around 430 °C. However, for Co/Mixed and Co/R, the both of temperatures in reduction steps were higher than those of Co/P25. It was due to the higher interaction between cobalt particles and the titania supports. Moreover, the reduction temperature around 500 °C correspond to the reduction of species being in chemical interaction with titania (cobalt titanate) (Michalak, 2009). For Ru-promoted catalysts, the reduction temperatures were lower than those unpromoted catalysts. It was found that ruthenium could decrease the reduction temperature of cobalt oxide (Jongsomjit,

2006). Nevertheless, the addition of ruthenium did not affect to the formation of cobalt titanate because the reduction temperature could be observed around 520 °C. Some of the Co strong interaction with the titanate ($Co_XO_Y–TiO_2$) can be reduced at lower temperature, besides; the Ru promotion can prevent the formation of the Co titanate. The low temperature peak indicates that the bond strength of Co–H_2 on these promoted catalysts was significantly weakened.
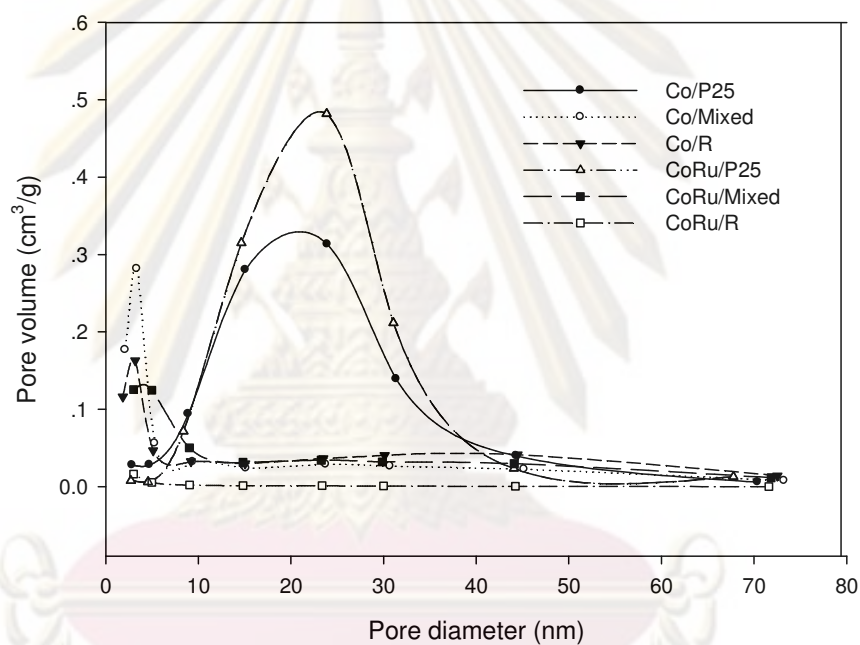
Figure 5.13 Pore size distributions of the Co-catalysts on various supports with Ru-promoted and without Ru-promoted.
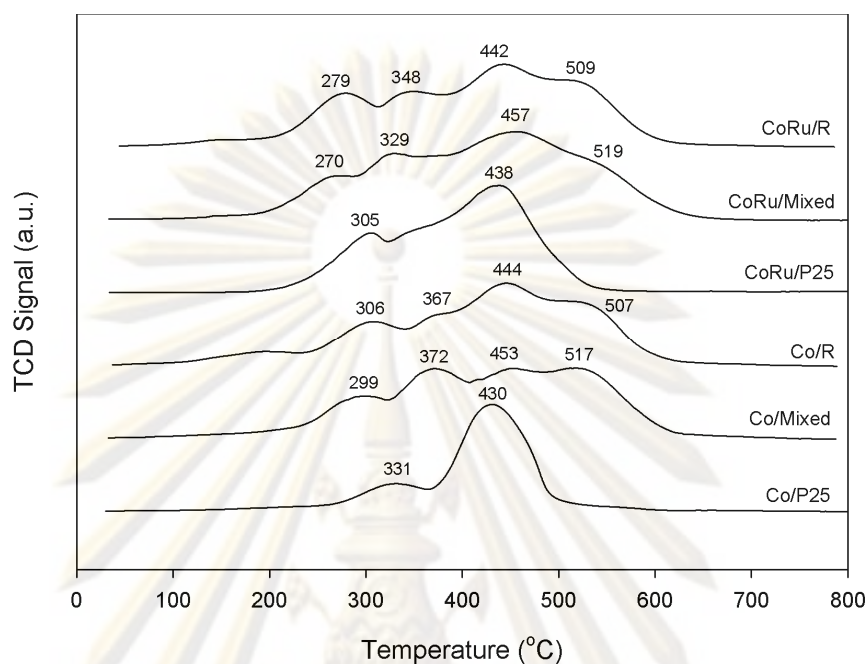
Figure 5.14 Reduction behaviors of the Co-catalysts.

5.2.4 SEM/EDX

Figures 5.15 and 5.16 show Ti and Co dispersion on the unpromoted and Ru-promoted Co-catalysts, respectively. From the ruthenium promoted effect, it reduced reduction temperature of cobalt oxide on the catalysts, which was corresponded to the above TPR results. It was found that all of the Co-catalysts exhibit similar dispersion of both Ti and Co, while the amount of Co metal on Ru-promoted Co-catalysts was brighter than that the unpromoted one. Therefore, the Ru-promoted Co-catalyst should present higher number of active sites. Ruthenium atom could not be detected with this technique because of very low concentration (<1%). The dispersion of ruthenium atom did not show in the figures.
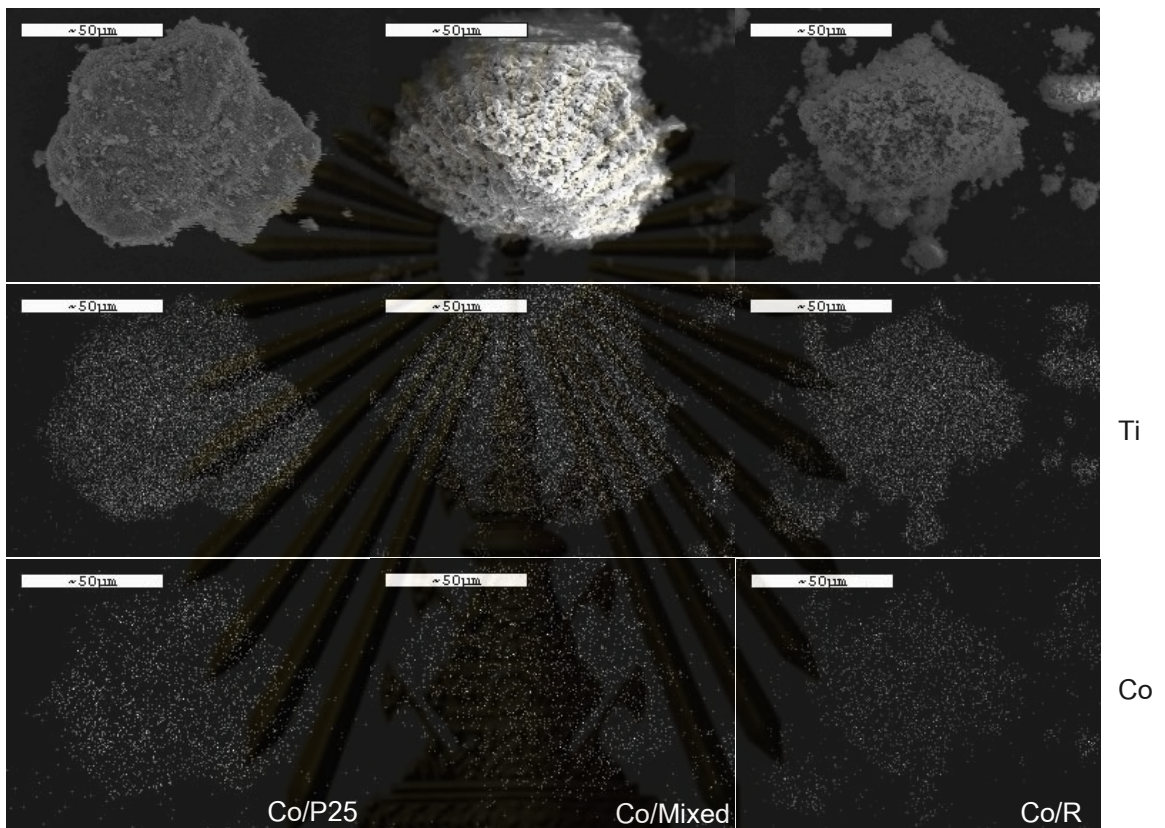
Figure 5.15 SEM/EDX images of the unpromoted Co-catalysts.
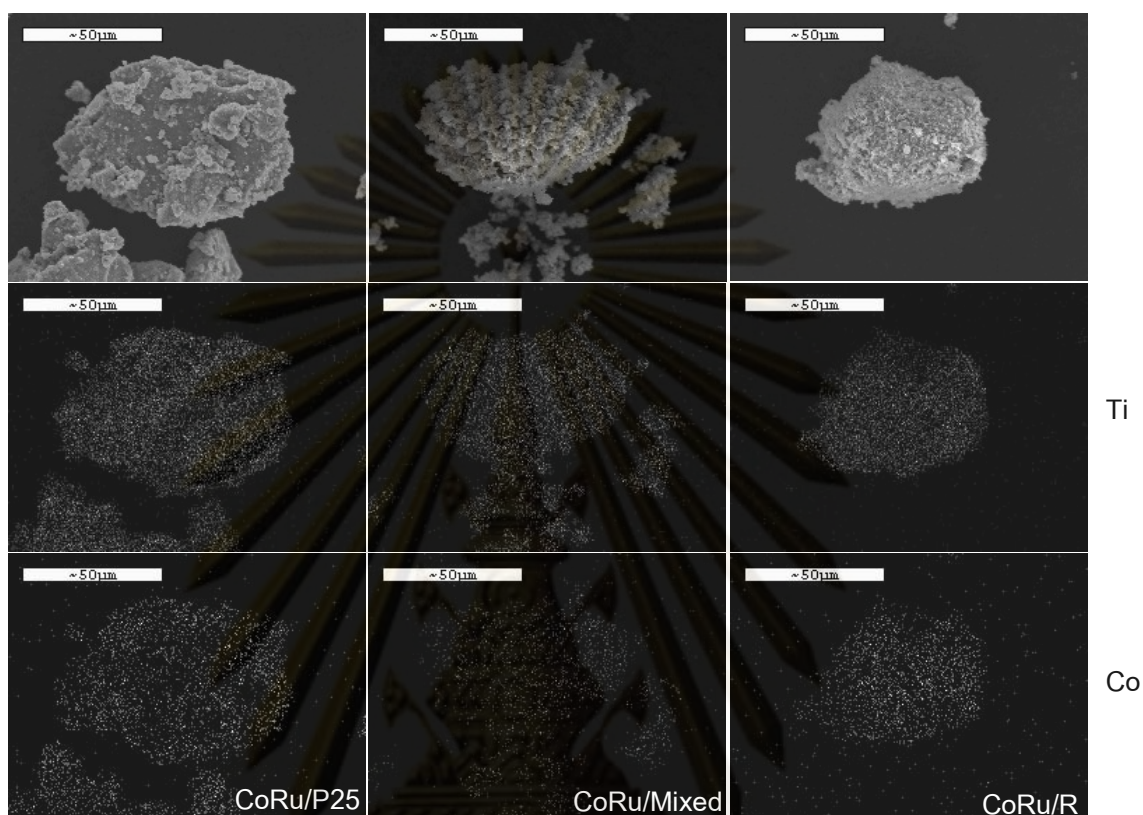
Figure 5.16 SEM/EDX images of the Ru-promoted Co-catalysts.

5.2.5 TEM

TEM micrographs of Ru-promoted and unpromoted Co-catalysts are shown in **Figures 5.17** and **5.18**, respectively. For cobalt catalysts, the dark spots represented cobalt oxide species dispersing on the different Co-catalysts. When the cobalt particles were compared with supports from the images, they were different from TiO_2 crystallite size. It was found that the dispersion of cobalt oxide species was good. The crystalline size of cobalt was very small (less than 10 nm) and agglomerated as the polycrystals. However, the cobalt particles on Ru-promoted and un-promoted catalysts shown in TEM observation appeared larger cobalt oxide granules.
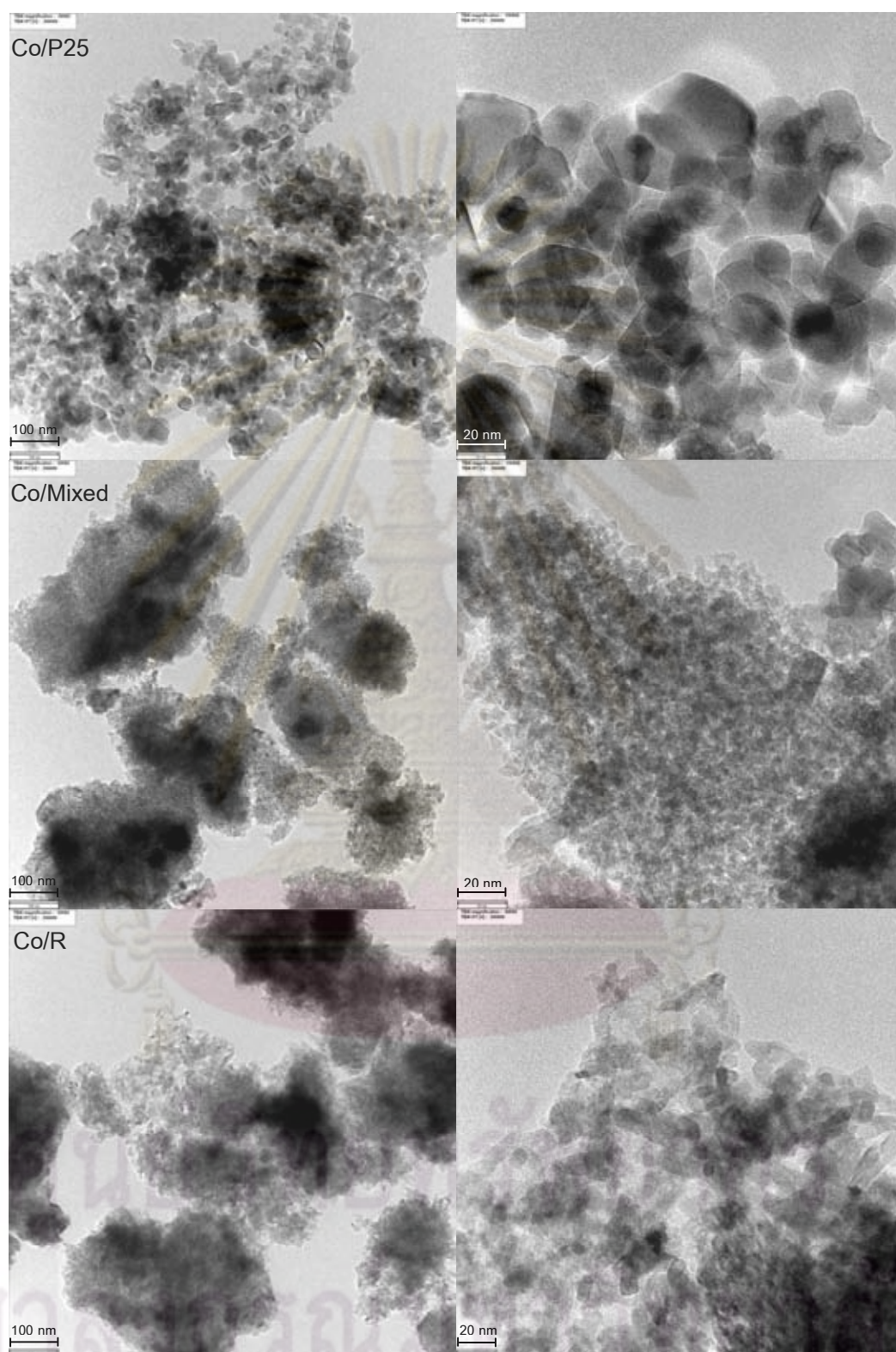
Figure 5.17 TEM images of unpromoted Co-catalysts.
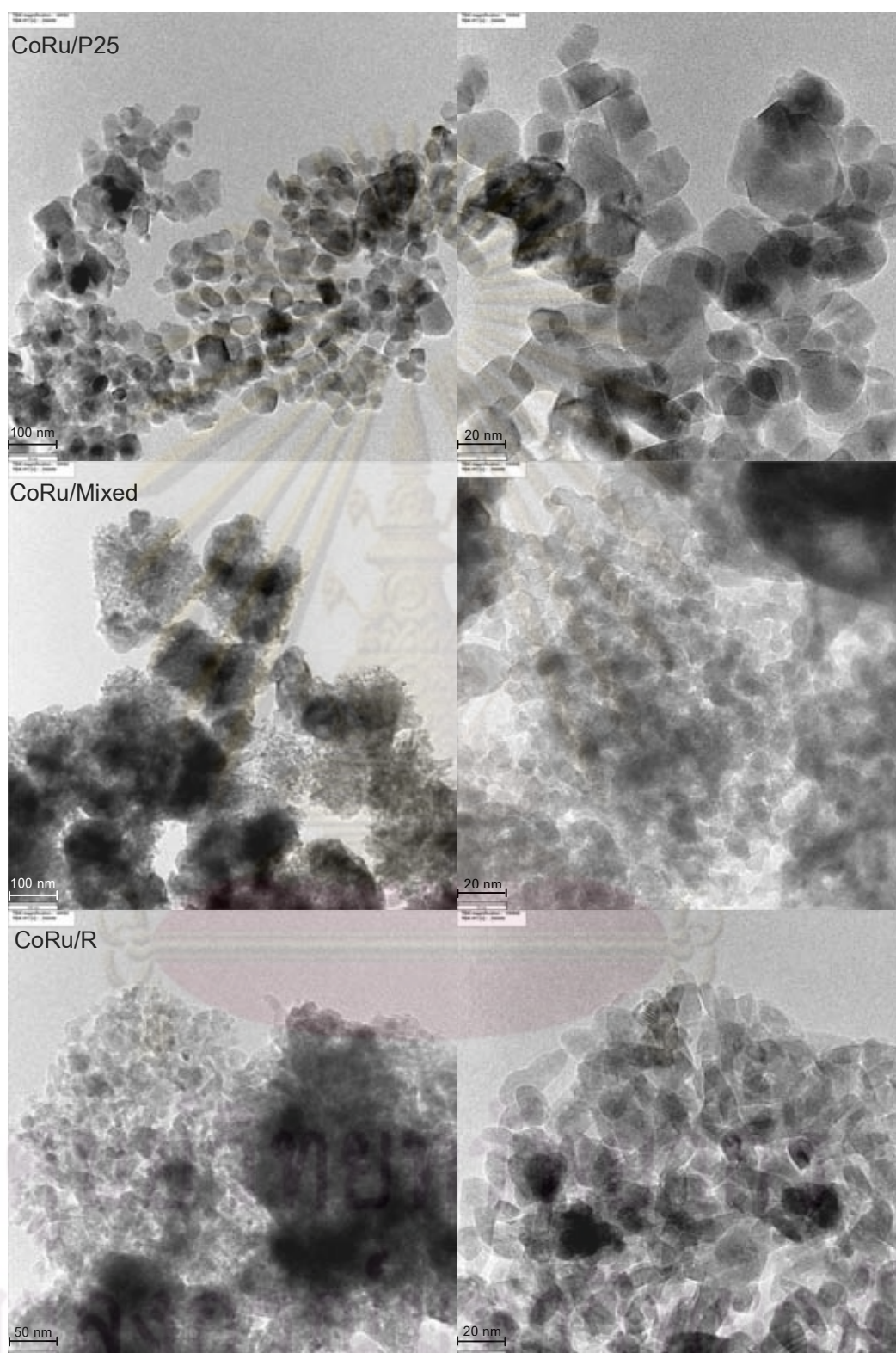
Figure 5.18 TEM images of Ru-promoted Co-catalysts.

5.2.6 CO-pulse chemisorptions

The characterization results of CO chemisorptions for the catalyst samples are illustrated in **Table 5.5**. Cobalt content of all catalysts was within the range of 19-21%wt. For the un-promoted cobalt catalysts, the Co/Mixed showed the highest number of active sites whereas Co/P25 and Co/R had the similar value. The mixed phases support could provide the dispersion of metal more than the pure phase. According to Jongsomjit *et al*. (2005), they found that the mixed phases between rutile (19%) and anatase (81%) could provide the highest dispersion of cobalt. Moreover, the number of active sites and the amount of CO uptake on catalytic phase of the Ru-promoted catalysts were higher than those in un-promoted catalysts due to spillover effect with Ru-promotion. In addition, it was found that the addition of ruthenium resulted in higher dispersion of cobalt on the support.

5.2.7 Carbon content

Figure 5.19 illustrates the carbon content of the TiC precursor, obtained support and all Co-catalysts, before and after CO_2 hydrogenation. It was found that, with unpromoted catalysts, both of Co/Mixed and Co/R have similar carbon level at 0.9%wt. In the past, the promoted catalysts were calcined at 500 °C. It resulted in decreasing carbon content compared to unpromoted catalysts. All of the promoted catalysts showed similar carbon content which closed to carbon content on Co/P25 catalysts (at 0.2-0.4%).

Table 5.5 Co content, active site, total CO-chemisorptions, %Co dispersion and active metal surface area of the Co-catalysts.

Sample	Co content[a] (%wt)	CO-pulse chemisorptions			
		Active site (x10^{-19} site/g.cat)	Total CO chemisorptions (μmol CO/g.cat)	% Co Dispersion	Active metal surface area (m^2/g.metal)
Co/P25	21.5	1.51	0.34	0.69	4.6
Co/Mixed	19.5	2.02	0.46	1.01	6.8
Co/R	17.3	1.12	0.24	0.63	4.3
CoRu/P25	21.4	1.83	0.47	0.83	5.6
CoRu/Mixed	21.0	3.12	0.81	1.46	9.8
CoRu/R	20.0	1.34	0.28	0.66	4.5

[a]= determined by ICP

Figure 5.19 The carbon content of all precursors and the Co-catalyst, before and after the reaction.

5.2.8 Raman spectroscopy

Raman spectra of Degussa-P25 and the Co-catalysts are shown in **Figure 5.20**. The Raman bands of CoTiO$_3$ exhibited bands at 695, 604, 455, 382, 336 and 266 cm^{-1} which are similar to the ones reported by Brik *et al*. (2001) and Jongsomjit *et al*. (2004) The strong Raman bands at 630, 504, and 389 cm^{-1} indicating the TiO$_2$ in its anatase phase (Brik, 2002) and at 235, 440 and 605 cm^{-1} indicating the TiO$_2$ in its rutile phase (Gole, 2008). The Raman spectrum of the Co-catalysts exhibited Raman bands at 630, 507, and 389 cm^{-1} as seen in those for TiO$_2$ including two shoulders at 685 and 476 cm^{-1}, assigned to Co$_3$O$_4$ (Jongsomjit, 2001, 2002, 2003). It indicated that "Co-titanate" was invisible in Raman spectroscopy. The invisible "Co-titanate" bands was probably caused by (i) its highly dispersed form and (ii) the Raman signals were hindered due to the highly strong Raman intensities of TiO$_2$ support.
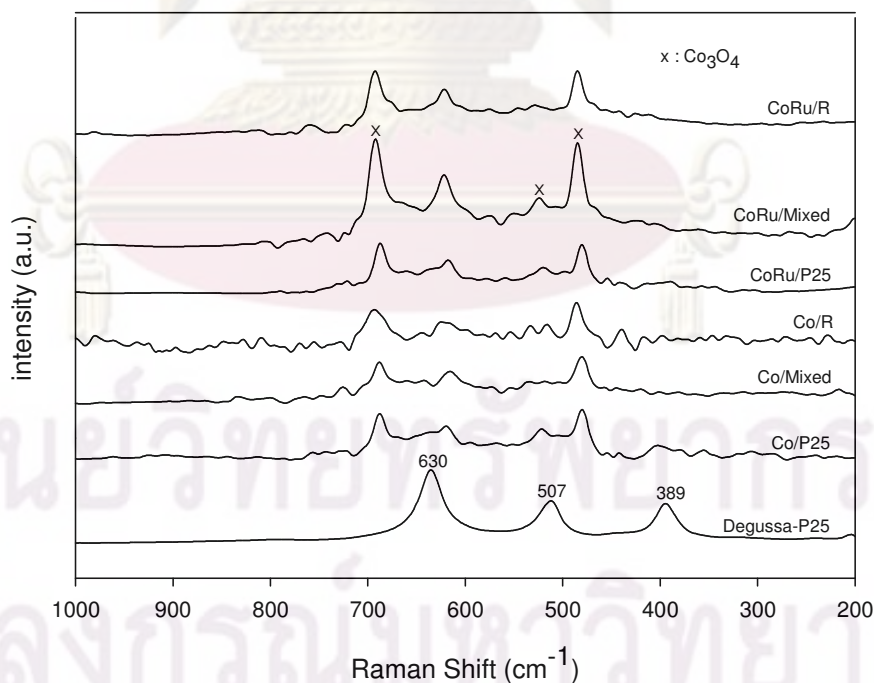
Figure 5.20 Raman spectroscopy results of the Co-catalysts.

5.2.9 XPS

XPS analysis was carried out to examine the surface species on the cobalt catalysts and also to determine the relative amount of element on the surface. The samples were analyzed in the Co 2p, Ti 2p, O 1s, and Ru3d with regards to the binding energy regions. For cobalt in an oxide state, the binding energies of Co $2p_{3/2}$ in catalysts reflect the total values for that of both Co_3O_4 and of surface phase (Zang, 2003). The peaks of Ru 3d would be detected around 280 eV. The binding energy values corresponding to Co 2p and Ti 2p were hardly affected by the small amount of Ru modification with the values at ∼780 eV and ∼459.1 eV, respectively. However, the binding energy of Ru could not be observed. The binding energy, the ratio of percentages of atomic concentration of Co $2p_{3/2}$ Ru and Ti 2s are also given in **Table 5.6**. The ratios of atomic concentrations of Co/Ti of Ru-modified supported catalysts were lower than those of unmodified supported catalysts, indicating that the addition of ruthenium resulted in higher dispersion of cobalt on supports (Pansaga, 2008). The binding energies of $Co2p_{3/2}$ for all catalysts were consistent with that of Co_3O_4. It revealed that interaction between cobalt species and support was similar. This observation was consonant with XRD patterns which showed the peaks of Co_3O_4 for all catalysts. The deconvoluted XPS spectra for the Co $2p_{3/2}$ core level region of cobalt catalysts on P25, Mixed, and R are shown in **Figures 5.21 to 5.22**.
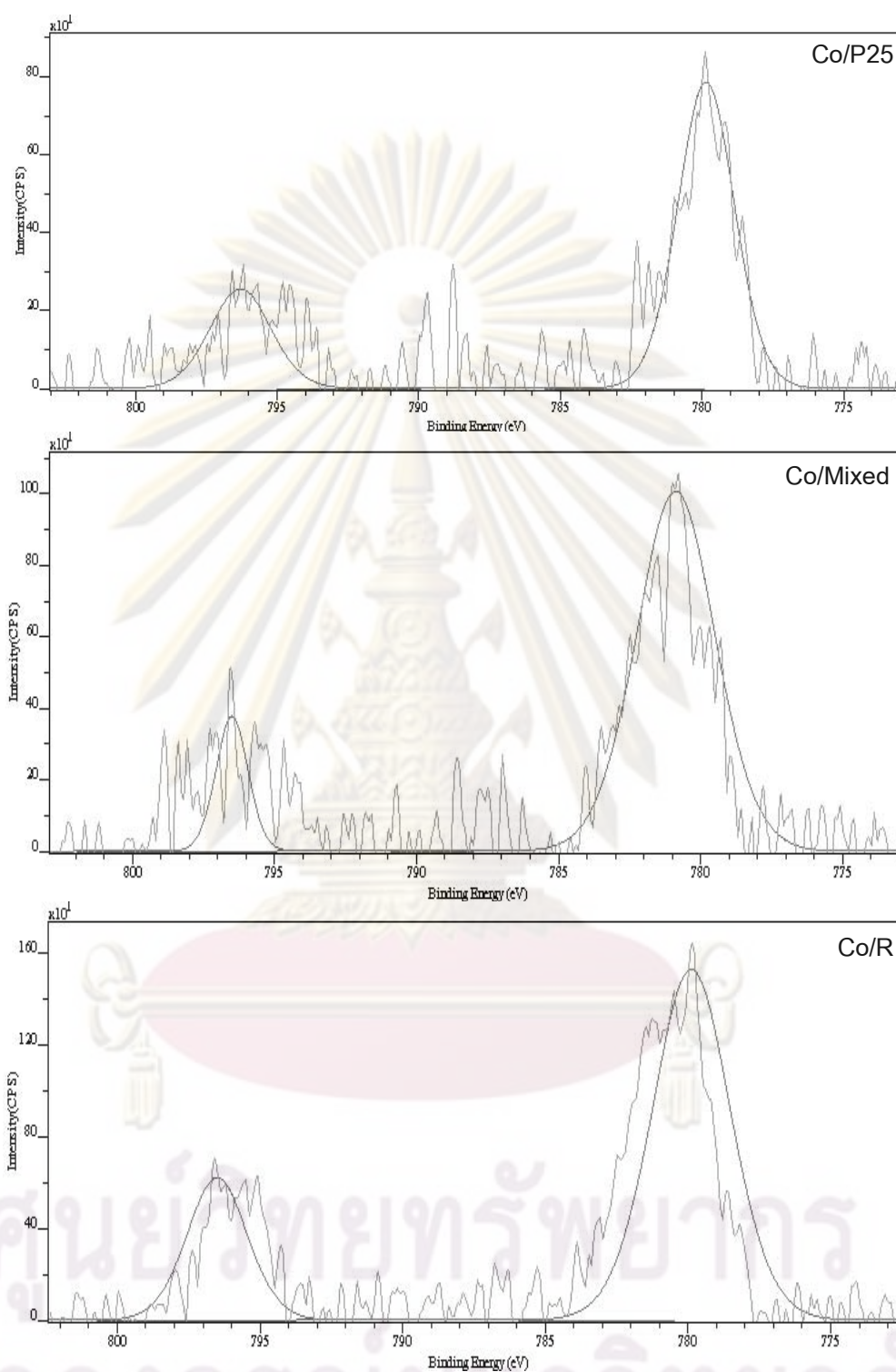
Figure 5.21 The deconvolution of Co2p$_{3/2}$ of XPS spectra of Ru-unmodified Co-catalysts.
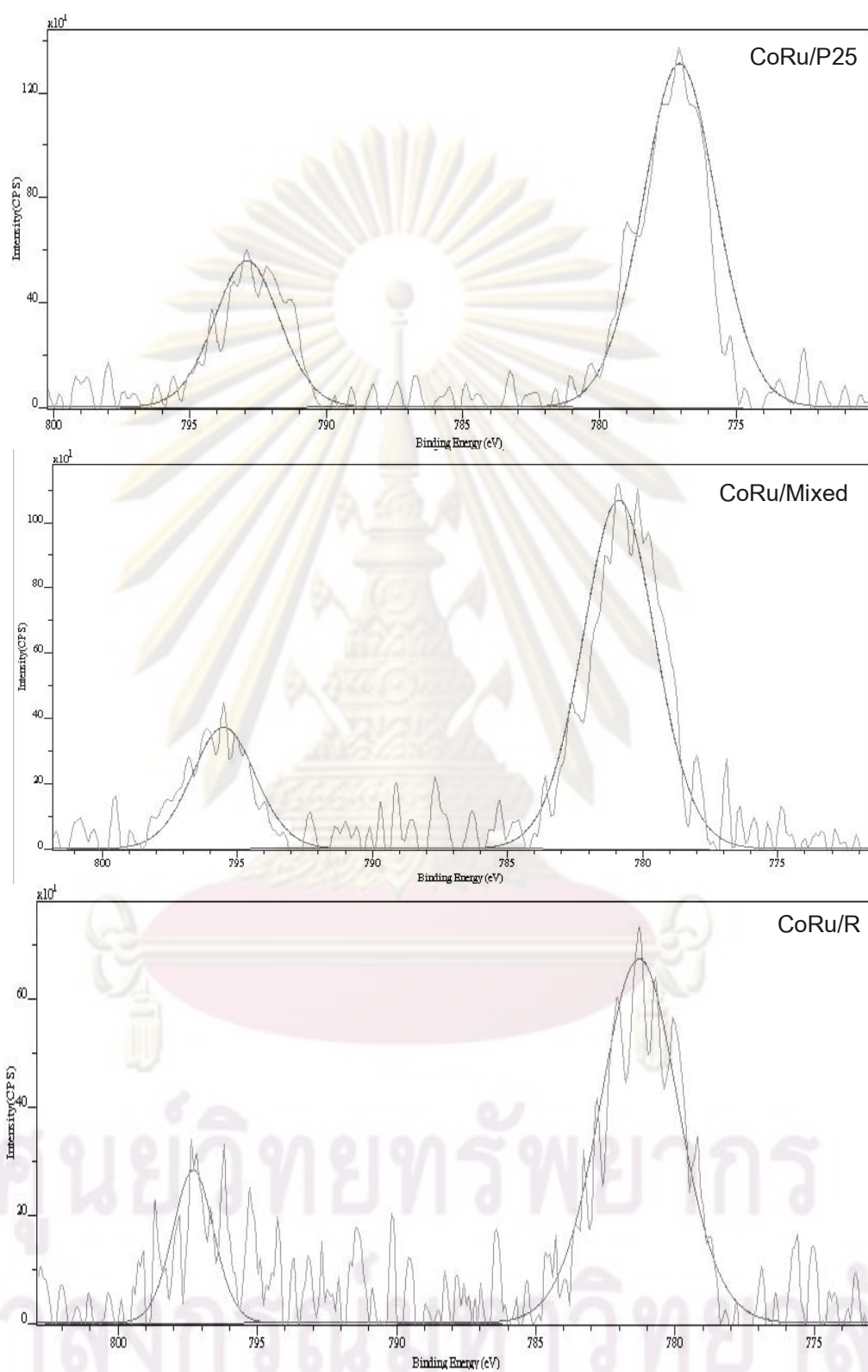
Figure 5.22 The deconvolution of Co2p$_{3/2}$ of XPS spectra Ru-promoted Co-catalysts.

Table 5.6 The binding energy, the ratio of percentages of atomic concentration, and FWHM of various elements.

Sample	Binding energy (eV) Co(II) $2p_{3/2}$	Ti 2p B.E. (eV)	Ti 2p FWHM	Atomic Concentration % Ti/O	Atomic Concentration % Co/Ti
Co/P25	779.9	458.95	1.497	0.216	0.52
Co/Mixed	780.9	459.25	2.485	0.175	0.45
Co/R	779.2	459.05	2.534	0.158	0.43
CoRu/P25	779.3	458.95	1.512	0.170	0.45
CoRu/Mixed	780.9	458.95	2.532	0.165	0.37
CoRu/R	781.3	459.85	2.797	0.173	0.34
[a]Co_3O_4	780±0.7				
[b]Co_2TiO_3	781.2				
[b]Co_2TiO_4	781.0				
Co[a]	778.1±0.1				

[a] Z. Zsoldos and L. Guczi, 1992

[b] Brik, Y. 2001

5.2.10 CO_2 hydrogenation study

The conversion, reaction rate, TOF (based on the number of reduced surface cobalt atoms measured from CO chemisorptions), and product selectivity during CO_2 hydrogenation at steady-state are given in **Table 5.10**. The conversion of Co/Mixed was higher than that of Co/R. It was due to higher number of active sites and higher dispersion. Moreover, the mixed phases of support had effect on catalytic activity. According to Jongsomjit *et al.*, (2005), they revealed that the fraction of anatase and rutile phase at 19% and 81%, respectively showed the highest activity of CO hydrogenation. However, these

catalytic activities were lower than that Co/P25 because higher amount of carbon content resulted in formation of coke and cobalt titanate. After addition of ruthenium, the catalytic activities were higher than those of unpromoted catalysts. For CoRu/Mixed and CoRu/R, the conversion dramatically increased from 6 to 20% and 3 to 22%, respectively, indicating that promotion with ruthenium had impact on the catalytic activity. The Ru would help dispersed cobalt on the surface and reduce cobalt oxide to cobalt metallic more easily. However, the activity of CoRu/P25, CoRu/Mixed, and CoRu/R had similar because some properties were similar. The low amount of carbon content after Ru-promoted conditions also resulted in the decrease of formation of coke which could become the deactivation of the catalysts. The rate vs. time on stream of the cobalt catalysts are given in **Figure 5.21**. The catalytic activity of Ru-promoted catalysts performed the stable rate probably because ruthenium may help provide stability of cobalt particles on the surface more than without promotion.

Since CO_2 hydrogenation is a structure insensitive reaction, therefore the catalytic activity depends only on the number of reduced Co metal surface atoms. The calculated TOFs at steady state of the samples are concluded in **Table 5.10**. They are in the range of 1×10^{-2} s^{-1} typical of Co catalyst under this condition (Kogelbauer, 1996, Jongsomjit, 2002, Kittiruangrayab, 2008). It was found that TOFs of Ru-promoted and unpromoted catalysts on all catalysts can be considered essentially similar. Since TOF can be derived from the intrinsic rate by definition, indicating that the intrinsic activity of the samples remain constant.
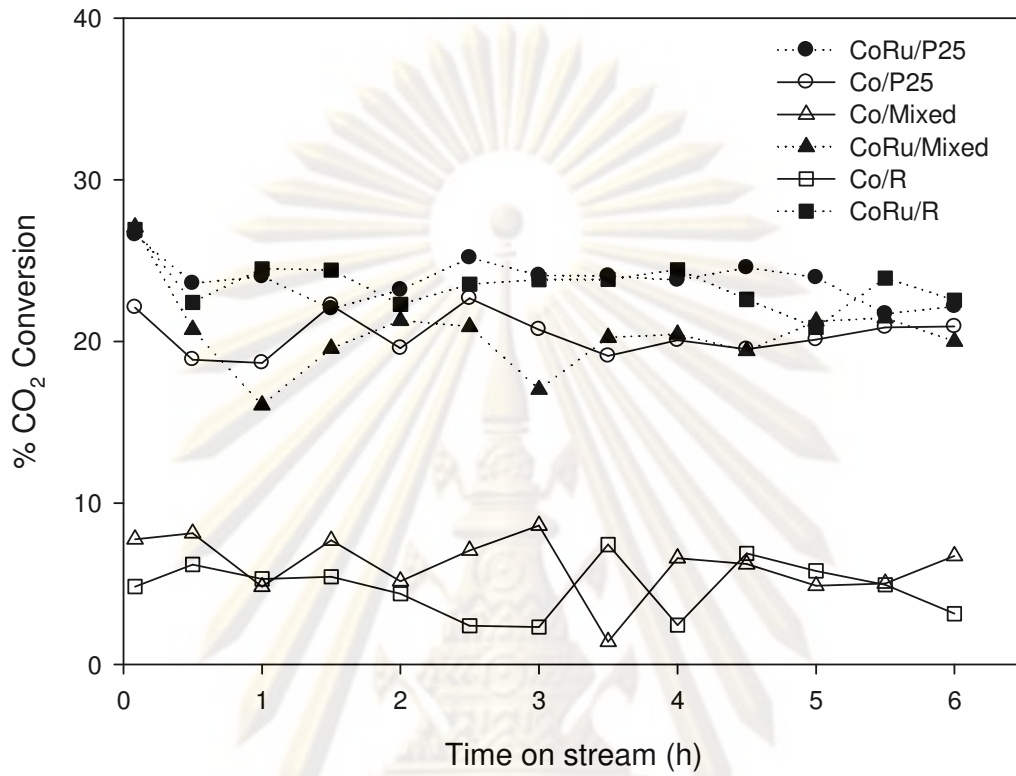
Figure 5.23 The rate vs. time on stream of the cobalt catalysts

Table 5.7 The conversion, reaction rate, TOF and product selectivity during CO_2 hydrogenation at initial and steady-state conditions.

| Sample | Conversion[a] (%) | | Rate ($\times 10^{-2}$ g CH_2/g.cat h) | TOF[d] ($\times 10^3$ s^{-1}) | Product selectivity[c] (%) |
	Initial[b]	Steady state[c]			CH_4
Co/P25	22.1	20.9	16	6.4	100
Co/A+R	7.8	6.7	5	1.4	100
Co/R	4.8	3.1	4	1.3	100
CoRu/P25	26.6	22.2	17	4.9	100
CoRu/A+R	27.1	20.0	15	2.6	100
CoRu/R	26.9	22.5	16	3.9	100

[a] CO hydrogenation was carried out at 220 °C, 1 atm, and $H_2/CO_2/Ar$ = 20/2/8, GSHV= 11400 h^{-1}.

[b] After 5 min of reaction.

[c] After 5 h of reaction.

[d] The TOF calculation was based on CO chemisorptions

CHAPTER VI

CONCLUSIONS AND RECOMMENDATIONS

6.1 Conclusions

6.1.1 The study of mesoporous titania synthesis from acid catalyzed-TiC

The high specific surface area TiO_2 was prepared via template-free, one step method using TiC as a precursor. The TiC was oxidized by aqueous nitric acid with the desired reaction time, acid concentration and reaction temperature to identify those reaction parameters on properties of TiO_2 obtained. The prepared TiO_2 with 306 m^2g^{-1} can be obtained using 5 M HNO_3 at 70 °C for 8 (calcined at 200 °C for 30 min). Summary is given as follows:

1. TiC precursor was completely oxidized, having 45% and 55% of anatase and rutile TiO_2, respectively. There were simultaneously produced during the reaction. When the reaction time increased, amount of the rutile phase continuously increased, and then it was completely transformed to pure rutile TiO_2 phase at 48 h.
2. The transformation rate from anatase to rutile could be accelerated when both of the reaction temperature and HNO_3 concentration increased. However the mesoporous framework could collapse during the oxidizing process leading to the reduction of specific surface area and pore volume.

3. Carbon residue remains in the prepared-TiO_2 approximately 3.8%. TiC contains carbon content at 16.4%. It was severely oxidized with aqueous nitric solution in the early 8 h. After that, the slow oxidation takes place, the carbon content gradually decreased.

4. Considering the acid condition, peptization process was adopted to describe the effects of all reaction parameters. With increasing reaction time or acidity (H^+ concentration), more oxolation bonds among titanium atoms were broken and produced more OH groups around a single titanium atom leading to structural rearrangements towards the more formation of corner-shared octahedral chains characteristic of the rutile phase.

6.1.2 Comparison of catalytic activity between Co-catalyst on prepared-TiO_2, with and without ruthenium promoted, with commercial grade TiO_2 (Degussa-P25).

In spite of Co-catalyst prepared from higher surface area and pore volume (mixed and pure rutile form acid catalyst-TiC) leading to higher value of active site, %dispersion and active metal surface area, low conversion value (%5) of CO_2 hydrogenation was obtained (compare with conversion from degussa-P25 support, 21%). It due to;

1. Carbon residue from TiC precursor. It remains on mixed and pure rutile support around 3.8% and 2.9% after treating with the acid, respectively. It reduced to 0.9% after impregnation. From the impregnation process, the catalysts were calcined at 300 °C and a number of carbons should be oxidized in this step. High carbon content can lead to blockage of metal

site, encapsulation of metal crystallites and blockage of pores in the catalyst support.

2. The deactivate behavior of Co-support compound formation (Co-SCF) refered to $CoTiO_x$ which should be form on synthesis catalysts. The formation of Co-titanate resulted in a decrease in the degree of reduction without any significant effect in the reduction behaviors which leads to a lower reducibility of catalysts.

3. All Ru-promoted catalysts showed higher conversion than commercial one (without Ru-promotion).Ruthenium metal can enhance dispersion of cobalt metal and stability of support crystal. From condition of Ru-promoted synthesis catalysts, 500 °C calcinations temperature was used; therefore amount of carbon residue should be dramatically decreased.

6.2 Recommendations

1. The carbon residue in the prepared TiO_2 should be investigated and eliminated in order to improve its physicochemical and chemical properties.

2. Should find the method to stabilize catalysts for high temperature condition.

3. C-doped TiO_2 from this synthesis method should be performed in photo-catalyst process.

REFERENCES

Antonelli, D., M.; Ying, Y., J. Synthesis of Hexagonally Packed Mesoporous TiO_2 by a Modified Sol-Gel Method. Angewandte Chemie-International Edition in English. 34 (1995): 2014-2017

Arakawa, H. Advances in Chemical Conversions for Mitigating Carbon Dioxide; Studies in Surface Science and Catalysis 114: (1998) 19-30

Aresta, M. Carbon Dioxide Utilization: Greening Both the Energy and Chemical Industry: An overview. Recovery and Utilization of Carbon dioxide Report 1 (1998): 2-39

Bacsa, R., Gratzel, M. Rutile Formation in Hydrothermally Crystallized Nanosized Titania. Journal of American Ceramic Society 79 (2005): 2185-2188

Bando, K., K.; Sayama, K.; Kusama, H.; Okabe, K.; Arakawa, H. In-situ FT-IR study on CO_2 hydrogenation over Cu catalysts supported on SiO_2, Al_2O_3 and TiO_2. Applied Catalysis A 165 (1997): 391-409.

Bischoff, B., Anderson, M., A. Peptization Process in the Sol-Gel Preparation of Porous Anatase (TiO_2). Chemical Material 7 (1995): 1772-1778

Borg, Ø.; Walmsley, J., C.; Royal, D.; Tanem, B., S.; Blekkan, E., A.; Eri., S.; Rytter., E. and Holmen., A. Electron microscopy study of γ-Al_2O_3 supported cobalt Fischer-Tropsch synthesis catalysts. Catalysis Letter 126 (2008): 224-230.

Brik, Y., Kacimi, M., Ziyad, M., Bozon-Verduraz, F. Titania-Supported Cobalt and Cobalt-Phosphorus Catalysts: Characterization and Performances in Ethane oxidative Dehydrogenation. Journal of Catalysis 202 (2001): 118-128

Brik, T., Kacimi, M., Bozon-Verduraz, F., Ziyad, M. Characterization and Comparison of the Activity of Boron-Modified Co/TiO_2 Catalysts in Butan-2-ol Conversion and Oxidative Dehydrogenation of Ethane. Journal of catalysis 211 (2002): 470-481

Chu, W., Chernavskii, P., A., Gengembre, L., Pankina, G., A., Fongarland, P., Khodakov, A., Y. Cobalt species in promoted cobalt alumina-supported Fischer-Tropsch catalysts. Journal of Catalysis 252 (2007): 215-230

Dry, M., E. The Fischer-Tropsch process: 1950-2000. Catalysis Today 71 (2002): 227-241

Dubois, J., Sayama, K., Arakawa, H. Conversion of CO2 to Dimethylether and Methanol over Hybrid Catalysts. Chemistry Letters 21 (1992): 1115-1118

Fisher, I., A., Bell, A., T. In-Situ Infrared Study of Methanol Synthesis from H_2/CO_2 over Cu/SiO_2 and $Cu/ZrO_2/SiO_2$. Journal of catalysis 172 (1997): 222-237

Fornika, R., Gorls, H., Seemann, B., Leitner, W. Complexes $[(P_2)Rh(hfacac)]$ as Catalyst for CO_2 hydrogenation: Correlations between solid-state structures, [103]Rh NMR Shifts and catalytic activities. Journal of Chemistry Society (1995): 1479-1481

Fujishima, A., Hashimoto, K., Watanabe, T. TiO_2 Photocatalysis: Fundamentals and Applications. BKC Tokyo (1999)

Gines, M., J., L., Marchi, A., J., Apesteguia, C., R. Kinetic study of the reverse water-gas shift reaction over $CuO/ZnO/Al_2O_3$ catalysts. Applied Catalysis A 154 (1997): 155-171

Gole, J., L., Prokes, S., M., Glembocki, O., J. Efficient Room-Temperature Conversion of Anatase to Rutille TiO_2 Induced by High-Spin Ion Doping. Journal of Physical Chemistry 112 (2008): 1782-17880

Hong, J., Chernavskii, P., A., Khodakov, A., Y., Chu, W. Effect of promotion with ruthenium on the structure and catalytic performance of mesoporous silica (smaller and larger pore) supported cobalt Fischer-Tropsch catalysts. Catalysis Today 140 (2009): 135-141

Huang, D., Luo, G., Yang, L., Wang, Y. Synthesis of mesoporous TiO_2 materials with high specific area using inorganic acids as catalysts. China Particuology 3 (2005): 176-180

Iglesia, E. Design, synthesis, and use of cobalt-based Fischer-Tropsch synthesis catalysts. Applied Catalysis A 161 (1997) 59-78

Jacobs, G., Das, T., K., Zhang Y., Li, J., Racoillet, G., Davis, B., H. Fischer–Tropsch synthesis: support, loading, and promoter effects on the reducibility of cobalt catalysts. Applied.Catalysis.A 233 (2002): 263-281

Jongsomjit, B., Panprenot, J., Goodwin Jr, J., G. Co-Support Compund Formation in Alumina-Supported Cobalt Catalysts. Journal of Catalysis 204 (2001): 98-109

Jongsomjit, B., Goodwin Jr, J., G. Co-support compound formation in Co/Al$_2$O$_3$ catalysts: effect of reduction gas containing CO. Catalysis Today 77 (2002): 191-204

Jongsomjit, B., Panpraont, J., Goodwin Jr, J., G. Effect of zirconia-modified alumina on the properties of Co/γ-Al$_2$O$_3$ catalysts. Journal of Catalysis 215 (2003): 66-77

Jongsomjit, B., Chitlada Sakdamnuson, C., Goodwin, J., G., Praserthdam, P. Co-support compound formation in titania-supported cobalt catalyst. Catalysis Letters 94 (2004): 209-215

Jongsomjit, B., Wongsalee, T., Praserthdam, P. Characteristics and catalytic properties of Co/TiO$_2$ for various rutile:anatase ratios. Catalysis Communication 6 (2005): 705-710

Jongsomjit, B., Wongsalee, T., Praserthdam, P. Study of cobalt dispersion on titania consisting various rutile: anatase ratios. Materials Chemistry and Physics 92 (2005) 572-577

Jongsomjit, B., Sakdamnuson, C., Panpranot, J., Praserhdam, P. Role of ruthenium in the reduction behavior of ruthenium-promoted cobalt/titania fischer-tropsch catalysts. Reaction of Kinetic Catalysis Letters 88 (2006): 65-71

Jung, H., Shin, H., Kim, J., Kim, J., Hong, K. In Situ Observation of the stability of anatase Nanoparticles and Their Transformation to Rutile in an Acidic Solution. Langmuir 20 (2004): 11732-11737

Khodakov, A., Y., Chu, W., Fongarland, P. Advances in the Development of Novel Cobalt Fischer-Tropsch Catalysts for Synthesis of Long-Chain Hydrocarbons and Clean Fuels. Chemical Reviews 107 (2007): 1692-1744

Kittiruangrayab, S.; Burakorn, T.; Jongsomjit, B. and Praserthdam, P. Characterization of Cobalt Dispersed on Various Micro- and Nanoscale Silica and Zirconia Supports. Catalysis Letter. 124 (2008): 376-383.

Kluson, P., Kacer, P., Cajthaml, T., Kalaji, M. Preparation of titania mesoporous materials using a surfactant mediated sol-gel method. Journal of Material Chemistry 11 (2001): 644-651

Kogelbauer, A., Goodwin Jr., J. G., and Oukaci, R. Ruthenium Promotion of Co/Al$_2$O$_3$ Fischer–Tropsch Catalysts. Journal of Catalysis. 160 (1996): 125-133.

Kraum, M., Baerns, M. Fischer-Tropsch synthesis: the influence of various cobalt compounds applied in the preparation of supported cobalt catalysts on their performance. Applied Catalysis A 186 (1999): 189-200

Kryukova, G., N.; Zenkovets, G., A.; Shutilov, A., A.; Wilde, M.; Gunther, K.; Fassler, D.; Richter, K. Structural peculiarities of TiO$_2$ and Pt/TiO$_2$ catalysts for the photocatalytic oxidation of aqueous solution of Acid orange 7 Dye upon ultraviolet light. Applied Catalysis B 71 (2007): 169-176.

Kusama, H., Okabe, K., Sayama, K., Arakawa, H. CO2 hydrogenation to ethanol over promoted Rh/SiO$_2$ catalyst. Catalysis Today 28 (1996): 261-266

Lahtinen, J., Anraku, T., Somorjai, G., A. C, CO and CO$_2$ hydrogenation on cobalt foil model catalysts: evidence for the need of CoO reduction. Catalysis Letters 25 (1994) 241-255

Lee, S., Jang, J., Lee, B., Kim, J., Kang, M., Lee, S., Choi, M., Choung, S. Promotion of hydrocarbon selectivity in CO$_2$ hydrogenation by Ru component. Journal of Molecular Catalysis A 210 (2004): 131-141

Leitner, W. Carbon Dioxide as a Raw Material: The Synthesis of Formic Acid and Its Derivatives from CO_2. Angewandte Chemie Inernational Edition in English 34 (1995): 2207-2221

Li, X., Fryxell, G., Engelhard, M., Wang, C. The synthesis of cadmium doped mesoporous TiO_2. Inorganic Chemistry Communication 10 (2007): 639-641

Liu, C., Fu, L., Economy, J. Simple template-free route for the synthesis of mesoporous titanium dioxide materials. Journal of Material Chemistry 14 (2004): 1187-1189

Liu, R., Ren, Y., Shi, Y., Zhang, F., Zhang, L., Tu, B., Zhao, D. Controlled Synthesis of Odered Mesoporous C-TiO_2 Nanocomposites with Crystalline Titania Frameworks from Organic-Inorganic-Amphiphilic Coassembly. Chemistry Material 20 (2008): 1140-1146

Matijevic, E. Monodispersed Metal (Hydrous) Oxides – A Fascinating Field of Colloid Science. Accounts of chemical research 14 (1981): 22-29

Mori, T., Taniguchi, S., Mori, Y., Hattori, T., Murakami, Y. High methanation activity of titania-supported Pd catalyst in the SMSI state. Journal of Catalysis 108 (1987): 501-502

Nagaoka, K., Takanabeb, K., Aika, K. Influence of the phase composition of titania on catalytic behavior of Co/TiO_2 for the dry reforming of methane. Chemical Communuty (2002): 1006-1007

Noyori, R., Jessop, P., G., Hsiao, Y., Ikariya, T. Homogeneous Catalysis in Supercritical Fluids: Hydrogenation of Supercritical Carbon Dioxide to Formic Acid, Alkyl Formates, and Formamamides. Journal of the American chemical society 118 (1996): 344-355

Othmer, K. Encyclopedia of Chemical Technology, A Wiley-Interscience Publication, John Wiley and Son, New York, 4th ed. 1 (1991): 948-972.

Ozcan, O.; Yukruk, F.; Akkaya, E., U.; Uner, D. Dye sensitized artificial photosynthesis in the gas phase over thin and thick TiO_2 films under UV and visible light irradiation. Applied Catalysis B 71 (2007): 291-297.

Pansanga, K.; Panpranot, J.; Mekasuwandumrong, O.; Satayaprasert, C. and Praserthdam, P. Synthesis of nanocrystalline alumina by thermal decomposition of aluminum isopropoxide in 1-butanol and their application as cobalt catalyst support. Korean Journal of Chemical Engineering 24 (2007): 397-402

Pansanga, K.; Panpranot, J.; Mekasuwandumrong, O.; Satayaprasert, C.; Goodwin, G.; J. and Praserthdam, P. Effect of mixed γ- and χ-crystalline phases in nanocrystalline Al_2O_3 on the dispersion of cobalt on Al_2O_3. Catalysis Communications 9 (2008): 207-212.

Perez-Alonso, F., J., Ojeda, M., Herranz, T., Rojas, S., Gonzalez-Carballo, J., M., Terreros, P., Fierro, J., L., G. Carbon dioxide hydrogenation over Fe-Ce catalysts. Catalysis Communication 9 (2008): 1945-1948

Rajesh, B., Sasirekha, N., Chen, Y. Influence of acid precursors on physicochemical properties of nanosized titania synthesized by thermal-hydrolysis method. Material Research Bulletin 43 (2008): 682-692

Raveendran, P., Eswaramoorthy, M., Bindu, U., Chatterjee, M., Hakuta, Y., Kawanami, H., Mizukami, F. Template-Free Formation of Meso-Structured Anatase TiO_2 with Spherical Morphology. Journal of Physical Chemistry 112 (2008): 20007-20011

Sakurai, H., Haruta, M. Carbon dioxide and carbon monoxide hydrogenation over gold supported on titanium, iron, and zinc oxides. Applied Catalysis A 127 (1995): 93-105

Sakurai, H., Haruta, M. Synergism in methanol synthesis from carbon dioxide over gold catalysts supported on metal oxides. Catalysis Today 29 (1996): 361-365

Shen, M., Wu, Z., Huang, H., Du, Y., Zou, Z., Yang, P. Carbon-doped anatase TiO_2 obtained from TiC for photocatalysis under visible light irradiation. Materials Letters 60 (2006): 693-697

Shieh, D., Li, J., Shieh, M., Lin, J. A novel approach to mesoporous anatase TiO_2: Oxidation of TiC by nitric acid. Microporous and Mesoporous Materials 98 (2007): 339-343

Shimada, S. A thermoanalytical study of oxidation of TiC by simultaneous TGA-DTA-MS analysis. Journal of Material Science 31 (1996): 673-677

Shimada, S., Mochidsuki, K. The oxidation of TiC in dry oxygen, wet oxygen and water vapor. Journal of Material Science 39 (2004): 581-586

Soled, S., L., Iglesia, E., Fiato, R., A., Baumgartner, J., E., Vroman, H., Miseoa, S. Control of metal dispersion and structure by changes in the solid-state chemistry of supported cobalt Fischer–Tropsch catalysts. Topics in Catalysis 26 (2003): 101-109

Storsaeter, S.; Totdal, B.; Walmsley, J., C.; Tanem, B., S.; Holmen, A. Characterization of alumina-, silica-, and titania-supported cobalt Fischer-Tropsch catalysts. Journal of Catalysis 236 (2005): 139-152.

Suo, Z.; Kou, Y.; Niu, J.; Zhang, W.; Wang, H. Characterization of TiO_2-, ZrO_2- and Al_2O_3-supported iron catalysts as used for CO_2 hydrogenation. Applied Catalysis A 148 (1997): 301-313.

Trovarelli, A., Mustazza, C., Dolcetti, G., Kaspar, J., Graziani, M., Carbon dioxide hydrogenation on rhodium supported on transition metal oxides: Effect of reduction temperature on product distribution. Applied Catalysis 65 (1990): 129-142

Ushikoshi, K., Mori, K., Watanabe, T., Takeuchi, M., Saito, M. A 50 kg/day class test plant for methanol synthesis from CO_2 and H_2. Study of Surface Science and Catalyst 114 (1998): 357–362

Vannice, M., A., Twu, C., C. SMSI effects on CO adsorption and hydrogenation on Pt catalysts: PartII. Influence of support and crystallite size on the kinetics of methanation. Journal of Catalysis 82 (1983): 213-222

Wang, C., B., Tang, C., W., Tsai, H., C., Chien, S., H. Characterization and catalytic oxidation of carbon monoxide over supported cobalt catalysts Catalysis Letters 107 (2006): 223-230

Wang, Y., Jiang, Z., Yang, F. Preparation and photocatalytic activity of mesoporous TiO_2 derived from hydrolysis condensation with TX-100 as template. Material of Science and Engineering B 128 (2006): 229-233

Wang, Y., Ma, C., Sun, X., Li, H. Synthesis and characterization of amorphous TiO_2 with wormhole-like framework mesostructure. Journal of Non-Crystalline Solids 319 (2003): 109-116

Wu, M., Wang, G., Xu, H., Long J, Shek, F., Lo, SM., Williams, I., D., Feng, S., Xu, R. Hollow Spheres Based on Mesostructured Lead Titanate with Amorphous Framework. Langmuir 19 (2003): 1362-1367

Yaccato, K., Carhart, R., Hagemeyer, A., Lesik, A., Strasser, P., Volpe, A., F., Turner, H., Weinberg, H., Grasselli, R., K., Brooks, C. Competitive CO and CO_2 methanation over supported noble metal catalysts in high throughput scanning mass spectrometer. Applied Catalysis A 296 (2005) 30-48

Yang, J., Mei, S., Ferreira, J., Norby, P., Quaresma, S. Fabrication of rutile rod-like particle by hydrothermal method: an insight into HNO_3 peptization. Journal of Colloid and Interface Science 283 (2005): 102-106

Yang, J., Mei, S., Ferreira, J. Hydrothermal Synthesis of Nanosized Titania Powder: Influence of Peptization and Peptizing Agents on the Crystalline Phases and Phase Transitions. Journal of American Ceramic Society 83 (2000): 1361-1368

Young, R., S., Victoria, B., C., Cobalt: Its Chemistry, Metallurgy and Uses. <u>ACS Monograph</u> 83 (1960): 4112-4113

Yu, K. and Lee, G., W., M. Decomposition of gas-phase toluene by the combination of ozone and photocatalytic oxidation process (TiO_2/UV, TiO_2/UV/O_3, and UV/O_3). <u>Applied Catalysis B</u> 75 (2007) 29-38.

Zhang, J.; Chen, J.; Ren, J.; Li, Y. and Sun, Y. Support effect of Co/Al_2O_3 catalysts for Fischer-Tropsch synthesis. <u>Fuel</u> 82 (2003): 581-586.

Zhang, R., Gao, L. Effect of peptization on phase transformation of TiO_2 nanoparticles. <u>Materials Research Bulletin</u> 36 (2001): 1957-1965

Zhang, Y., Jacobs, G., Sparks, D., E., Dry, M., E., Davis, B., H. CO and CO_2 hydrogenation study on supported cobalt Fischer-Tropsch synthesis catalysts. <u>Catalysis Today</u> 71 (2002): 411-418

APPENDICES

APPENDIX A

CALCULATION FOR CATALYST PREPARATION

Preparation of 20%Co/TiO$_2$ is shown as follows:

Calculation for the preparation of cobalt loading catalyst (20%Co/TiO$_2$)

Example calculation for the preparation of 20%Co/TiO$_2$

Based on 100 g of catalyst used, the composition of the catalyst will be as follows:

Cobalt	=	20 g	
TiO$_2$	=	100-20 =	80 g

For 1 g of Al$_2$O$_3$

Cobalt required	=	$1 \times (20/80)$	=	0.25 g

Cobalt 0.25 g was prepared from $Co(NO_3)_2 \cdot 6H_2O$ and molecular weight of Co is 58.93

$$Co(NO_3)_2 \cdot 6H_2O \text{ required} = \frac{MW \text{ of } Co(NO_3)_2 \cdot 6H_2O \times \text{cobalt required}}{MW \text{ of } Co}$$

$$= (291.03/58.93) \times 0.25 = 1.23 \text{ g}$$

Calculation for the preparation of the 0.5% Ru-modified TiO$_2$ support

Based on 100 g of catalysts used, the composition of the catalyst will be as follow:

Cobalt	=	20 g	
Ruthenium	=	0.5 g	
Titania	=	100— (20+0.5) =	79.5 g

For 1 g of titania

Cobalt required	=	1× (20/79.5)	=	0.251 g
Ruthenium required	=	1 × (0.5/79.5)	=	0.0063 g

Ruthenium 0.0063 g was prepared from $(Ru(NO)(NO_3)_3)$ solution in dilute nitric acid 1.5 wt%

$Ru(NO)(NO_3)_3$ required = ruthenium required × fraction of Ru in nitric sol^n

= 0.0063 × (100/1.5) = 0.42 g

$Co(NO_3)_2 \cdot 6H_2O$ required = $\dfrac{\text{MW of Co(NO}_3)_2 \cdot 6H_2O \ \times \text{cobalt required}}{\text{MW of Co}}$

= (291.03/58.93) × 0.251 = 1.24 g

APPENDIX B

CALCULATION OF THE CRYSTALLITE SIZE

Calculation of the crystallite size by Scherrer equation

The crystallite size was calculated from the half-height width of the diffraction peak of XRD pattern using the Debye-Scherrer equation.

From Scherrer equation:
$$D = \frac{K\lambda}{\beta \cos \theta} \qquad (B.1)$$

where
  D = Crystallite size, Å

  K = Crystallite-shape factor = 0.9

  λ = X-ray wavelength, 1.5418 Å for CuKα

  θ = Observed peak angle, degree

  β = X-ray diffraction broadening, radian

The X-ray diffraction broadening (β) is the pure width of a powder diffraction free of all broadening due to the experimental equipment. Standard α-alumina is used to observe the instrumental broadening since its crystallite size is larger than 2000 Å. The X-ray diffraction broadening (β) can be obtained by using Warren's formula.

From Warren's formula:
$$\beta^2 = B_M^2 - B_S^2 \qquad (B.2)$$
$$\beta = \sqrt{B_M^2 - B_S^2}$$

Where B_M =   The measured peak width in radians at half peak height.

B_S =   The corresponding width of a standard material.

Example: Calculation of the crystallite size of Co_3O_4 on P25

The half-height width of peak   = 0.34° (from Figure B.1)

= $(2\P \times 0.34)/360$

=   0.0059 radian

The corresponding half-height width of peak of α-alumina   =   0.0042 radian

The pure width   = $\sqrt{B_M^2 - B_S^2}$

= $\sqrt{0.006^2 - 0.0041^2}$

=   0.004 radian

β =   0.004 radian

2θ = 37.26°

θ = 18.6° = 0.324 radian

λ =   1.5418 Å

The crystallite size   = $\dfrac{0.9 \times 1.5418}{0.004 \cos 0.324}$ =   365.9 Å
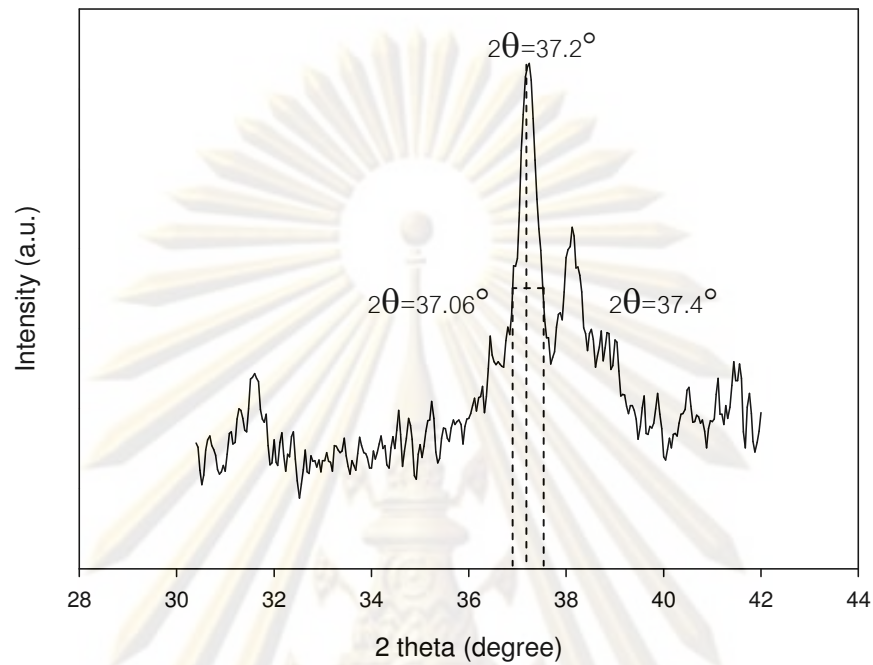
=   36.6 nm

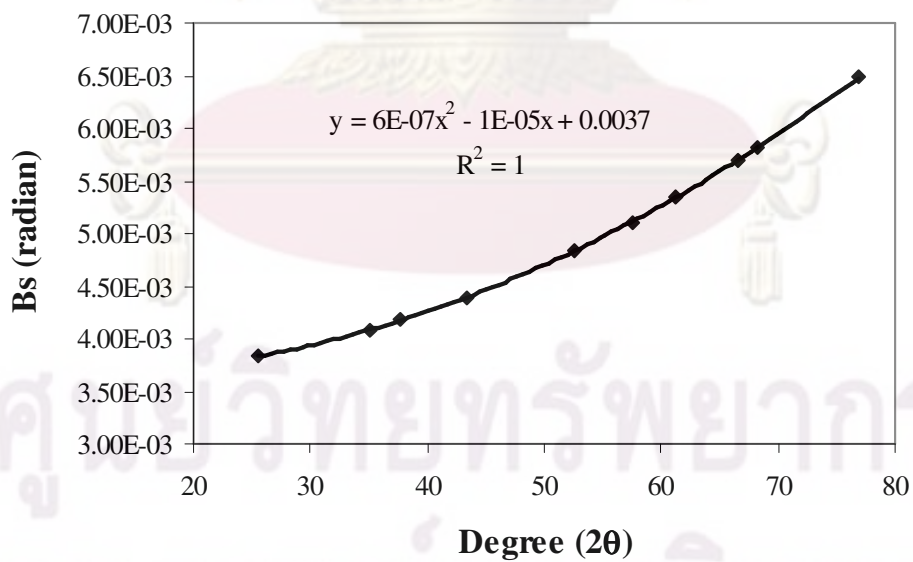Figure B.1 The measured peak of Co/P25 to calculate the crystallite size.

Figure B.2 The plot indicating the value of line broadening due to the equipment. The data

were obtained by using α-alumina as standard.

APPENDIX C

CALCULATION FOR TOTAL CO CHEMISSORPTION AND DISPERSION

Calculation of the total CO chemisorption and metal dispersion of the catalyst, a stoichiometry of CO/Co = 1, measured by CO chemisorption is as follows:

Let the weight of catalyst used	=	W	g
Integral area of CO peak after adsorption	=	A	unit
Integral area of 30 µl of standard CO peak	=	B	unit
Amounts of CO adsorbed on catalyst	=	B-A	unit
Concentration of Co	=	C	%wt
Volume of CO adsorbed on catalyst	=	$30 \times [(B-A)/B]$	µl
Volume of 1 mole of CO at 30°C	=	24.86	µl
Mole of CO adsorbed on catalyst		$= [(B-A)/B] \times [30/24.86]$	µmole

Molecule of CO addorbed on catalysts

$$= [(B-A)/B] \times [30/24.86] \times [6.02 \times 10^{23}] \quad \text{µmole}$$

Total CO chemisorption $\quad = [(B-A)/B] \times [1.08 \times 10^{24}] \times [1/W] \qquad$ µmole/g cat

(Metal active site)

Molecular weight of cobalt $\qquad = 58.993$

Calculation of %metal dispersion

Definition of % metal dispersion:

Metal dispersion (%) = 100×[molecules of Co from CO adsorption/molecules of Co loaded]

In this study, the formula from Chemisorb 2750 Operator's Manual can used for determined the % metal dispersion as follow:

$$\%D = S_f \times \left[\frac{Vads}{Vg} \right] \times \left[\frac{m.w.}{\%M} \right] \times 100\% \times 100\% \dots\dots\dots\dots(C.1)$$

Where

%D	=	%metal dispersion
S_f	=	stoichiometry factor, (CO on Co* =1)
V_{ads}	=	volume adsorbed (cm^3/g)
V_g	=	molar volume of gas at STP = 22414 (cm^3/mol)
m.w.	=	molecular weight of the metal (a.m.u.)
%M	=	%metal loading

Example: %Dispersion of Co/P25

Calculation Volume Chemisorbed (V_{ads})

$$V_{ads}(cm^3/g) = \left[\frac{Vinj}{m} \right] \times \sum_{i=1}^{n}\left(1 - \frac{Ai}{Af}\right) \dots\dots\dots\dots\dots(C.2)$$

Where:

V_{ing}	=	volumn injected (cm^3) = 27.1 µL=0.271 cm^3
m	=	mass of sample (g)
Ai	=	area of peak i
Af	=	area of last peak

To replace values in equation (1) and (2);

$$V_{ads} = \left[\frac{0.271}{0.1} \right] \times \left[\left(1 - \frac{0.00021}{0.00533}\right) + \left(1 - \frac{0.00153}{0.00533}\right) + \left(1 - \frac{0.00510}{0.00533}\right) + \left(1 - \frac{0.00526}{0.00533}\right) + \left(1 - \frac{0.00495}{0.00533}\right) + \left(1 - \frac{0.00508}{0.00533}\right) \right]$$

$$= 0.5544 \ cm^3/g$$

$$\%D = 1 \times \left[\frac{0.5544}{22414} \right] \times \left[\frac{58.993}{21.54} \right] \times 100\% \times 100\% = 0.68\%$$

%Co dispersion is 0.68%

APPENDIX D

CALIBRATION CURVES

This appendix showed the calibration curves for calculation of composition of reactant and products in CO_2 hydrogenation reaction. The reactant is CO_2 and the main product is methane. The other products are linear hydrocarbons of heavier molecular weight that are C_2-C_4 such as ethane, ethylene, propane, propylene and butane.

The thermal conductivity detector, gas chromatography Shimadzu model 8A was used to analyze the concentration of CO_2 by using Porapak Q column.

The VZ10 column are used with a gas chromatography equipped with a flame ionization detector, Shimadzu model 14B, to analyze the concentration of products including of methane, ethane, ethylene, propane, propylene and butane. Conditions uses in both GC are illustrated in Table D.1.

Mole of reagent in y-axis and area reported by gas chromatography in x-axis are exhibited in the curves. The calibration curves of CO_2, methane, ethane, ethylene, propane, propylene and butane are illustrated in the following figures.

Table D.1 Conditions use in Shimadzu modal GC-8A and GC-14B.

Parameters	Condition	
	Shimadzu GC-8A	Shimadzu GC-14B
Width	5	5
Slope	50	50
Drift	0	0
Min. area	10	10
T.DBL	0	0
Stop time	8	20
Atten	2	2
Speed	10	3
Method	1	1
Format	1	1
SPL.WT	100	100
IS.WT	1	1
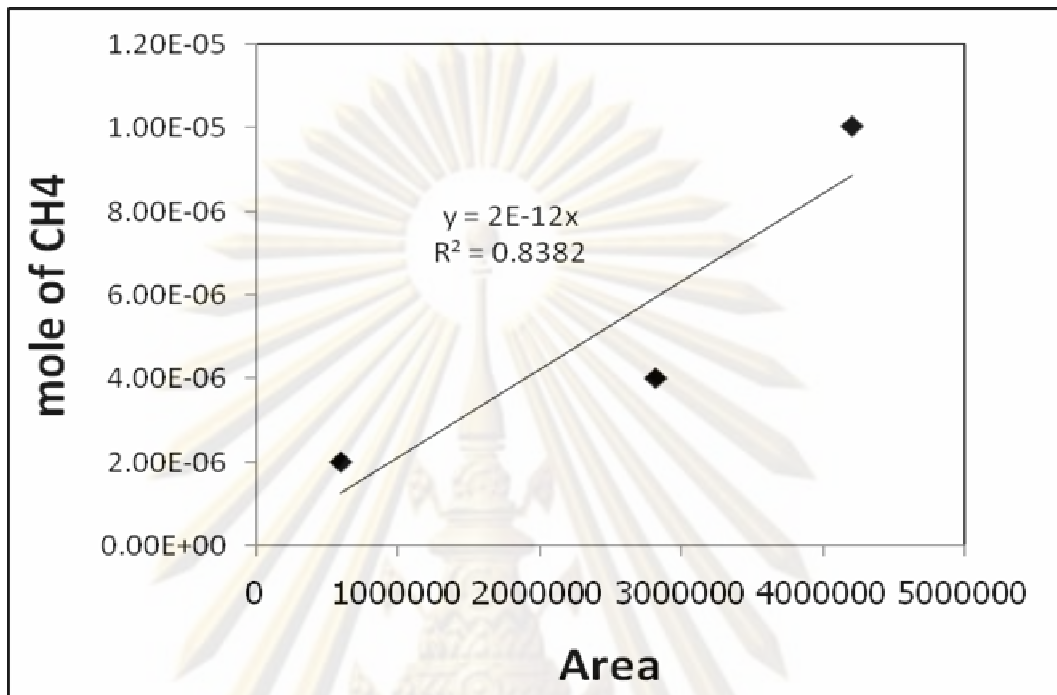
Figure D.1 The calibration curve of methane
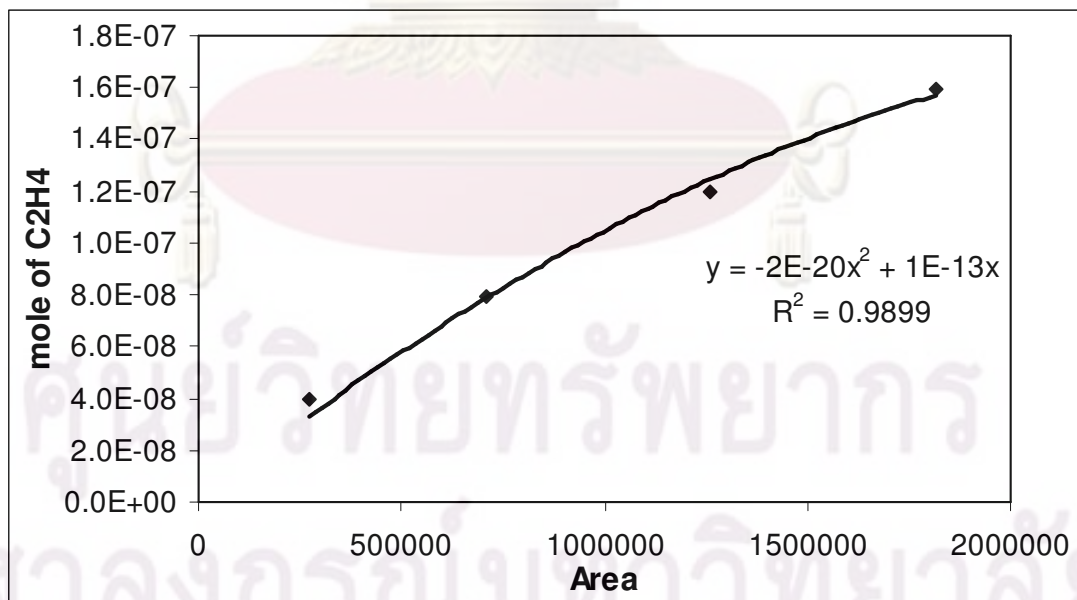
Figure D.2 The calibration curve of ethylene
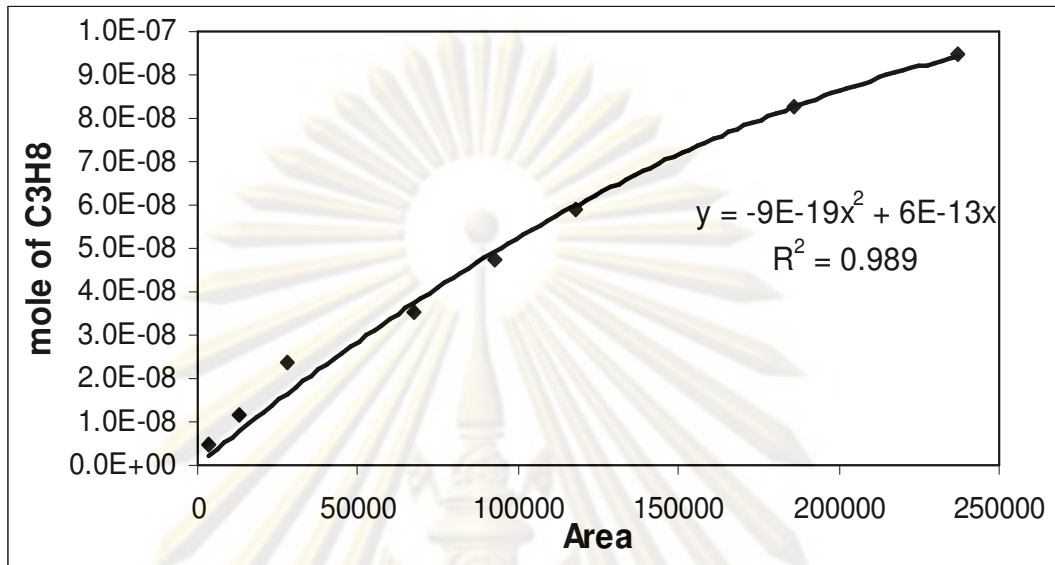
Figure D.3 The calibration curve of propane

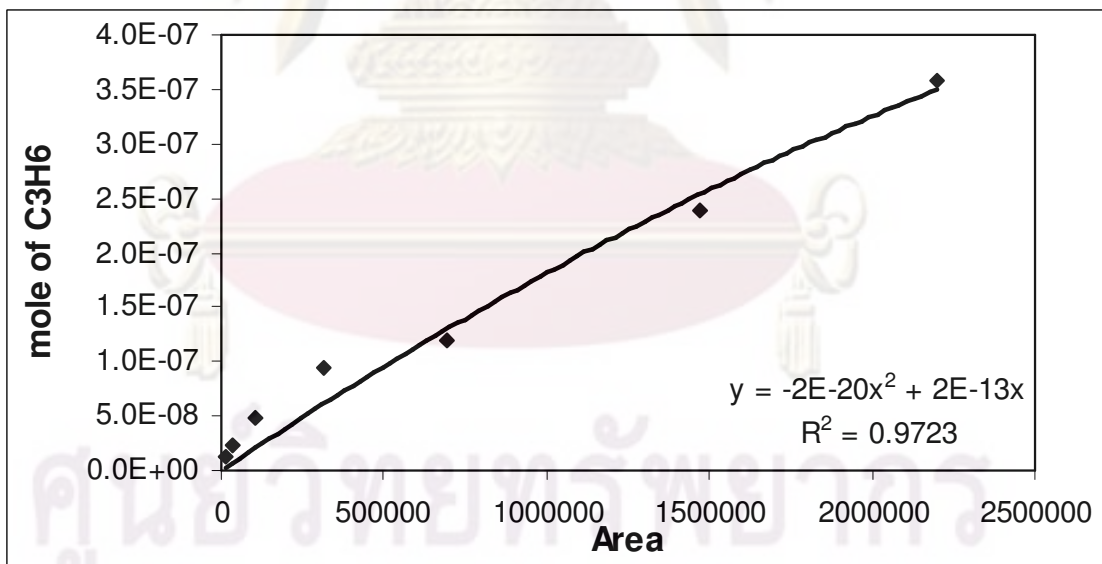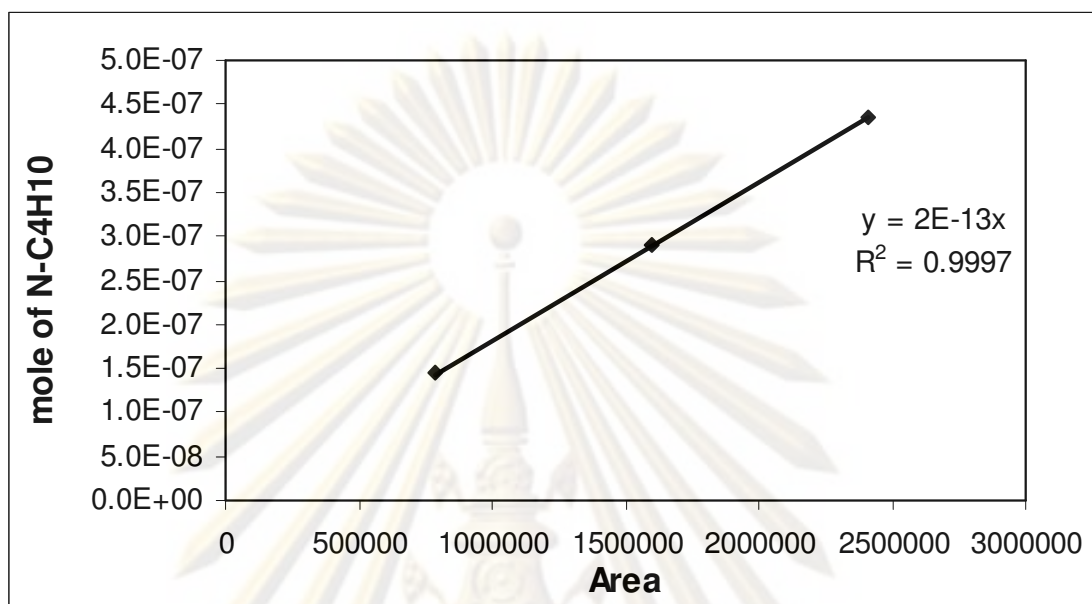**Figure D.4** The calibration curve of propene

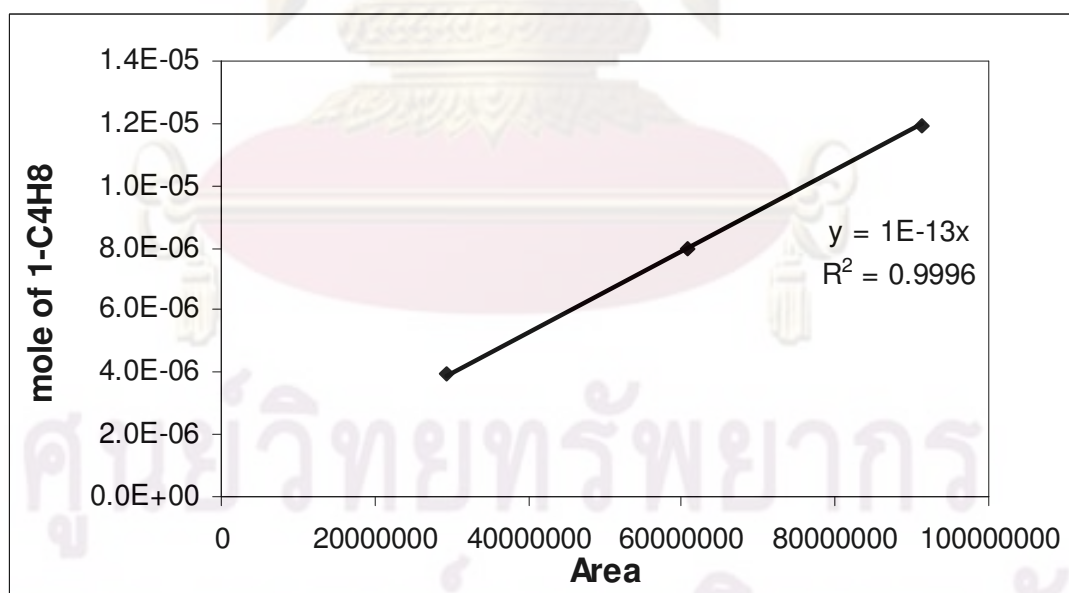**Figure D.5** The calibration curve of butane

Figure D.6 The calibration curve of butene

Figure D.7 The chromatograms of catalyst sample from thermal conductivity detector, gas

chromatography Shimadzu model 8A (Porapak Q)

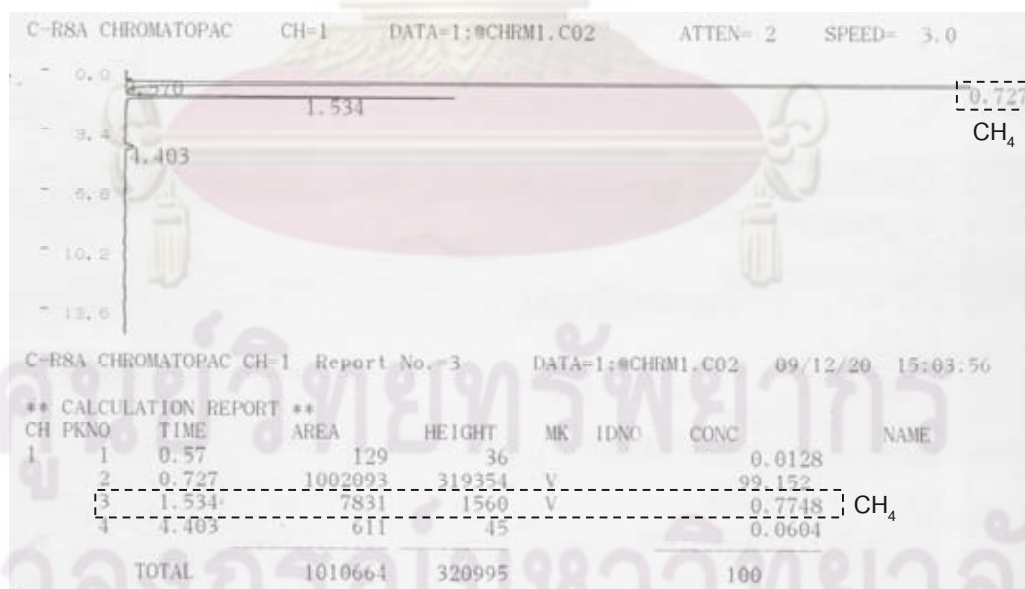**Figure D.8** The chromatograms of catalyst sample from flame ionization detector, gas

chromatography Shimadzu model 14B (VZ10 column)

APPENDIX E

CALCULATION OF CO_2 CONVERSION, REACTION RATE AND SELECTIVITY

The catalyst performance for the CO_2 hydrogenation was evaluated in terms of activity for CO_2 conversion rate and selectivity.

Activity of the catalyst performed in term of carbon monoxide conversion and reaction rate. Carbon monoxide conversion is defined as moles of CO_2 converted with respect to CO_2 in feed:

$$CO_2 \text{ conversion (\%)} = \frac{100 \times [\text{mole of } CO_2 \text{ in feed} - \text{mole of } CO_2 \text{ in product}]}{\text{mole of } CO_2 \text{ in feed}} \quad \text{(i)}$$

Reaction rate was calculated from CO_2 conversion that is as follows:

|			
Let the weight of catalyst used	=	W	g
Flow rate of CO_2	=	2	cc/min
Reaction time	=	60	min
Weight of CH_2	=	14	g
Volume of 1 mole of gas at 1 atm	=	22400	cc

$$\text{Reaction rate (g } CH_2/\text{g of catalyst)} = \frac{[\% \text{ conversion of } CO_2/100] \times 60 \times 14 \times 2}{W \times 22400} \quad \text{(ii)}$$

Selectivity of product is defined as mole of product (B) formed with respect to mole of CO_2 converted:

$$\text{Selectivity of B (\%)} = 100 \times [\text{mole of B formed/mole of total products}] \quad \text{(iii)}$$

Where B is product, mole of B can be measured employing the calibration curve of products such as methane, ethane, ethylene, propane, propylene and butane

$$\text{mole of CH}_4 = (\text{area of CH}_4 \text{ peak from integrator plot on GC} - 14\text{B}) \times 8 \times 10^{12} \quad \text{(iv)}$$
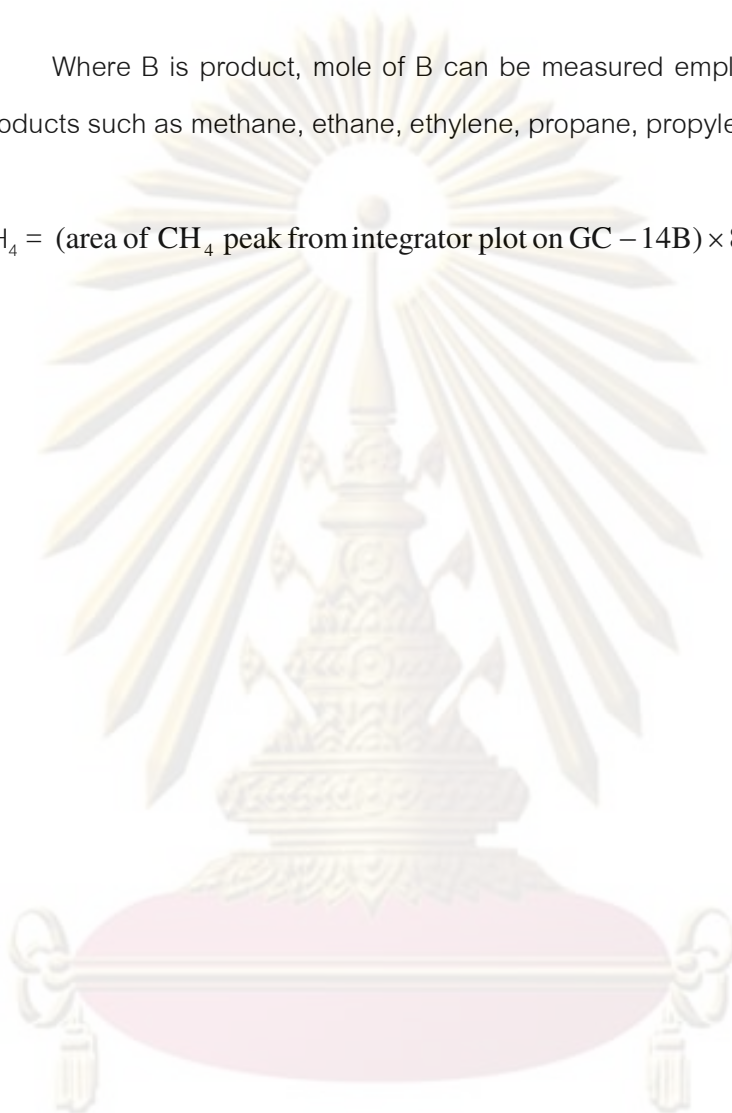
APPENDIX F

CALCULATION OF TURNOVER OF FREQUENCY

Metal active site $\quad = \quad$ y $\quad$ molecule/g catalysts

$$\text{TOF} \quad = \quad \frac{\text{rate}}{(\text{number of active site})}$$
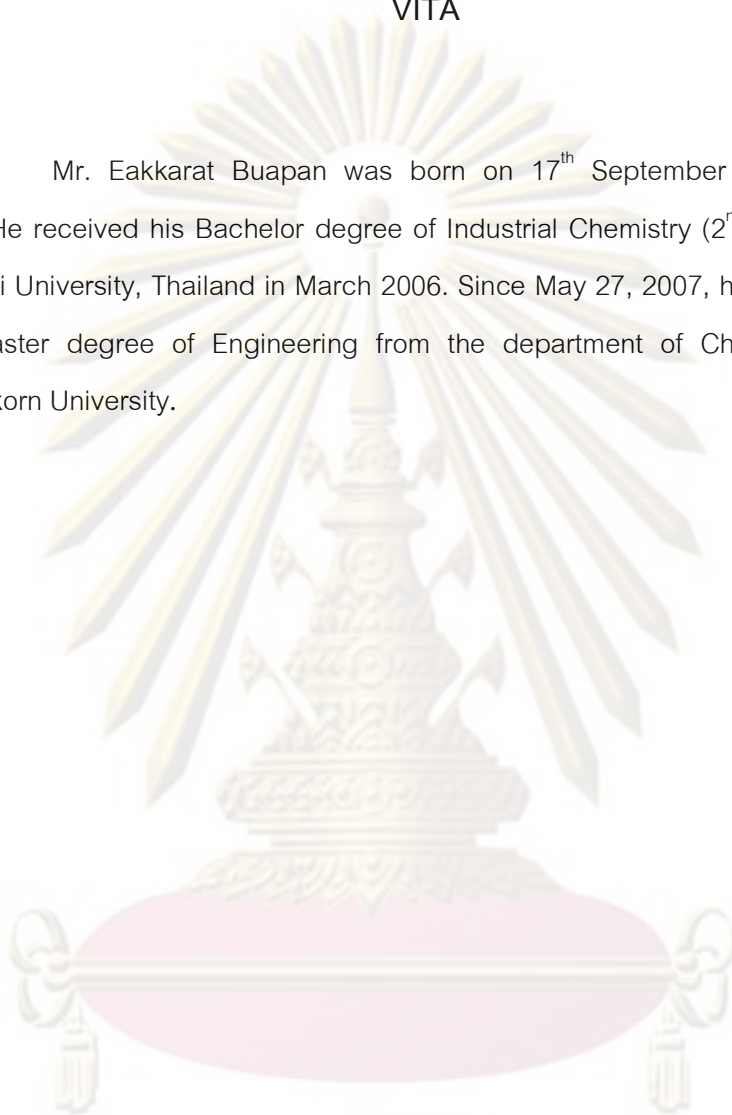
$$= \quad \frac{[\text{molecule substrate conveted}]}{[\text{g cat.}][\text{min}]} \left| \frac{[\text{g cat.}]}{\text{y [active site]}} \right| \frac{[\text{min}]}{[\text{s}]}$$

$$= \quad [\text{s}^{-1}]$$

VITA

Mr. Eakkarat Buapan was born on 17th September 1983, in Chonburi, Thailand. He received his Bachelor degree of Industrial Chemistry (2nd class honors) from Chiang Mai University, Thailand in March 2006. Since May 27, 2007, he has been studying for his Master degree of Engineering from the department of Chemical Engineering, Chulalongkorn University.